FAILURE CHARACTERIZATION OF THE INTERFACE BETWEEN CONCRETE SUBSTRATES AND FIBER REINFORCED CONCRETE REPAIRS

by

Bardia Kabiri Far

B.Sc., International University of Imam Khomeini, 2014

M.Sc., University of Bologna, 2016

A DISSERTATION SUBMITTED IN PARTIAL FULFILLMENT OF

THE REQUIREMENTS FOR THE DEGREE OF

DOCTOR OF PHILOSOPHY

in

THE FACULTY OF GRADUATE AND POSTDOCTORAL STUDIES

(Civil Engineering)

THE UNIVERSITY OF BRITISH COLUMBIA

(Vancouver)

April 2021

The following individuals certify that they have read, and recommend to the Faculty of Graduate and Postdoctoral Studies for acceptance, the dissertation entitled:

Failure characterization of the interface between concrete substrates and fiber reinforced concrete repairs

submitted by Bardia Kabiri Far in partial fulfillment of the requirements for

the degree of Doctor of Philosophy

in Civil Engineering

Examining Committee:

Cristina Zanotti, Assistant Professor, Civil Engineering, UBC

Supervisor

Philip Evans, Professor, Wood Science, UBC

Supervisory Committee Member

Shahria Alam, Professor, School of Engineering, UBC Okanagan

University Examiner

Tom Troczynski, Professor, Materials Engineering, UBC

University Examiner

Additional Supervisory Committee Members:

Mattia Bacca, Assistant Professor, Mechanical Engineering, UBC

Supervisory Committee Member

Nemkumar Banthia, Professor, Civil Engineering, UBC

Supervisory Committee Member

Abstract

Concrete structures are severely susceptible to degradation as a result of mechanical or environmental processes. In most cases, retrofit is the only available option because reconstruction of the deteriorated structure is neither a feasible nor financially practical option. The overall performance of a repaired structure is highly dependent on the properties of its interface, which is the weakest part of the system.

Fiber reinforced concrete (FRC) is a recognized repair material, however, there are still some knowledge gaps including lack of comprehensive understanding of the synergistic effects of fiber addition and surface preparation on composite structure, long-term behavior and durability of interfaces, and lack of standard design equations for concrete-FRC interfaces.

In this study, synergistic effects of different fibers at various volume ratios and surface preparation on failure mechanism, bond strength, and crack growth resistance of concrete-FRC interfaces is investigated under Mode-I loading regime.

Based on experimental data, design equations are proposed for concrete-FRC interfaces under Mode-I. These models address tensile strength and crack growth resistance of concrete-FRC interfaces encompassing various variables including surface preparation, type of repair material, and ductility of substrate and repair layers.

Furthermore, the micromechanical properties of concrete-FRC interfaces are studied and the impact of fiber addition and curing condition on microhardness, porosity, durability, and water absorption of composite structures is assessed using micro-indentation, scanning electron microscopy (SEM), and micro-computed x-ray tomography (CT-scanning) techniques.

Results indicate that there is a strong relationship between surface treatment, fiber content, and composite mechanical behavior. Fiber addition and improved surface treatment enhance response of composite systems in Mode-I. Semi-empirical models exhibit saturating trend between mechanical response improvement and surface preparation/fiber content. Moreover, micromechanical results indicate effectiveness of fibers in mitigating pre-loading and shrinkage damages.

In conclusion, FRC can be considered as a promising repair material for repair of deteriorated concrete structures. It can effectively mitigate pre-loading damages as well as mitigating failure under tensile stresses leading to improved mechanical performance and durability of repaired systems. Suggestive models can be employed for numerical simulations and can be used by practitioners for design purposes and to predict composite response of repaired structures.

Lay Summary

Over time, concrete infrastructures start to deteriorate mainly due to mechanical loads and deteriorating mechanisms. These degraded structures need to be enhanced before losing their functionality. To have a sustainable repaired system, not only the maximum load bearing capacity of the structure needs to be addressed, but also its durability. Various characteristics of FRC-concrete interfaces are investigated using tensile tests, capillary absorption, micro-hardness, SEM and CT-scans. Effectiveness of FRC in mitigating pre-loading damages and improving tensile behavior is demonstrated and the role of surface preparation, ductility, and properties of repair material on composite response is addressed in proposed semi-empirical models. Results indicate that FRC is an assuring repair material capable of enhancing load bearing capacity, improving crack nucleation and propagation resistance, and mitigating pre-loading damages. Proposed design equations can be used by practitioners in the field. They can also be employed in numerical simulations of composite elements.

Preface

I hereby declare that this thesis, completely made and drafted by Bardia Kabiri Far, which includes the conducted research, as part of a doctoral program, under the primary supervision of Dr. Cristina Zanotti, assistant professor of civil engineering at UBC. Identification and design of the research program was done by Bardia Kabiri Far. All experimental work was carried out at Civil Engineering Materials laboratory at UBC by Bardia Kabiri Far under supervision of Dr. Zanotti. Data collection, analysis, result presentation, and writing were conducted by Bardia Kabiri Far.

The research work presented in Chapter 3 has led to the following published papers:

Journal paper:

Kabiri far B., Zanotti C., "Concrete-concrete bond in Mode-I: a study on the synergistic effect of surface roughness and fiber reinforcement", Journal of Applied Sciences, Special Issue "Fiber-Reinforced Concrete, 2019.

Conference paper:

Kabiri far B., Zanotti C., "Concrete-FRC bond in mode-I: A crack growth resistance analysis", fib symposium 2019: Concrete - Innovations in Materials, Design and Structures, Krakow, Poland.

Table of Contents

List of Tables

List of Figures

List of Abbreviations

2D	Two-Dimensional
3D	Three-Dimensional
BFS	Blast Furnace Slag
CBM	Crack Band Model
CCM	Cohesive Crack Model
CDCB	Contoured Double Cantilever Beam
CDMP	Concrete Damage Plasticity
CFRP	Carbon Fiber Reinforced Polymer
CH	Calcium Hydroxide
CMOD	Crack-Mouth Opening Displacement [mm]
CSH	Calcium Silicate Hydrate
CTOD	Crack-Tip Opening Displacement [mm]
CT-scanning	Micro-computed X-ray Tomography
DIC	Digital Image Correlation
ECC	Engineered Cementitious Composites
ECM	Effective Crack Model
EDS	Energy Dispersive Spectroscopy
FCM	Fictitious Crack Model
FE	Finite Element
FPZ	Fracture Process Zone
FRC	Fiber Reinforced Concrete
FRCC	Fiber Reinforced Cementitious Composite
FRCM	Fiber Reinforced Cementitious Matrix
FRP	Fiber Reinforced Polymer
GU Cement	General Use Cement

HPFRC	High Performance Fiber Reinforced Concrete
HV	Hardness Value [GPa]
ITZ	Interfacial Transition Zone
LEFM	Linear Elastic Fractur Mechanics
MLEFM	Modified Linear Elastic Fracture Mechanics
MMOR	Modified Modulus of Rupture
MSSCT	Modified Slant Shear Cylinder Test
NSC	Normal Strength Concrete
PVA	Poly-Vinyl-Alcohol
P_{max}	Peak Indentation Load [gf]
RH	Relative Humidity [%]
ROI	Region of Interest
SCM	Supplementary Cementitious Material
SEM	Scanning Electron Microscopy, Size Effect Model
SIF	Stress Intensity Factor [MPa*mm$^{0.5}$]
SL	Splitting Load [kN]
SSD	Saturated Surface Dry
SP	Superplasticizer
TEM	Transmission Electron Microscopy
TPFM	Two-Parameter Fracture Model
UHPC	Ultra High-Performance Concrete
UHPFRC	Ultra High-Performance Fiber Reinforced Concrete
WDT	Wedge Driving Test
XRD	X-Ray Diffraction

List of Symbols

%	=	percentage
°	=	degrees
α	=	bond plane angle
δ	=	stress across a crack
Γ	=	interface toughness
Γ_c	=	toughness of repair/substrate layers
θ	=	the angle of reinforcement
K_I	=	stress intensity factor
K_{IC}	=	critical stress intensity factor
K_t	=	stress concentration factor
ν	=	Poisson's ration
σ_{max}	=	maximum stress
σ_N	=	normal stress
τ_{au}	=	adhesive shear bond strength
τ_{fu}	=	maximum frictional shear strength
φ	=	friction angle
μ	=	coefficient of friction
a	=	crack length
a_0	=	length of the notch
a_c	=	critical effective crack length
a_{eff}	=	effective crack length
c	=	cohesion
C	=	compliance
E	=	elastic modulus
E_{eff}	=	effective elastic modulus

E_o = elastic modulus of the overlay

E_s = elastic modulus of the substrate

f_c = compressive strength

f_t = tensile bond strength

f_y = yield strength

G = strain energy release rate of the interface cracking

G^t = strain energy release rate of the kinked cracking

G_c = critical strain energy release rate

G_F = specific fracture energy

gf = gram-force unit

GPa = giga-pascals unit

H = hardness

Hz = hertz unit

J_c = critical value in J-integral method

kg/m^3 = kilogram-per-cubic-meter unit

kN = kilo-newtons unit

kV = kilo-voltage unit

L_c = critical length

m = meter unit

mm = millimeters unit

min = minute

MPa = mega-pascals unit

nm = nanometer unit

Psi = pounds-per-square-inch unit

R^2 = coefficient of correlation

R_a = average roughness (2D)

R_{pm} = the mean peak height (2D)

S_a = average roughness (3D)

S_{pm} = the mean peak height (3D)

T = Temperature

U = strain energy

V_f = volume fraction of fiber reinforcement

$V_{f.critical}$ = critical fiber content

$V_{f.ultimate}$ = ultimate fiber content

W = energy for crack nucleation

Acknowledgments

I would like to appreciate Dr. Cristina Zanotti as the primary supervisor of this doctoral work. Without her support and cooperation, this work would have not been feasible. Also, I would like to appreciate the guidance of my thesis supervisory committee members, Prof. Philip Evans, Prof. Nemy Banthia, and Dr. Mattia Bacca.

I offer my gratitude to the administrative and technical staff at the Civil Engineering Department of the University of British Columbia for their help and support during this project. Specifically, the kind support of Mr. Harald Schrempp, Mr. John Wong, Mr. Doug Hudniuk, Mr. Scott Jackson, Mr. Simon Lee, and Mr. Sylvain Picard who helped me a great deal with instrumentation, data acquisition, and running various test setups; as well as Obinna Onuaguluchi, Ricky Ratu, Negar Roghanian, Farhad Pargar, Madhuvandi Ravi, Parisa Setayeshgar, Giulia Rostagno, Tahmineh Teymourian, Salman Soleimani-Dashtaki, Robert Shilton, Mohammed Farooq, and Joanna Suchta.

I owe an enormous debt of gratitude to my family who have always supported me and been there for me. This thesis is dedicated to my beloved mother, Nazi, who dedicated her life to her children, and to my sister, Niloufar, who did a great job during these years and in all circumstances always stood behind me.

Special thanks are owed to my close friends Hamed Mirzaei, Omid Fakourfar, Hossein Kavehsaz, Omid Alavi, Mohammad Faregh, Navid Salami, Pouya Rostam, Arman Ahmadi, and many others, who provided me with unbelievable support during these hard years.

Finally, I would like to acknowledge the financial support of the Natural Sciences and Engineering Research Council of Canada (NSERC).

Dedication

To my mother Nazi

Chapter 1: Introduction

1.1 Statement of the problem

Concrete is the most popular construction material around the world, used in various structures from bridges and dams to schools and hospitals due to its availability, formability, and low cost [Collin, 2014]. However, concrete has shortcomings as well. Concrete structures are highly vulnerable to deterioration from both mechanical and environmental means. The most important defects of concrete are low load bearing capacity, specifically under tension, and low durability. Moreover, concrete as the second most widely used material [Crow, 2008], accounts for 5-8% of global carbon dioxide emissions equivalent to 1.75-2.8 billion tonnes per year [Worrell et al., 2001]. These emissions are caused by calcination process (50%), burning fossil fuels (40%), and transportation (10%) [Schaefer et al., 2018]. Although load bearing capacity of concrete has been addressed in various research works, comprehensive investigations have not been conducted on the durability of concrete structures, which is highly important in terms of long-term behavior, sustainability, and controlling carbon emissions.

A remarkable amount of concrete infrastructure is in growing need of rehabilitation, retrofitting, repair, and rebuilding. From a survey undertaken by McGill University and the Federation of Canadian Municipalities (FCM), and the report of the Canadian Society of Civil Engineers, Canada’s municipal infrastructure deficit has been increased from CAN $44 billion in 1996 to CAN $60 billion in 2006 [McGill-FCM, 1996] [Mirza, 2006]. In United States, the American Society of Civil Engineers (ASCE) launched four consecutive detailed surveys of selected infrastructures categories from 1998 to 2005 [ASCE 1998, 2001, 2003, 2005]. The surveys investigated each category in all states. Their summarized results can be observed in Table 1.1.

Generally speaking, the overall condition for any specific infrastructure category either did not change remarkably or was downgraded from 1998 to 2005. While the average infrastructure grade was C in 1998, it changed to D in 2005, where projected 5-year needs boosted from US $ 1.0 trillion in 1988 to US $1.6 trillion in 2005.

It should be noted that an astonishing 79% of infrastructure in Canada is already beyond its expected service life [CSCE 2003]. All these deteriorated structures are in urgent need of maintenance and rehabilitation. Figure 1.1 depicts a qualitative relationship between the degradation of infrastructures in Canada and the level of maintenance, where maintenance cost is expressed as a percentage of the facility cost [Mirza, 2004]. Level of performance is scaled from 0 to 1, where 1 is perfectly functional structure. The higher the level of maintenance, the better performance during expected service life. If maintenance is neglected (0% maintenance), the structure needs to be replaced in 45 years. This increases to more than 60 years if equivalent to 1.5% of facility cost is dedicated to structure maintenance. Failure to properly address deteriorating structures will lead to an unsustainable infrastructure system.

Table 1.1: Summary of USA infrastructure survey findings [Mirza, 2006]

	1988	1998	2001	2003	2005
Infrastructure category evaluated					
Aviation	B–	C–	D	→	D+
Bridges	C+	C–	C	→	C
Dams	—	D	D	→	D
Drinking water	B–	D	D	→	D–
Energy	—	—	—	—	D
Hazardous waste	D	D–	D+	→	D
Navigable waterways			D+	→	D–
Public parks and recreation	D				C–
Rail	—	—	—	—	C–
Roads	C+	D–	D+	→	D
Schools		F	D–	→	D
Security	—	—	—	—	I
Solid waste	C–	C–	C+	→	C+
Transit	C–	C	C–	→	D+
Waste and Energy	—	—	D+	D	—
Wastewater	C	D+	D	→	D–
Water resources	B	—	—	—	—
Infrastructure GPA	C	D	D+	D+	D
Total investment needs (CAN$ trillion)[a]	1.0	1.3	1.3	1.6	1.6

Note: Adapted from ASCE (1998, 2001, 2003, 2005). Grading criteria: A, exceptional (90%–100%); B, good (80%–89%); C, fair (70%–79%); D, poor (41%–69%); F, inadequate (<40%); →, condition remained unchanged; I, insufficient information. The 1988 data, for comparison, are from NCPWI (1988).

[a]Estimated 5-year needs.

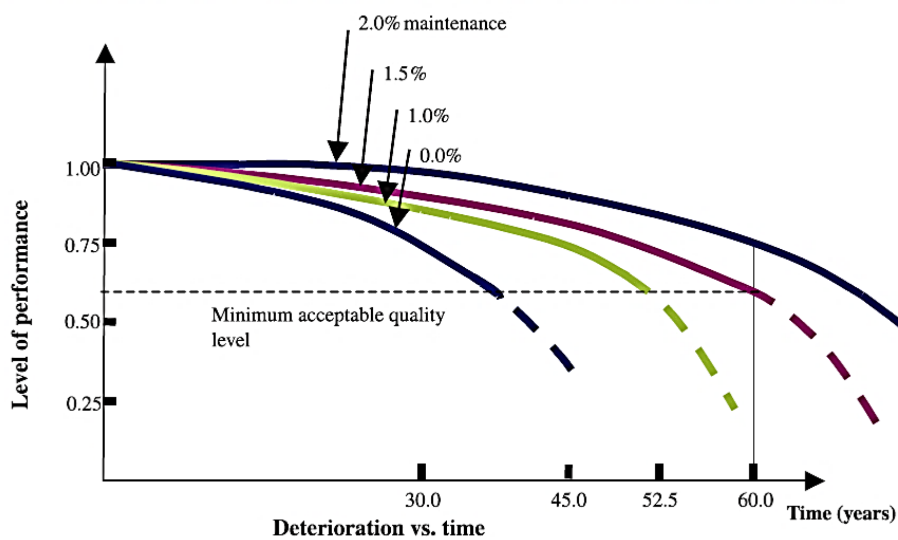

Figure 1.1: Qualitative degradation versus time for different levels of maintenance [Mirza, 2004]

In order to extend the service life of deteriorating reinforced concrete structures, and to ensure safety in case of increased loading demand, interventions of repair and rehabilitation have become of frequent practice worldwide. The annual cost of concrete repair in the United States is between $18 billion and $21 billion [Vision 2020, 2016]. In Europe, 50% of the construction budget is spent on maintenance, strengthening and repair [Tilly and Jacobs, 2007]. Since concrete production skyrocketed after the second world war, the number of concrete structures today which have significantly deteriorated is high and will continue to increase.

Unfortunately, there are many gaps in the state of knowledge of repair and rehabilitation of concrete structures. For instance, many previously repaired structures are suffering from a lack of durability. There is lack of comprehensive knowledge of failure mechanism of repaired systems both in macro and micro scales, and there is no standard design equation for repairing concrete structures. Research studies indicate that in Europe, 20% of the repairs failed within 5 years, 55% within 10 years, and 90% within 25 years [Tilly and Jacobs, 2007]. In the United States, almost 50% of the repairs fail to exhibit a satisfactory performance [McDonald et al, 1985]. Poor compatibility (shrinkage, thermal, mechanical etc.), cracking, and debonding of the repair material are some of the most common contributing factors. In order to solve these problems, better understanding of composite behavior of cementitious materials is required.

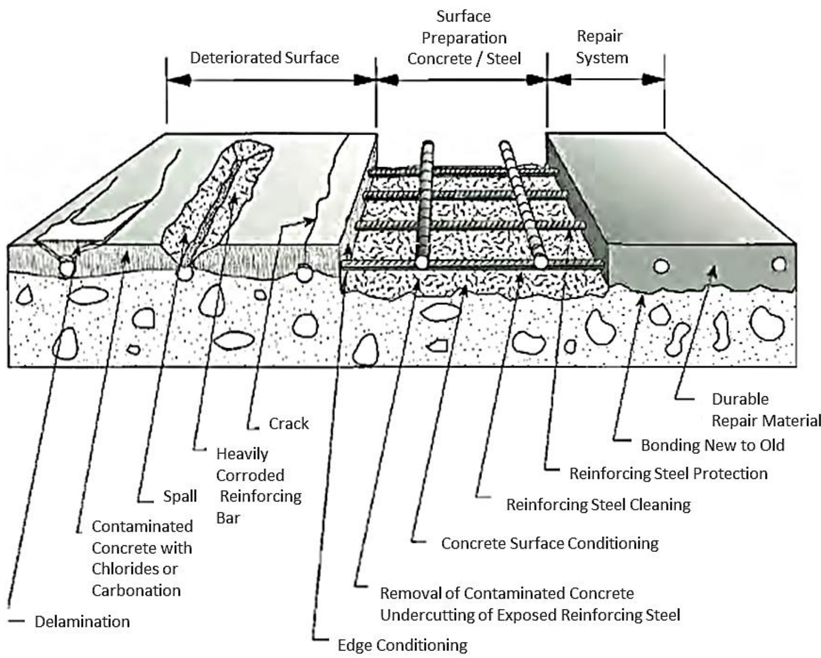

Figure 1.2 Anatomy of concrete repair [Emmons, 1994]

In a repaired system (Figure 1.2), the interface between the concrete substrate and the new repair layer is typically weaker than the materials on either side [Zanotti et al., 2018]. Due to this weakness combined with stress concentrations (emphasized where there is poor substrate-repair compatibility), the interface is much more vulnerable to cracking and failure. As a result, the performance of repaired systems and, thus, their safety and durability, are highly dependent on the properties of the interface [Sadowski, 2017] [Sadowski and Stefaniuk, 2017] [Courard et al., 2014] [Xiong et al., 2002] [Sadowski et al., 2017].

There are various repair and rehabilitation techniques used for concrete structures; among them, using Fiber Reinforced Concrete (FRC) as a repair layer is recognized as a promising option [Banthia et al., 1994]. Microfibers are able to improve durability of concrete [Barkhordari et al., 2017] [Banthia et al., 2014] [Bentur and Mindess, 2007] [Qi et al., 2003]. These benefits become even more relevant in repaired structures, where fibers can help to improve compatibility between old and new layers or, at least, reduce the extent of damage arising from poor compatibility e.g. shrinkage or thermal gradients [Banthia et al., 2014] [Banthia and Gupta, 2006]. As a result, FRC is chosen as the repair material in this study.

Previous studies have shown that FRC can be beneficial to concrete bond. However, earlier research on concrete-FRC bond mostly focused on bond strength only and the effect of different fibers added to repair layer on the micromechanical behavior of concrete-FRC interfaces is not well-addressed in existing literature. Overall, the data available is too limited and thus no general conclusions can be drawn nor can some standard equations accounting for the FRC effect be developed as there is a lack of comprehensive knowledge on the influence of various controlling factors on interfacial failure modes

The study presented here is a description of the research works done as a PhD thesis on “Failure characterization of the interface between concrete substrates and fiber reinforced concrete repairs” which is a subproject of a larger project known as “Durable Repair of Concrete Structures”. This research work is a continuation of previous studies done under Dr. Zanotti’s supervision in the UBC Civil Engineering Materials Lab during the last 5 years on failure of concrete-FRC repaired systems. In this PhD thesis various macro and micro scale properties of concrete-FRC interfaces are investigated. Knowledge gained through experimental study culminated in a proposed design equation for concrete-FRC composite systems.

1.2 Objectives

By means of experimental and analytical tools, this study aims to gain a better understanding of concrete-FRC interfaces. Considering that the performance of composite specimens is affected both by material properties, as well as environmental conditions, various repair materials are to be studied under different environmental and loading conditions. The main objectives of this PhD are as follows:

1. Investigate the role of metallic (steel) and synthetic (Poly-Vinyl-Alcohol (PVA)) fibers at different volume ratios (0-1%), as well as the effect of surface preparation and morphology (attained by sandblasting) on failure mechanisms, bond strength, and crack growth resistance of concrete-FRC composite systems in Mode I.
2. Develop a semi-empirical model to describe the failure of concrete-FRC interfaces under Mode-I that could be adopted by standards and codes for structural design as well as by concrete engineers to design their FRC repair material with the scope to optimize bond and durability.
3. Transitioning from the macroscale to the microscale and evaluating the micromechanical properties of concrete-FRC interfaces and the effectiveness of steel and PVA fibers in harsh environmental condition.

1.3 Methodology and Outline of the Thesis

It is a significant undertaking to investigate all of the known factors that govern damage development and failure of concrete-FRC interfaces. Some parameters were covered in previous studies such as the influence of water/cement ratio, the influence of substrate saturation level, and the influence of supplementary cementitious materials [Lukovic, 2016]. Thus, the general approach is to evaluate selected parameters of primary interest and to leave other variables unchanged.

This study can be divided into three main sections dealing with characterization of repair materials and investigation of the effect of microfibers and surface preparation on failure of concrete-FRC interfaces in mode-I, modelling the failure of concrete-FRC interfaces in mode-I and developing a design equation, and microscale characterization of concrete-FRC interfaces.

For the first part of the study (Chapter 3 of this thesis), two different classes of tests are conducted. The first set of the tests (monolithic specimens) are dedicated to study of the pure material properties, effectiveness of fibers, and the failure behavior of different repair mixes. The ideal repair material exhibits high performance, ductile behavior under tension, and high ultimate stress capacity [Zanotti et al., 2014b]. It also needs to meet certain service condition requirements, to be durable, easily accessible, and affordable [ACI 563, 2018]. In the second set of the tests, the previous materials are applied directly to sandblasted substrate surface, as a repair layer, in order to investigate the composite behavior of concrete-FRC systems. The substrate mix design and curing regime are consistent for all specimens, while repair mix design and surface preparation are subject to change. Various fibers at different volume fractions are used in both monolithic and composite (substrate-repair) specimens. The Mode-I failure of repair materials and the concrete-FRC interfaces is investigated at the macroscale using Contoured Double Cantilever Beam (CDCB) tests. Through analysis of the full load-displacement curve of the failed specimens, not only maximum load bearing capacity under Mode-I loading regime, but also crack nucleation and crack growth resistance of interfaces are studied. Mechanical properties and ductility of substrate and repair are evaluated based on splitting, compressive and modulus of elasticity tests. It needs to be highlighted that the goal is not to develop a perfect repair material which can be used in all conditions. The main goal of this chapter is to cover knowledge gaps and to study complex interactions among different factors so as to enable informed development of FRC repairs. A part of this work has been published in the Journal of Applied Sciences, Special Issue on Fiber Reinforced Concrete, [Kabiri Far and Zanotti, 2019].

The next stage of the research (Chapter 4 of this thesis) deals with developing a standard equation for characterizing Mode-I bond failure of concrete-FRC composite systems taking into account the most important variables including surface roughness, incompatibility between two layers, and characteristics of repair overlay. CDCB tests are used for load bearing capacity and crack growth resistance of both monolithic and composite specimens. Surface preparation is quantified by means of 2D and 3D laser scanning. Ductility of substrate and repair layers is investigated by compressive, splitting, and elastic modulus tests. Various regression models are employed to investigate the relation between variables and output and suggestive design equations are proposed. The outcomes of this chapter are expected to be useful for predicting the performance of repaired systems in the future.

The last section (Chapter 5) deals with the characterization of micro-properties of selected repair mix designs based on the results of the previous work. The complexity of concrete microstructure comes from both the binder phase and the aggregate-binder interfaces. In the case of repaired systems, the interface between substrate and repair layers further contributes to the complexity of the system. This interfacial transition zone (ITZ) is the place for the nucleation of the first microcracks because of its weakness and complex stress state. Micromechanical properties such as micro-hardness is determined using micro-indentation tests. Porosity and pore-connectivity are investigated by means of micro-computed x-ray tomography (CT-scanning). Capillary water absorption is studied by employing gravimetric absorption tests. Finally, the micro-features of repair and substrate layers, as well as the interface are investigated based on scanning electron microscopy (SEM).

Chapter 2: Literature Review

This chapter provides required background information on main subject areas relevant to this thesis. Firstly, quantification methods for bond strength, which requires comprehensive knowledge of various bond evaluation techniques, are reviewed. Then advantages of fiber reinforced concrete as a repair material, which requires familiarity with fibers' behavior in cementitious materials and cementitious interfaces, are discussed. Moreover, fracture behavior of cementitious materials and interfaces is reviewed. Finally, previous efforts on micro analysis and modelling interfacial bond of cementitious interfaces are discussed.

2.1 Test Methods for Evaluation of Concrete-Concrete Bond

In order to have functional and durable composite cementitious systems, development and maintenance of a sound bond is necessary. The interface must maintain its integrity and strength to be able to endure imposed stresses as well as degradation processes. Reliable test methods are required for assessment of failure modes and quantification of bond between new and old concrete layers. Employing suitable quantification techniques is quite important for an understanding of the load transfer mechanisms in structures subjected to repair and retrofit. To have a durable repair, the two layers should have a sufficiently strong bond to prevent delamination and avoid ingression of contaminants such as chloride. The measured bond strength is highly dependent on the test method. Some of test methods report inflated values. There are many different test methods to study the bond between concrete layers, but most of these methods are only appropriate for laboratory tests.

Numerous studies have been devoted to the bond characterisation of cementitious composite systems, focusing on either suitability of tests or their comparability. An ideal testing method should have a convenient setup, provide reliable and comprehensive output, simulate site conditions, induce stress states typical of service, evaluate *in-situ* bond strength, and have a wide range of applications [Momayez et al., 2005]. Some test methods are more common due to their simplicity such as the pull-off test. Figure 2.1 shows various test methods for evaluation of interfacial bond strength. These test methods can be categorized based on the state of stress imposed on the interface and failure mode. Tensile and shear bond tests are two main types of bond strength tests.

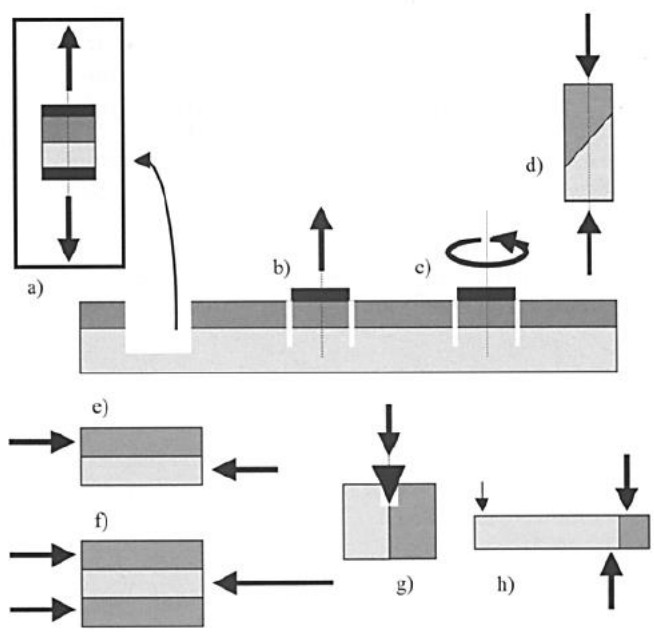

Figure 2.1: Different test methods to study interfacial bond strength a) Pull off test carried out in the lab, b) in-situ pull off test, c) in-situ torsion test, d) slant shear test, e and f) direct shear tests, g) wedge splitting test, and h) guillotine test [Silfwerbrand, 2003]

2.1.1 Tensile Bond Tests

Tensile tests are increasing in popularity, however, performing a reliable tensile test is complex and time consuming. Tensile bond testing techniques can be divided into direct and indirect tests. In the direct tensile tests, the tensile load is transmitted to the concrete by glued metal or grips and failure occurs on a plane perpendicular to the axial load, e.g. pull-off test and direct tensile test (Figure 2.1 a & b). Eccentricity can cause significant error in direct tensile tests. The other type of tensile test is indirect, such as the flexural test and the splitting test. The main governing factors for any tensile bond test are material properties, surface preparation, geometry, load axiality, and incompatibility of the two adjacent layers.

Pull-off Test

This is the most common bond test used on site [ASTM D4541]. This test can be carried out in the laboratory, to study material characteristics and failure modes, or in-situ for quality control. A core is drilled through new and old concrete layers and then the core is loaded in tension either by gluing steel pates to the core, by means of a suitable epoxy adhesive, or by friction grips clamping around the core (Figure 2.2). Disregarding eccentricity, the failure load is the pure tensile load bearing capacity. After carrying out the test, the failure mode needs to be carefully investigated to see if interfacial bond strength or material strength is measured. Three different failure modes can be identified, namely interfacial, cohesive material, and combined. Failure at locations other than the interface is known as cohesive failure of the overlay/substrate. Such failure indicates that the strength of the interface is greater than the failed material. In this case, the measured strength value is a lower bound of the bond strength. This testing method is highly sensible to instrumental parameters, load axiality and eccentricity, drilling-induced damage and related stress disturbances, and inaccurate gluing of the steel plate [Chmielewska et al., 2003; Austin et al., 1995]. Load eccentricity depends on normality of the core drilling and accuracy of locating the metal dolly on top of the core. In addition, the drilling depth of the core beyond the interface and into the substrate, as well as the thickness of repair layer influence the results. The effect of different geometries was addressed in an elastic finite element analysis run by Austin et al. [1995]. Smaller core diameter leads to increased ratio of cut surface area to volume, as well as increased intensity of damages occurring during drilling process. Hence, pull-off strength is expected to decrease by reducing core diameter. Moreover, it is expected that increasing drilling depth exacerbates core damage due to the vibration. Very shallow drilling depths, on the other hand, can also deliver increased bond strengths. The effect of the loading rate on the pull-off strength is addressed by Bonaldo et al., suggesting that there is a trend of increasing pull-off strength corresponding to an increased rate of loading [2005].

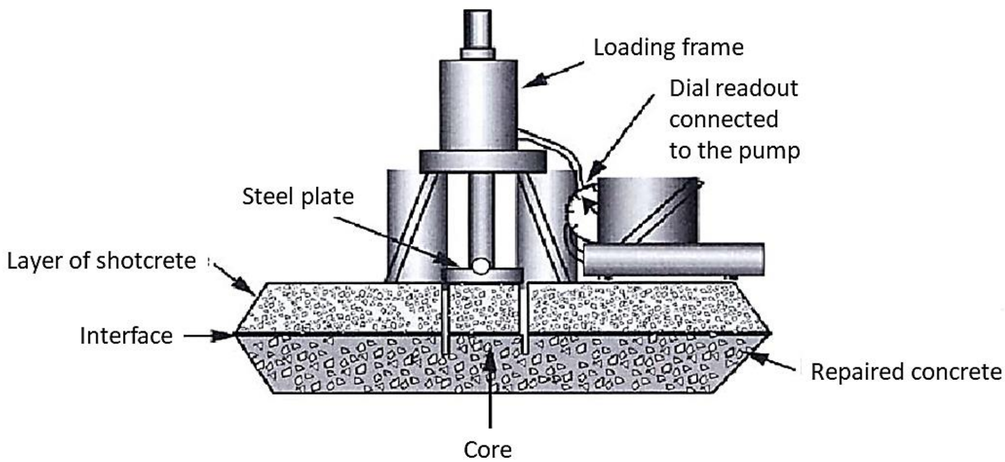

Figure 2.2: Pull-off test setup [Beaupre, 1999]

Other Tensile Tests

Splitting test or Brazilian test is one of the most common indirect tensile tests. It was first proposed by Japanese researchers [Akazawa, 1943] and later modified in Brazil [Carneiro and Barcellos, 1949]. This test method consists of a cylindrical specimen that is subjected to a diametral compressive force along its length [ASTM C496]. This technique was later used for tensile bond assessment of composite cylinder and prism specimens [Ramey and Strickland, 1984]. Since the areas of load application are in a state of triaxial compression, they can withstand much higher compressive stresses than uniaxial compressive strength. Hence, tensile failure happens before compressive failure (Figure 2.3). This test can be employed either for laboratory specimens or *in-situ* drilled cores.

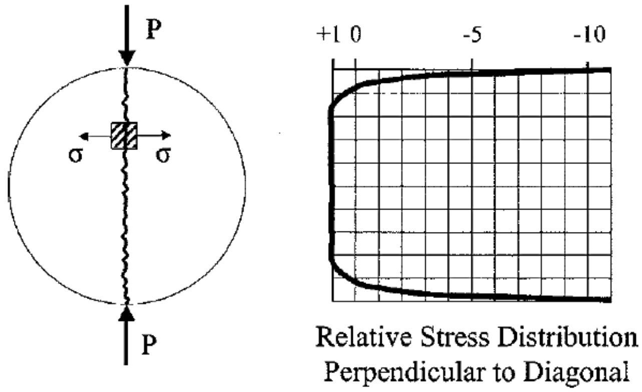

Figure 2.3: Setup and stress distribution of splitting test representing the difference between magnitude and pattern of compressive versus tensile stresses [Nilson, 1961]

The other type of indirect tensile tests is the flexural method. For example, Abu-Tair et al.'s modified modulus of rupture (MMOR) test to evaluate bonding under tensile stresses. It is been shown that MMOR is a useful and reliable indicator of repair effectiveness in tension. However, MMOR is sensitive to changes in repair materials. Moreover, the test suffers from low efficiency due to small bonded interface compared to the specimen volume [Abu-Tair et al. 1996].

The other indirect tensile test is the wedge splitting method (Figure 2.1 g). This method was first developed by Tschegg for fracture analysis of concrete [1991]. Later, it was used for determination of fracture properties of the cementitious interfaces [Tschegg et al., 2000]. During this test, notched cubic or cylindrical specimens are split using a wedge splitting device and the load-deformation curve is measured until full material separation occurs. The main advantage of this test setup is possibility of obtaining fracture properties of the specimen. This method is explained more in detail in the methodology for this chapter.

2.1.2 Shear Bond Tests

Bond strength is not routinely quantified in a pure shear stress state. A pure shear stress state can be evaluated as a combination of corresponding axial stresses occurring at 45° to the shear plane, where failure depends on the relative values of compressive and tensile strength and the bond strength. For cementitious materials as tension-weak brittle materials, the compressive strength is much higher than tensile strength and under shear stress, failure is most likely governed by tensile cracking rather than shear slipping. In other words, failure load is an indication of tensile strength, rather than shear strength. In case of a smooth interface, there is not any extra mechanical interlock and the shear failure line can pass along the bond interface. In this case, measuring true shear bond strength is more probable. In case of rough surfaces, however, there is a mechanical interlock from the uneven surface resulting in remarkable tensile cracking contribution (Figure 2.4) [Austin, 1999]. Shear bond tests can be divided into pure shear methods, e.g. mono-surface and bi-surface methods, and combined shear and axial stresses, e.g. slant shear test.

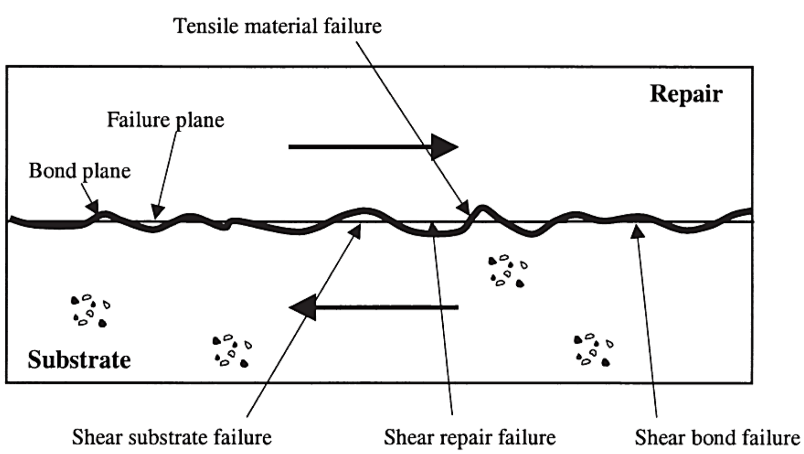

Figure 2.4: Interfacial failure under shear load [Austin et al., 1999]

Slant Shear Test

This is one of the most common bond strength evaluation techniques in which the interface is subjected to combined state of compression/tension and shear stresses [ASTM C882]. This test method is only useful for laboratory investigations and can not be used on site. This test was first introduced as "Arizona Slant Shear Test" by Kreigh [1976] and later modified by Tabor [1978]. The test specimen is a composite cylinder with a diagonal bonded plane at an angle of 30˚ (Figure 2.1 d). The test is still employed for characterization of repair materials, but the method has several shortcomings, as follows.

Firstly, the failure strongly depends on the angle of the interface [Austin et al., 1999]. In the standard test setup, the angle of the plane is fixed, which hinders the possibility of achieving different failure planes (where there might be a more significant stress combination). Based on Coulomb theory, the maximum load of failure depends on the angle of the interface. There is also a critical angle, which is the inclination at which the stress corresponding to bond failure is minimum, for each surface roughness. Austin et al. developed an analytical method to quantify the critical angle [Austin et al., 1999]. Figure 2.5 depicts ratio of the failure stress to the adhesion strength versus angle of bond plane. It can be observed that the critical angle tends to decrease as surface roughness increases. The critical bond angles corresponding to smooth, medium rough, and rough surfaces are 27˚, 23˚, and 19˚ respectively. This means although the failure stress corresponding to smooth surface is close enough to the minimum failure stress, the failure stress for a rough surface with an interface angle of 30˚ is much higher than the minimum stress at the critical angle of 19˚. In other words, by keeping bond angle constant and increasing surface roughness, failure mode switches from bond failure to compressive failure of either repair or substrate layer.

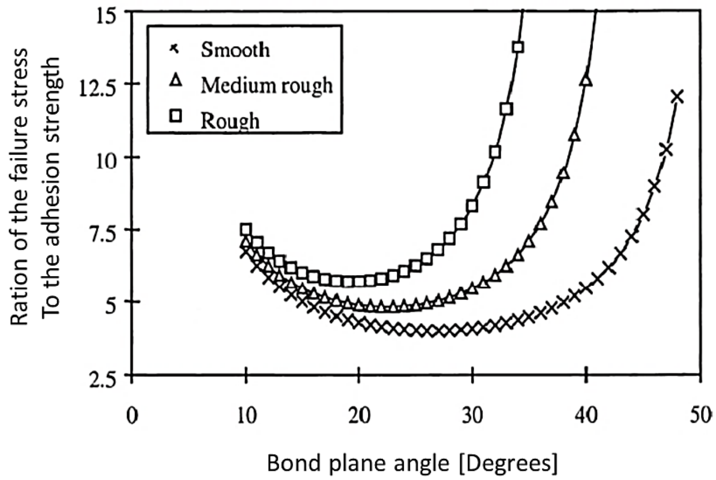

Figure 2.5: Influence of surface roughness on critical angle [Austin et al., 1999]

Secondly, the test is rather insensitive to surface preparation and surface roughness [Austin et al., 1999]. While the test is able to capture bond strength increases for smooth surface and rough surfaces, it can not appropriately address corresponding changes for various roughness levels. Moreover, higher roughness might affect failure surface, in that case, failure and bond surface are no longer the same. This insensitivity to roughness can be mitigated by employing tensile slant shear test, in which specimens are subjected to a combination of tensile and shear stresses. This test procedure was first introduced by Chestney [1996]. This methodology produces a different but still a realistic stress state, e.g. in repairs to beams, which provides a more comprehensive picture of bond characteristics.

Additionally, in case of compressive slant shear test, the compressive stress increases friction and interlocking mechanisms at the interface leading to greater bond strengths. This means that even for weakly bonded interfaces, the slant shear test might give high bond strength [Neshvadian, 2010]. Lastly, slant shear test is highly sensitive to elasticity mismatch. This is mainly due to extra stress concentration at the interface which acts as additional shear stress at the interface. In addition, it might develop some load eccentricities which can result in a lower failure load [Austin et al., 1999].

Modified Slant Shear Cylinder Test (MSSCT)

In order to address the issue of changing critical angles, Zanotti et al. proposed a variable bond angle approach for slant shear test method, known as modified slant shear test [Zanotti et al., 2014b]. Two additional bond plane angles were employed (α = 20˚ and 25˚), in addition to the standard inclination angle (α = 30˚) (Figure 2.6). Having data for three different test setups allows inherent bond properties (cohesion and internal angle of friction) to be quantified. This approach is quite helpful to eliminate the effect of bond angle.

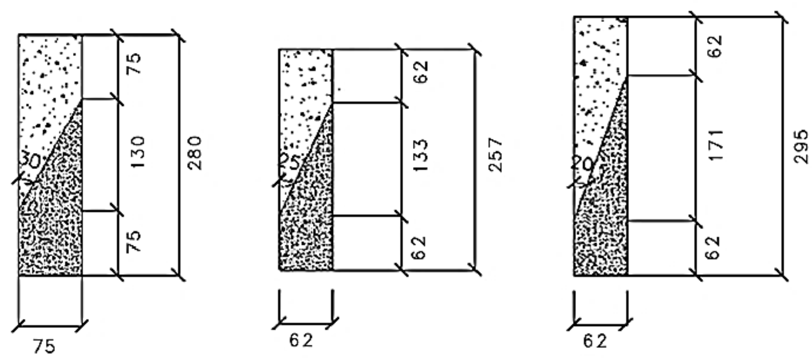

Figure 2.6: Geometry of cylinders for modified slant shear test [Zanotti et al., 2014b]

Twist-off Test

Most shear test methods have one common disadvantage: test specimens need to be prepared in the laboratory. In other words, most accepted shear test methods can not be conducted on site. Silfwerbrand proposed a new method which can be employed in-situ [Silfwerbrand, 2003]. The test specimen is the same as pull-off test specimen. However, the core is subjected to torsional moment rather than a tensile force (Figure 2.1 c). The steel plate is glued to the drilled core and a torsional moment is applied to the core. Failure shear stress can be derived from the maximum torsional moment. Similar to the pull-off method, the failure mode needs to be investigated thoroughly to see if the failure value corresponds to the interface failure or material failure. It can be expected that tensile cracks develop at the periphery of the bond plane, however, because of high tensile strengths of substrate and repair layers, microcracks do not propagate into the repair or substrate layers. Instead, microcracks propagate moderately into the bond plane until failure occurs.

One possible source of error for the twist-off test is development of normal forces when running the test due to poor workmanship. It is also important to note that in some studies, almost none of the cores showed failure at the interface [Silfwerbrand, 2003]. This suggests that test geometry is not appropriate for the applied forces. In another study, Neshvadian suggested that based on the failure envelope of concrete, as a brittle material, failure under pure torsion occurs on an inclined plane rather than on a plane perpendicular to the axis of torsion [Neshvadian, 2010]. Hence, it would be better to have an inclined interface surface which can lead to more interfacial failures and less error.

Other Shear Tests

The simplest shear test setup is called a mono surface shear test (Figure 2.1 e) in which forces are applied parallel to the bond plane causing shear stress at the interface. This test is vulnerable to extra moment caused by shear forces and load eccentricity. This flaw led to the development of the Push-out Specimen Method [Chen et al., 1995]. Having three forces in two different directions, eliminates the adverse impact of extra moments (Figure 2.1 f). This test, however, does not represent the real condition of repaired systems as such specimens contain two parallel interfaces. In addition, the interface is exposed to small bending moment and tensile stresses caused by tiny eccentricities between applied load and support points which results in lower bond values [Zanotti et al., 2019]. The Guillotine test method eliminates the problem of extra moments as test specimens do not have two interfaces (Figure 2.1 h). This test takes advantage of a long span rather than a large extra force to counteract the effects of additional moment. In this way, vulnerability of test specimen to material shear failure decreases. This test method can be used for both on-site cores and laboratory specimens.

2.1.3 Fracture Bond Tests

Fracture behavior is the other fundamental aspect of repaired systems. As mentioned above, crack growth resistance is a fundamental aspect governing long-term behavior of the cementitious repaired systems. Fracture tests are those carried out on specimens with notches or initial cracks. These tests can be performed under various loading configurations. Tests involving opening or tensile displacements are called mode-I tests, e.g. wedge splitting test. The ones which involve opening displacement and shear (sliding) displacements are called mixed mode tests. Considering the complexity of mixed mode tests and low tensile strength of concrete, mode-I tests are preferred [Gettu et al., 1996]. The resulting load-deformation curve provides required information for evaluation of concrete fracture.

Several research works are dedicated to the development of testing methods for fracture characterisation of concrete and FRC as well as cementitious interfaces. These include Jenq and Shah's research on concrete fracture testing methods [Jenq and Shah, 1989], a study on testing methods to determine fracture energy of concrete by Rokugo et al. [1989], Tschegg's proposed method for fracture tests on concrete [Tschegg, 1991], Elser and co-workers' study of fracture behavior of FRC under biaxial loading [Elser et a., 1996], the investigation by Banthia and Nandakumar on crack growth resistance of hybrid fiber reinforced cement composites [Banthia and Nandakumar, 2001], and a recent study on fracture characterisation of FRC-concrete interfaces by Zanotti et al. [2014]. Fracture bond tests are further explained in the methodology section of this chapter.

2.1.4 Comparability of Bond Tests

Different test setups give different bond values because of different modes of loading, specimen sizes, loading rates, etc. Various studies have focused on developing a relationship between different test methods. Delatte et al. investigated tensile and shear bond strengths of high-early-strength bonded overlays [Delatte et al. 2000], employing direct shear and pull-off test methods. Their results indicate that shear bond strength is approximately twice the value of tension bond strength. In another study, pull off and torsion tests were employed to investigate tensile and shear bond strength of concrete overlays, respectively [Silfwerbrand, 2003]. Results suggested that shear bond strength is much higher than the tensile bond derived from the pull off and torsion tests. Additional research work was concerned with comparability of pull-off, slant shear, splitting prism and bi-surface shear tests [Momayez et al., 2005]. The highest bond strength was achieved with the slant shear tests, mainly due to the high compressive stresses, followed by bi-surface shear tests, splitting tests, and pull-off tests. The authors suggested that the pull-off test provides the most conservative bond measurements as it is not affected by friction or any other extra force [Momayez et al., 2005]. They concluded that in the case of cementitious materials, the most conservative results correspond to tensile tests. In a more comprehensive study, Zanotti and Randl investigated the comparability of slant shear, push out, direct splitting, and pull off tests [Zanotti and Randl, 2019]. In their study, size effect and test geometry were addressed as well. It was suggested that specimen geometry affected bond values, as well as failure modes. The smaller the specimen, the higher the bond strength. Their study also found that shear bond strength obtained from push-out tests were lower than the ones derived from slant shear tests. Finally, for each shear bond test setup, a constant cohesion-tensile bond ratio was derived [Zanotti and Randl, 2019].

2.2 Introduction to Fiber Reinforced Cementitious Composites

Using fibers to strengthen cementitious materials that are much weaker in tension than in compression dates back to ancient times. Asbestos cement was the first widely employed composite cementitious material, developed in 1900 [Li, 2011]. Since then, various types of fibers have been used in fiber reinforced cementitious composites (FRCC) including steel, glass, carbon, cellulose, etc. In recent decades, the popularity of fiber reinforced concrete has increased remarkably, due to the capacity of fibers to improve concrete's mechanical behavior and durability, as well as improving cementitious interfaces. FRCCs are cement-based composites with integrated fibers, mainly short and discontinuous. The goal of research on FRCC is to improve tensile strength by transferring stresses and loads across the cracks, as well as enhancing energy consumption capacity or toughness of the plain cement-based composites by providing energy absorption mechanisms related to the debonding and pull-out of the fibers [Li, 2011]. Fibers help both by mitigating crack propagation, and by improving the mechanical properties of the plain material [Zanotti et al., 2014]. Other advantages of adding fiber to concrete are enhancing impact resistance [Mindess et al., 1987] and changing the failure mode [Li and Leung, 1992].

2.2.1 Structure of Fiber Reinforced Cementitious Materials

The properties of FRCC depends on the characteristics of its three main components, as follows:

1. Bulk cementitious matrix which can be either concrete, mortar, or paste

2. Fibers that exhibit wide range of mechanical, physical, and chemical properties. Fibers can be either in the form of monofilaments or bundles. They can be divided into continuous and discrete fibers.
3. Fiber-matrix interface, known as interfacial transition zone (ITZ), has a different microstructure compared to bulk material. It is usually rich in calcium hydroxide (CH), and contains more pores due to bleeding and inefficient packing around the fiber surface. The structure of the ITZ is governed by various factors including type of fiber and nature of the matrix. ITZs affect FRCC behavior in different ways by controlling fiber-matrix bond and debonding processes.

2.2.2 Fiber-Cement Interactions

The performance of fibers in a brittle cementitious matrix is highly dependent on the interactions between fiber and matrix. Three main interactions can be recognized:

1. Physical and chemical adhesion
2. Friction
3. Mechanical anchorage

In the case of cementitious composites with added microfibers, friction and adhesion make significant contributions to bond development between fiber and cement. In conventional fiber reinforced composites, where fibers with bigger diameter and lower surface area are employed, the contribution of adhesive and frictional bonding is not enough, thus, mechanical anchoring is required.

In cementitious composites, fiber-cement interactions and stress-transfer effects must be addressed separately at pre-cracking and post-cracking stages. In the pre-cracking stage, elastic shear stress transfer is the main contributing mechanism and displacements of the fiber and matrix at the interface are geometrically compatible [Bentur and Mindess, 2007]. Further loading causes debonding across the interface. At this stage, frictional slip controls the process of stress transfer. This shear frictional stress is assumed to be uniformly distributed along the ITZ. This process is most important for post-cracking behavior of the composite and affects its ultimate strength and strain capacity as well as mode of failure. The transition between adhesive and frictional stress transfer occurs when the interfacial shear stresses exceed the fiber-matrix shear strength, or the adhesive shear bond strength (τ_{au}). The maximum frictional shear strength during pull-out process is called τ_{fu}. In practice, τ_{fu} may have slip softening or slip hardening behavior based on the nature of the interaction. Figure 2.7 shows a view of a partially debonded fiber and the ideal interfacial shear stress-displacement curve.

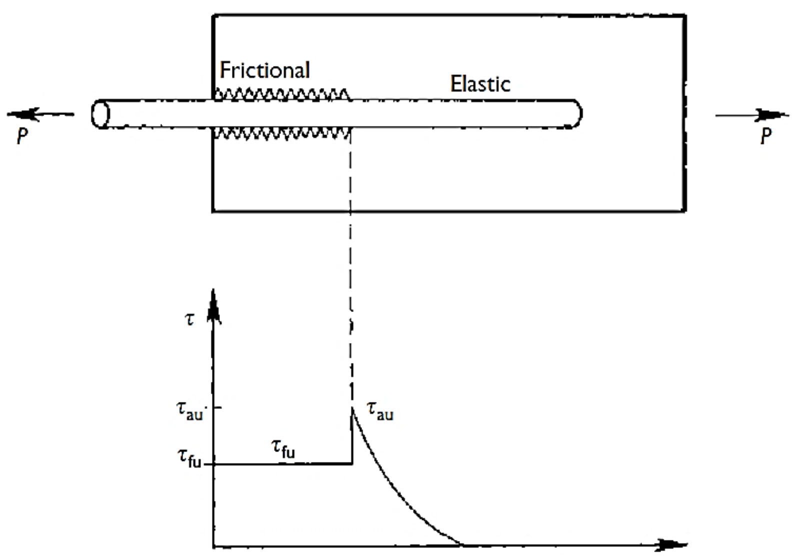

Figure 2.7: Partially debonded fiber configuration and the ideal interfacial shear stress-displacement curve [Bentur and Mindess, 2007]

The sequence of debonding and matrix cracking is controlled by the adhesive shear bond strength between fiber and matrix, and tensile strength of the matrix. If debonding occurs before cracking, the shear stress distribution will be of a combined mode, with frictional shear close to the crack tip and elastic shear elsewhere. If cracking happens before debonding, the stress distribution will be elastic followed by shear lag (Figure 2.8).

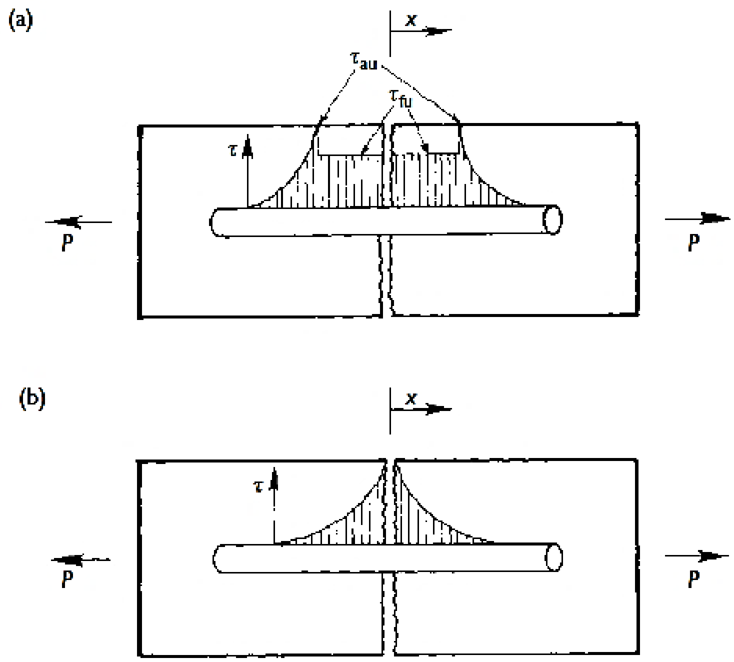

Figure 2.8: Interfacial shear stress distribution along a fiber a) debonding prior to cracking b) cracking before debonding [Bentur and Mindess, 2007]

2.2.3 Governing Factors for Overall Response FRCC

Overall response of FRCC to load can be characterized by the curve of the stress across a crack (σ) versus crack opening (δ). This stress-strain response is dependent on various factors including matrix composition, fiber content, type of fiber, bond-slip parameters, fiber geometry, proper mixing and homogenous spread of fibers, etc. It is quite important to understand the way these factors affect overall behavior of FRCC. In this section, some of the most important governing factors are discussed.

2.2.3 (a) Fiber Type

In terms of fiber material, carbon, glass, polymeric (synthetic), natural, and steel are among the most commonly used in FRCC, as mentioned above. These types of fibers have different elastic modulus, tensile strength, surface texture, strain capacity, and wettability values. These properties can affect the bond between fibers and the matrix, their ability to restrain cracks, and the overall response of FRCC [Li, 2011].

Steel fiber is the most common fiber used in FRCC with high elastic modulus and high tensile strength. Its high specific gravity, however, can induce extra dead load. Glass fiber is also commonly employed in FRCC, it has high tensile strength but low modulus of elasticity. Some glass fibers suffer from low durability due to their high vulnerability in alkaline environments. Their other shortcomings include low resistance to moisture, sustained and cyclic loads [Li, 2011]. Another popular fiber for FRCC is carbon fiber. Their high strength and high stiffness are some of the main advantages of carbon fibers, however they have low impact resistance, low ultimate strength and they are also expensive. Polymer fibers are increasingly used for the reinforcement of cementitious materials. The properties of synthetic fibers vary widely based on the strength and modulus of elasticity. Generally, they can be divided into low modulus and high modulus fibers. However, fibers in the same family can exhibit different characteristics such as ease of dispersion and alkali resistivity. Finally, natural fibers are the most widely available type of fibers in the world. They are inexpensive compared to other fibers, but they are sensitive to moisture. Such sensitivity to moisture can cause extra strain, affect the matrix-fiber bond, and influence mechanical properties. The hygroscopic nature of natural fibers can also have negative effect on their durability and long-term performance. Nevertheless, they are a good option for the production of low-cost cement composites and low-cost housing applications [Bentur and Mindess, 2007].

2.2.3 (b) Fiber Volume Fraction (V_f)

The volume fraction of fiber in FRCC has a remarkable effect on its mechanical properties, crack mitigation, and failure mode. FRCC can be classified based on their fiber volume fractions (Figure 2.9). Mix designs with low fiber volume fractions ($V_f < 1\%$), where fibers contribute to reducing cracks and improving mechanical properties to some extent. FRCC with moderate fiber volume fractions ($1\% < V_f < 2\%$), which exhibit more significant enhancement of mechanical properties and crack width control. A third group, known as high performance fibre reinforced concrete (HPFRC), has high volume fiber content ($2\% < V_f$). HPFRC is known for its apparent strain-hardening behavior, as well as very high cracking strength. However, it suffers from higher brittleness and lower ultimate strain capacity [Balagaru and Shah, 1992].

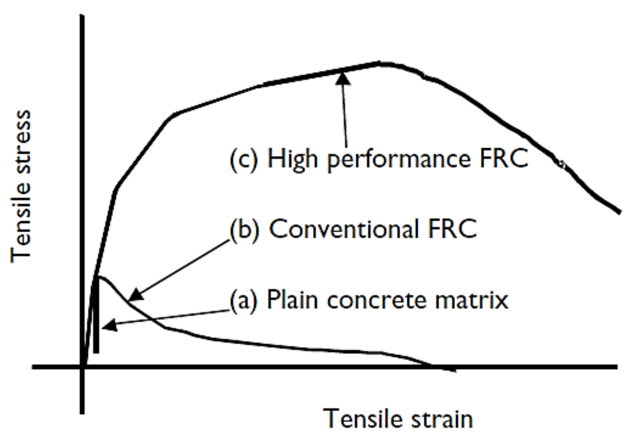

Figure 2.9: Typical stress-strain curve for plain concrete, FRC, and HPFRC [Bentur and Mindess, 2007]

The other important concept regarding fiber volume fraction, is the critical fiber content ($V_{f.critical}$). The overall contribution of fibers is assumed to be the integration of the contribution of all the fibers. However, the crack propagation mechanism will change as all fibers act together. Higher fiber contents might adversely affect homogenous dispersion of fibers in concrete. Hence, the concept of critical fiber content is necessary to classify the behaviour of fiber reinforced cementitious composites. The following categories have been identified:

1. $\boldsymbol{V_f < V_{f.critical}}$ → Brittle Behaviour

Due to small amount of fibers, failure is still governed by a single crack propagation in which load-displacement curve exhibits strain-softening behavior. Figure 2.8 b demonstrates stress-strain curve of cementitious composite with $V_f < V_{f.critical}$. Hence, the overall strength and strain capacity are governed by the elastic behavior corresponding to pre-crack region [Bentur and Mindess, 2007].

2. $\boldsymbol{V_{f.critical} < V_f \ll V_{f.ultimate}}$ → Tension Softening Behaviour

In this case, fiber content is more than the critical value but much less than ultimate one ($V_{f.ultimate}$). $V_{f.ultimate}$ can be considered as a representative value showing maximum amount of fiber content beyond which dispersion problems arise. Added fibers will noticeably contribute to strength improvement. They also help improve post-cracking toughness. This toughness is due to post-cracking deformations and multiple cracking, which is governed by various factors including type of fiber, fiber geometry, etc. The fracture mode occurring in this range of fiber volume can be characterized by the formation of multiple cracks. After crack nucleation, large volumes of fibers act as load carrying elements. This additional loading capacity leads to further cracking of the matrix, which still does not lead to failure of the system (Figure 2.10 a). The result is multiple crack failure rather than single crack failure as in case 1.

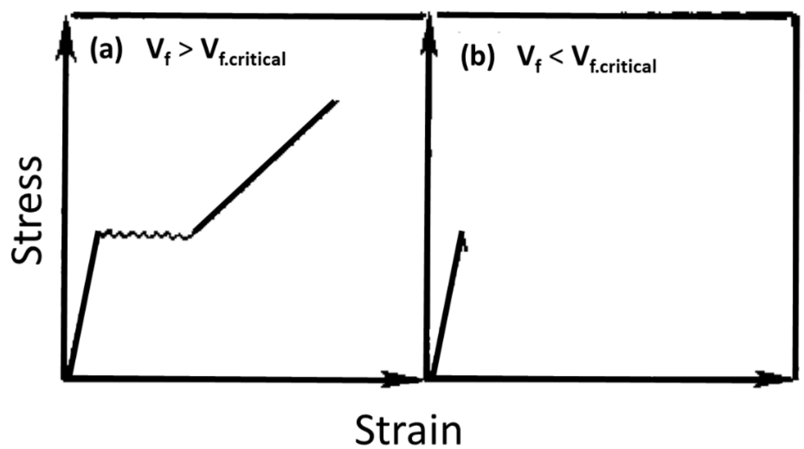

Figure 2.10: Schematic representation of the stress versus strain curves for V_f more and less then $V_{f.critical}$ [Bentur and Mindess, 2007]

3. $\boldsymbol{V_{f.critical} << V_f < V_{f.ultimate}}$ → Strain Hardening Behaviour

In this case, fiber content is still between critical and ultimate values, however, it is much closer to the ultimate value rather than the critical value (case 2). This type of fiber reinforced concrete tends to exhibit strain hardening behavior. It also has higher ultimate strength, energy absorption, toughness, and ductility. In this case, as fiber fracture does not occur, a great amount of energy will be consumed through fiber debonding and pullout. Figure 2.11 compares stress-strain curves of tension softening (case 1) versus strain hardening (case 2) composites. While in conventional FRC (case 1) post-cracking load bearing capacity dwindles, higher performance fiber reinforced concrete (HPFRC) demonstrates an increasing trend of post-cracking. This might be a result of microcracks stabilizing due to the interaction between the matrix and fibers which can postpone the formation of the first major crack in the matrix [Li, 2011]. This can also change the failure mode of FRC from quasi-brittle to ductile.

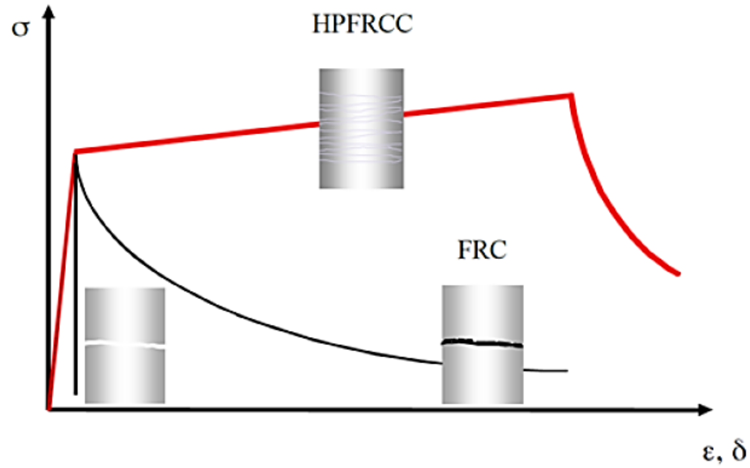

Figure 2.11: Schematic representation of the stress versus strain curves for FRC and HPFRC [Li, 2007]

4. $\boldsymbol{V_{f.ultimate} < V_f}$ $\rightarrow$ unworkable mix design with lack of homogenous fiber dispersion

Increasing fiber content is not always beneficial. Very high fiber content causes dispersion problems. It can also dramatically decrease workability of the fiber matrix mix. The maximum fiber content depends on the properties of mix design (such as gradation of aggregates and water/cement ratio) and the characteristics of fibers including geometry and water absorption capacity. Such an increase in fiber content not only adversely affects properties of wet concrete, but also worsens the mechanical properties of hardened concrete. [Bentur and Mindess, 2007].

2.2.3 (c) Fiber Length

The impact of fiber length on properties can be evaluated in terms of stress transfer mechanisms. The critical length, L_c, is the minimum fiber length required for formation of stress equal to its failure load. The value for critical length depends on stress transfer mechanisms. For $L < L_c$, the embedded length of the fiber is not sufficient to build-up a stress equal to the fiber strength, so fiber is not utilized efficiently (Figure 2.12). For the fiber to reach its tensile strength along a greater portion of its length, the length should exceed L_c.

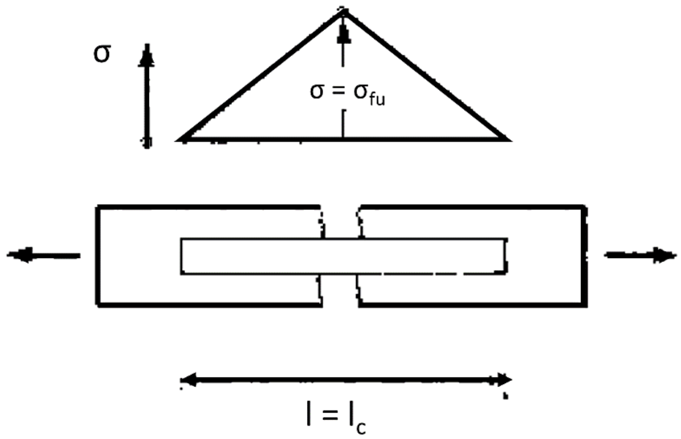

Figure 2.12: Stress distribution along the fiber [Bentur and Mindess, 2007]

2.2.3 (d) Fiber Orientation

In most of cases, fibers are not perpendicularly aligned to the crack surface. Two scenarios might occur in this case: 1. Fibers which are uniform along their length, and 2. Fibers with local bending at the crack surface (Figure 2.13). Case 1 mostly corresponds to the pre-cracking stage, while case 2 occurs post-cracking. Various studies show that efficiency and load bearing capacity of obliquely oriented fibers relative to a similar volume of perpendicular fibers are much lower in both pre-cracking and post-cracking stages [Krenchel, 1964].

Moreover, the local bending in the fiber around the crack (case 2) creates flexural stresses in the fiber and compressive stresses in the matrix. In the case of ductile fibers with low modulus, they will easily bend, and dowel action helps with additional pull-out resistance. In the case of brittle fibers with higher modulus, however, extra local flexural stresses are induced in the fiber, that are superimposed on the axial tensile stress. This can cause premature failure of the fiber and lower efficiency [Leung and Chi, 1995].

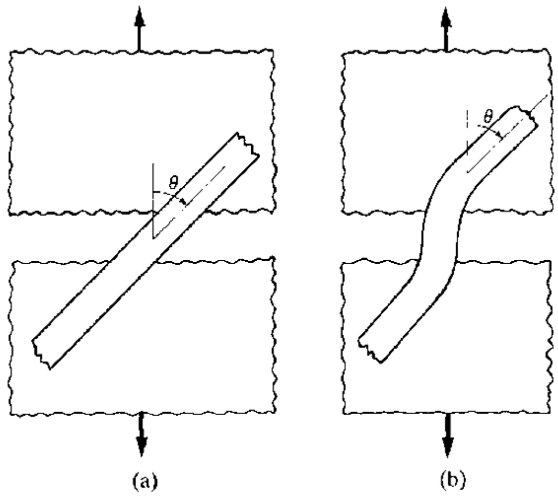

Figure 2.13: Fiber-crack intersection a) constant fiber orientation b) fiber with local bending [Bentur and Mindess, 2007]

2.2.3 (e) Fiber Coating and Surface Modification

Surface coatings can be employed to modify fiber-cement interaction and bond-slip behavior. Various studies have been carried out on the effects of coatings on pull-out behavior of fibers. Figure 2.14 demonstrates the effect of applying surface coating on Polyvinyl-alcohol (PVA) fibers in engineered cementitious composite (ECC). While untreated hydrophilic PVA fiber demonstrates high chemical and frictional bond with cementitious material, using a surface coating allows slippage to occur and improved tensile strain hardening response can be achieved [Li, 2003].

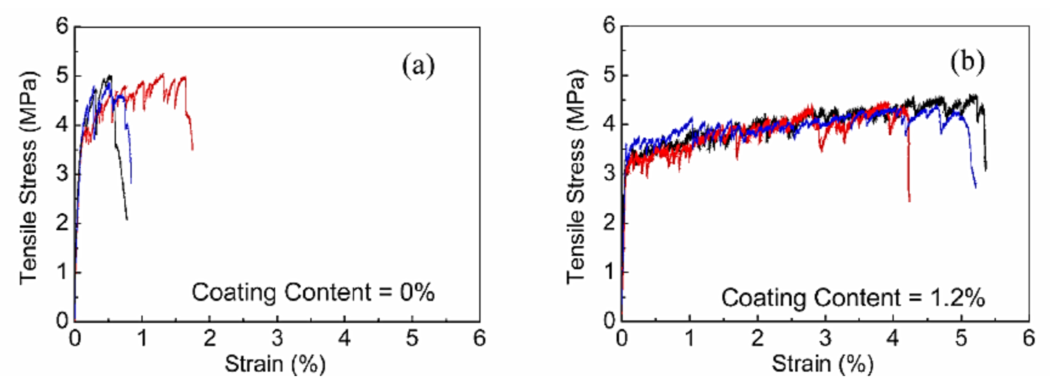

Figure 2.14: Effect of surface coating on tensile response of ECC [Li, 2003]

2.2.3 (f) Bulk Cementitious Matrix

The properties of the cementitious matrix can also influence the fiber-matrix ITZ and fiber bond-slip behavior. For example, aggregate properties such as angularity and gradation, chemical composition, and supplementary cementing materials (SCMs) affect the bond interface properties between fibers and matrix [Soleimani-Dashtaki, 2018]. Silica fume, a commonly used SCM, reacts with calcium hydroxide (CH) to convert it into calcium silicate hydrate (CSH). This leads to reduced average pore size and thinner interfacial transition zone, which improves the bond-slip behavior of the fibers. Silica fume can also act as a filler material and densifies cementitious binder. Fly ash, which is another highly used SCM, has high pozzolanic capacity and can improve matrix and ITZ properties. Due it its spherical shaped particles, fly ash also improves workability of the material helping with homogenous dispersion of fibers within bulk matrix leading to improved overall behavior of FRCC [Mindess et al., 2003].

2.2.4 FRCC as a Repair Material

Interfacial properties are critical to achieving strong and durable repairs. Interfacial bond strength is a property quantifying short-term behavior and strength of the material. Interfacial fracture toughness, on the other hand, is an interface property able to predict cracking and long-term behavior of repaired systems. The effect of adding fiber to the repair material on the overall behavior of repaired cementitious composites has been the subject of various research studies [Banthia and Dubeau, 1994; Wagner et al. 2013]. It has been shown that FRCC can be a promising repair option [Zanotti et al., 2018]. In repaired structures with FRCC repair layers, the extent of interfacial damage due to poor compatibility between two layers is reduced [Banthia and Gupta, 2006]. Moreover, fiber reinforcement can be helpful in improving the interfacial bond between substrate and repair layers, and with interfacial fracture behavior.

The quality of concrete-FRC bond depends on frictional/interlocking forces and cohesive/adhesive bonding [Zanotti and Randl, 2018]. In the case of tensile loading regime, cohesive/adhesive bonding plays the major role in the overall mechanical response of the material. Using FRC as repair material help to improve interfacial bonding by enhancing quality of the interfacial transition zone [Banthia and Dubeau, 1994; Lim and Li, 1997] . Fibers are able to decrease relative movements, mitigate ITZ damage prior and during loading, and to provide further interfacial bonding mechanisms which help with the enhancement of interfacial bond and crack growth resistance [Wagner et al., 2013; Zanotti et al., 2018].

The other governing factor of an effective and durable concrete repair is compatibility of repair and substrate. Repair of any concrete structure results in formation of a complex two-component system. Compatibility is considered as a basic requirement for a repair material [Garbacz et al., 2014]. Having very incompatible repair and substrate layers, increases vulnerability of composite structure to interfacial stress concentration and failure. One of the major benefits of using FRC as repair material, is improving compatibility or, at least, decreasing the intensity of incompatibility-induced damages [Banthia et al., 2014].

Two failure modes in composite structures can be identified in repaired composites, namely adhesive (delamination) and cohesive-adhesive modes. In the former case, the failure plane passes through the bond plane and interfacial cracks do not enter the substrate or the repair layer. In the latter case, however, some microcracks might kink-out and get diverted into the repair layer activating fiber-related toughening and strengthening mechanisms. This is called the trapping mechanism. This significantly increases the effectiveness of FRCC as a repair layer.

2.2.4.1 Trapping Mechanism in Repaired Cementitious Composites

Any rehabilitated system consists of an old layer (substrate), a new repair layer, and an interface between these two layers. Early nucleation of cracks can occur anywhere in this bi-material system, however, occurrence of cracks at the interface is usually due to the weakness of the bond plane compared to other parts of the system. Hence, a crack can either extend along the interface or kink into one of the adjoining materials. This competition is governed by the relatedness of the ratio of the energy release rate of the interface cracking (G) to kinked cracking (G^t) versus ratio of the interface toughness (Γ) to the toughness of repair/substrate layers (Γ_c) [He et al., 1991]. If the relative toughness of a system is greater than the relative driving force, interface cracks kink out from the interface. If the relative toughness is less than the relative driving force, no kinking can occur. The interface crack condition is as follows:

$$\frac{G}{G_{max}^{t}} < \frac{\Gamma}{\Gamma_c} \qquad 2.1$$

Interfacial crack propagation causes more brittle failure as there is no bridging interlocking along the interface. However, when cracks kink out from the interface, two different cracking behaviors can occur. If the repair material is brittle, a crack will not be stopped in the repair layer and surface spalling occurs. If the repair material exhibits rising fracture resistance, however, the kinked crack will be trapped (Figure 2.15).

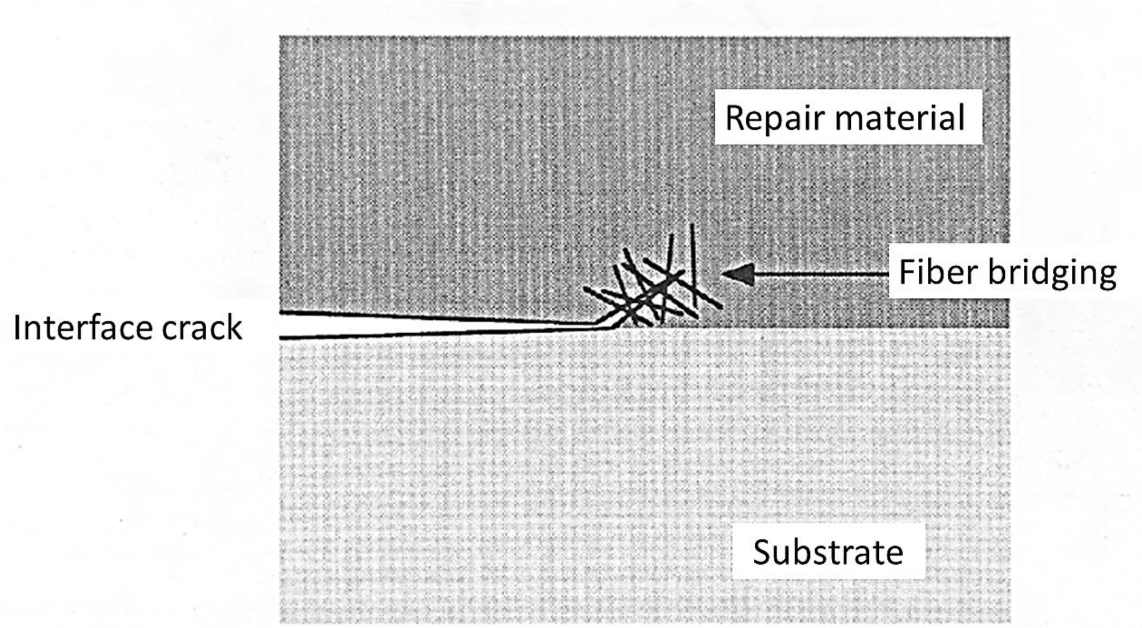

Figure 2.15: Fiber bridging and trapping mechanism for a kinked crack [Lim and Li, 1997]

After trapping the first kinked crack, further loading fosters the mother crack to propagate along the interface. Escaping from the first damage zone, relative toughness increases once again and the crack kinks out from the interface. This sequence of kinking, damaging, trapping, and interfacial propagation is responsible for a large amount of energy absorption and will continue up to failure [Lim and Li, 1997]. Figure 2.16 represents the conceptual trapping mechanism with load-displacement curve of repaired system.

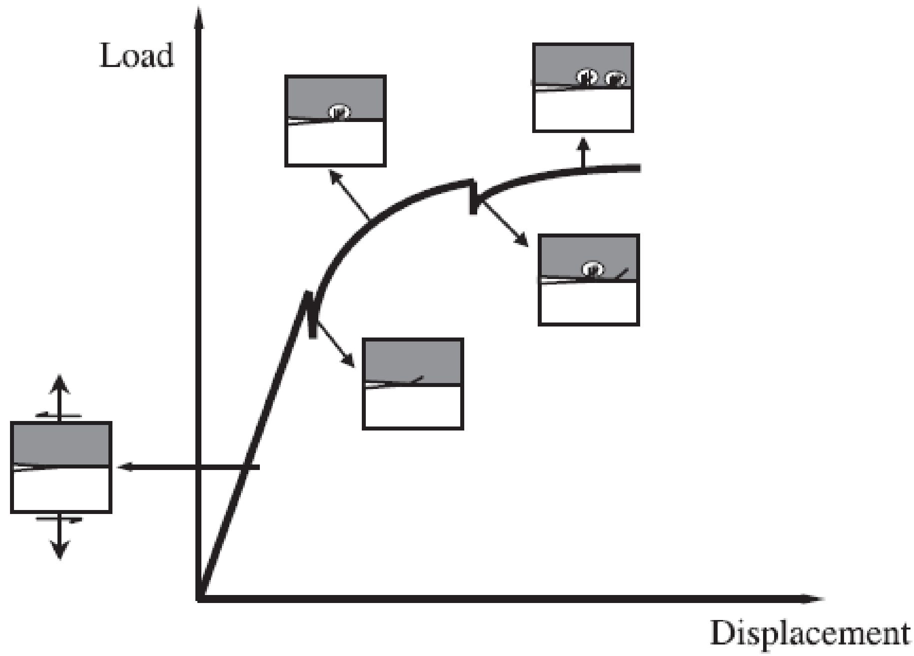

Figure 2.16: The conceptual trapping mechanism and load-displacement curve of a repaired system [Kamada and Li, 2000]

2.3 Introduction to Fracture Mechanics of Concrete

Fracture mechanics is a division of solid mechanics dealing with the behavior of a material and the quality of the region close to the crack and at the crack tip. It is concerned with the study of stress and displacement fields in the material adjacent to a crack. As there are many sources of microcracking within cement-based materials, the stress-strain behavior and the failure mode are governed by microcrack propagation. As a result, it is vital to understand fracture mechanisms to predict concrete behavior.

The study of fracture mechanics was triggered by the difference between the theoretical prediction of a material's strength, and its performance in the real world [Maiti, 2015]. This inequality is attributed to the pre-existing flaws inside a material capable of inducing stress concentrations and nonhomogeneous stress distributions. This stress concentration causes intensified stresses leading to local failure prior to reaching theoretical strength.

In fracture mechanics, materials are divided into brittle materials, quasi-brittle materials, and ductile materials, as is seen in the relevant tensile stress-strain curves. Brittle materials exhibit a sudden failure as soon as reaching the maximum stress. Quasi-brittle materials show a strain-softening behavior where stress diminishes with stress increase. Finally, ductile materials have a long, plastic plateau after failure (Figure 2.17).

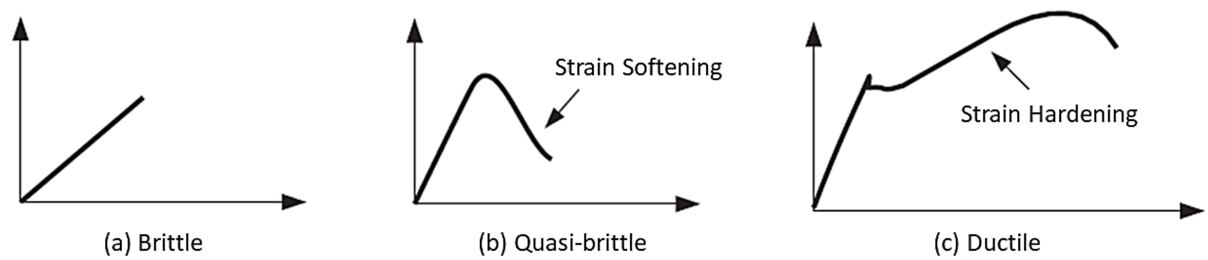

Figure 2.17: Three failure modes of materials [Li, 2011]

Linear elastic fracture mechanics (LEFM) theory was developed in 1920 by Griffith [1920]. Griffith observed a difference between the impacts of tiny imperfections versus large flaws on material properties. He suggested a novel energy-based criterion based on crack size. Using a compliance concept, Griffith showed that an instability criterion for cracks in brittle materials could be achieved by the variation of potential energy of the material. Griffith's theory was mainly applicable to highly brittle materials, specifically glasses and ceramics.

The other LEFM approach, known as stress based LEFM, was introduced by Inglis [1913]. Later, Irwin proposed the concept of the stress intensity factor and the critical stress intensity factor (K_{IC}). The idea behind LEFM is that crack propagation can be identified with only the value of the stress intensity factor (SIF) adjacent to the crack tip. However, cementitious materials, rocks, and fiber reinforced composites, known as quasi-brittle materials, need a different approach in fracture mechanics approach to model their fracture behavior.

In LEFM, stress values close to the crack tip are determined as a function of stress intensity factor (SIF) and can reach infinity. As this is not plausible in a real material, researchers suggested modelling an inelastic zone close to the crack tip. This idea led to the concept of nonlinear fracture mechanics, which mainly focuses on the determination of the size of the plastic zone adjacent to a crack tip. Some early research measured the size of the plastic zone and plastic zone correction [Irwin 1958, 1960], cohesive zone model [Dugdale 1960], and J-integral method [Rice 1968]. The results of these studies showed that there is a plastic zone in front of a crack tip. In materials with small plastic zones, LEFM remains applicable.

Concrete consists of various ingredients such as cement, fine and coarse aggregates, water, and admixtures. In addition, there are many voids inside the matrix including pores in hydrated cement and cracks at matrix-aggregate interface. These defects have a significant impact on the behavior of concrete. They aid the nucleation of microcracks close to the tip of a macro-crack, followed by a progressive failure due to further propagation of cracks. Concrete shows sub-critical crack growth prior to unstable crack propagation which is known as the slow crack growth region. Various experimental and numerical studies have shown that due to the large fracture process zone, the classical form of linear elastic fracture mechanics is not applicable to normal size concrete members.

Fracture mechanics was first applied to concrete by Kaplan [1961]. He tried to determine the applicability of Griffith crack theory to rapid crack growth and fracture of concrete. Due to the large fracture process zone in concrete, Kaplan [1961] concluded that LEFM could not be directly applied to concrete. In other words, in order to understand the fracture behavior of concrete, modified fracture mechanics approaches were required.

Hillerborg et al. [1976] proposed a fictitious crack model based on the cohesive crack model [Dugdale 1960, Barenblatt 1962]. Some other nonlinear approaches are the crack band model, based on the concept of strain softening [Bažant and Oh 1983], the two-parameter fracture model i.e. critical stress intensity factor at the tip of the effective crack and the elastic critical opening displacement [Jenq and Shah 1985], the size-effect model [Bažant 1984, Bažant et al. 1986], the effective crack model [Nallathambi and Karihaloo 1986], the K_R-curve method based on cohesive force [Xu and Reinhardt 1998, 1990], the double-K fracture model [Xu and Reinhardt 1999], and the double-G fracture model [Xu and Zhang 2008].

The science of concrete structure design has already gone through two main phases. The first one was based on elastic no-tension analysis and the second one was concerned with the plastic limit theory. Many researchers now believe that the third phase of this evolution might be based on the design of concrete structures governed by fracture mechanics parameters [Kumar and Barai 2011].

2.3.1 Linear Elastic Fracture Mechanics (LEFM)

The aim of linear elastic fracture mechanics is to investigate the stress and deformation distributions close to the crack tip of brittle materials by means of a single fracture parameter. There are two different approaches in LEFM: Stress-based and energy-based. In the former, fracture is determined by the stress intensity factor while in the energy-based approach, the surface energy release rate is the index of fracture.

Stress-based LEFM

Stress concentration factor

Defects influence stress distribution in materials and alter their mechanical properties. The presence of a crack in the plate changes the stress distribution in the adjacent area and favors a maximum stress (σ_{max}) formed at the edge of the hole (Figure 2.18). σ_{max} is significantly greater than the normal stress σ_N. This is known as the stress concentration.

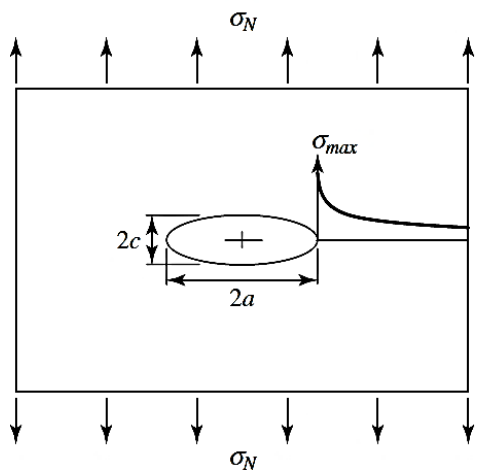

Figure 2.18: A specimen with an elliptical hole under tensile loading [Li, 2011]

The stress concentration factor, K_t, is a function of the shape of the hole and the loading pattern. In case of a very narrow ellipse or a sharp crack, K_t approaches infinity. Considering that this is not possible in the real world, the concentration factor is not applicable to a material containing a sharp crack. In this case, fracture mechanics needs to be considered.

$$K_t = \frac{\sigma_{max}}{\sigma_N} = 1 + \frac{2a}{c} \qquad 2.2$$

where a and c are the long and short radii of the ellipse.

Stress intensity factor

In fracture mechanics, cracks can be divided into three different modes, i.e. mode I (opening mode), mode II (sliding mode), and mode III (tearing mode). Figure 2.19 represents various cracking modes. Stress intensity factor, K_I, is based on specimen geometry and loading pattern.

$$K_I = \sigma\sqrt{\Pi a f(\frac{a}{b})} \tag{2.3}$$

where σ is the normal stress on the structure, a the crack length, b the size of the structure, and f (a/b) the geometry factor.

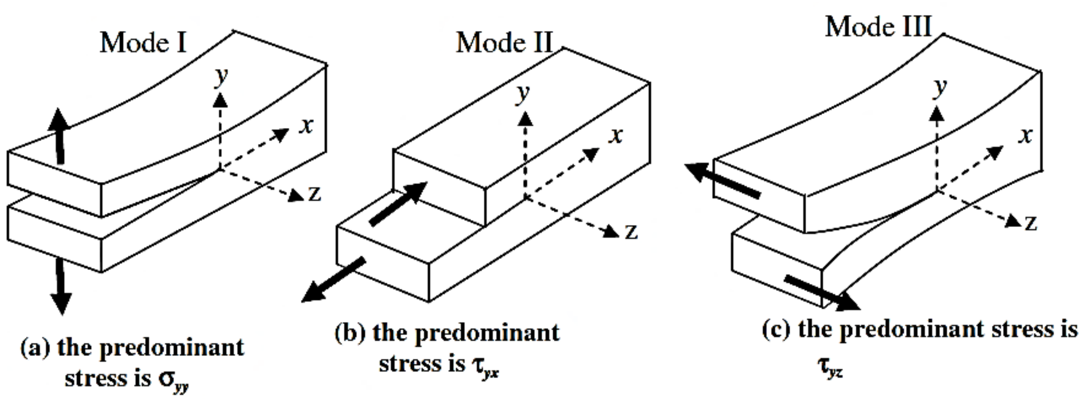

Figure 2.19: Cracking modes: a) mode I (opening mode), b) mode II (sliding mode), c) mode III (tearing mode) [Kumar and Barai 2011]

Both stress concentration factor, K_t, and stress intensity factor, K_I, can be used to determine the increase of stresses resulting from the presence of a defect. In the case of a sharp crack, K_I has a limiting value while K_t reaches infinity. The value of K_I represents the singularity of the stress field in the crack tip, which is governed by geometry, loading patterns, size, boundary conditions, and crack length.

Linear elastic fracture mechanics uses the stress intensity factor at the crack tip to determine crack behavior. The stress intensity factor, also called fracture toughness, is a very important concept in fracture mechanics. A crack propagates as soon as the critical fracture toughness of the material is reached.

$$K_I = K_{Ic} \tag{2.4}$$

where K_{Ic} is the critical stress intensity factor. K_{Ic} is the material fracture parameter in linear elastic fracture mechanics.

Energy-based LEFM

Crack development can also be explained by an energy-based criterion that was first developed by Griffith [1921]. This energy-based fracture criterion is based on an equilibrium state of a cracked structure. The total potential energy in the structure is as follows:

$$\Pi = U - F + W \tag{2.5}$$

where U is the strain energy of the structure, which is governed by crack length and strain, F is the work done by the external load, and W is the energy for crack nucleation. To maintain equilibrium state, the first-order derivative of total potential energy needs to equal zero during small crack extension. The strain energy release rate, G, for the propagation of a unit length of a crack in a structure with unit thickness is defined as:

$$G = \frac{1}{B}\,\frac{\delta}{\delta_a}(F - U) \tag{2.6}$$

Since G provides the energy for a crack growth, it is also known as the crack-driving force. The value of G can be determined using a load-displacement curve. F is a function of the applied load, structural geometry, and boundary conditions. As soon as G reaches the critical strain energy release rate, G_c, the initial crack propagates and causes failure of a linear elastic material. The critical strain energy release rate, $G_{c.}$ is a material constant for linearly elastic materials.

There exists a relationship between G and K for a linearly elastic material as follows [Maiti, 2015]:

$$G_I = \frac{K_I^2}{E} \qquad \text{(plane stress condition) 2.7}$$

$$G_I = \frac{K_I^2}{(1-\nu^2)E} \qquad \text{(plane strain condition) 2.8}$$

where G_I is strain energy release rate (J/m^2), K_I is stress intensity factor (MPa.mm$^{0.5}$), E is elastic modulus (GPa), and ν is Poisson's ratio (-).

2.3.2 Nonlinear Fracture Mechanics

Fracture behavior of concrete is strongly governed by the fracture process zone. LEFM is not directly applicable to concrete due to its large fracture process zone, aggregate bridging, and crack deviation. The nonlinear fracture models are based on two different approaches:

1. Using finite element or boundary element method: fictitious, cohesive, and crack band models fall within this group.

2. Using adaptations of LEFM concept: examples are the two-parameter fracture model, size-effect model, and effective crack model.

Cohesive Crack Model (CCM) or Fictitious Crack Model (FCM)

The cohesive crack model was first introduced by Barenblatt [1962] and Dugdale [1960]. Barenblatt applied CCM to brittle materials while Dugdale used it to model ductile fracture behavior. Hillerborg et al. [1976] applied the cohesive crack method (or fictitious crack model) to study the fracture of concrete structures. Later, FCM was also extended to fiber reinforced concrete [Hillerborg et al. 1980].

Fictitious crack model was based on the assumption of strain localization and the softening curve of the cohesive stress vs. crack width. In this model, the elastic section of the stress – deformation curve is disregarded, and the post-peak response is identified by a stress – deformation curve. Three material properties including specific fracture energy G_F, uniaxial tensile strength f_t, and the shape of σ (w) are required for the fictitious crack model. G_F is the amount of energy required for creating one unit of crack length.

Determination of the σ (w) relationship

In order to describe the fictitious crack model, a unique σ (w) curve is needed. σ (w) function affects the structural response, the energy dissipation, and local fracture behavior. This relationship can follow a linear, bilinear, trilinear, exponential, or power function (Figure 2.20).

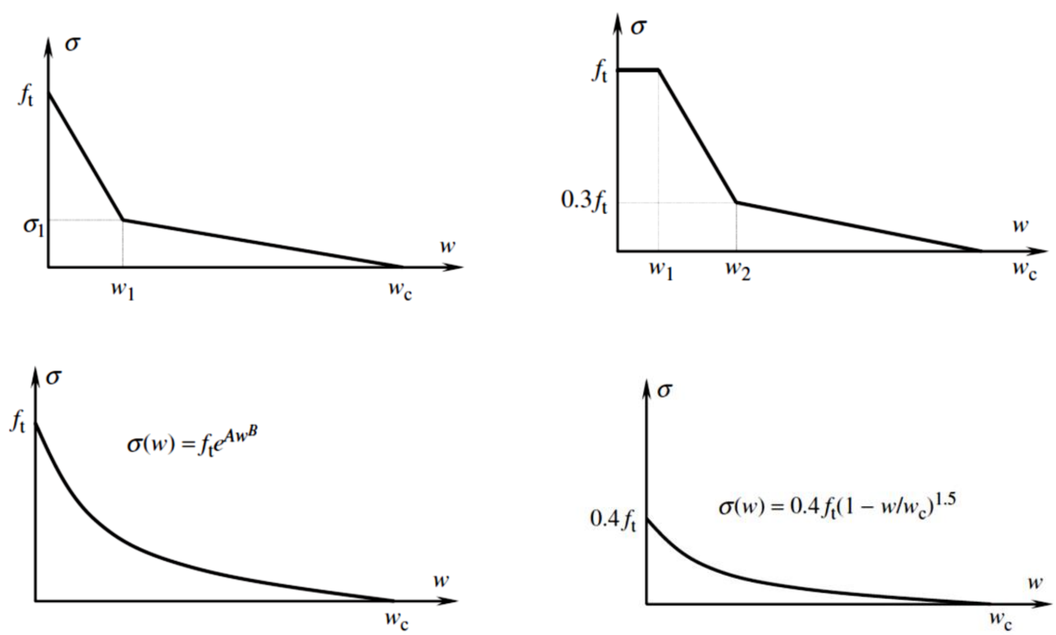

Figure 2.20: σ (w) curve modelling: a) Bilinear curve, b) Trilinear curve, c) Exponential curve, d) Power curve [Li 2011]

Determination of GF

Hillerborg [1985] suggested the use of a three-point bending beam test to measure G_F. Using this test, the area below the load – displacement curve is first quantified followed by a correction corresponding to the self-weight of the specimen.

$$G_F = \frac{W_o + 2W_s\delta_0}{A_{lig}} \qquad 2.9$$

where W_0 is the area below load –displacement curve, W_s is self weight of the beam, δ_o is the deformation at final failure, and A_{lig} area of the beam section.

Two-Parameter Fracture Model (TPFM)

The two-parameter fracture model proposed by Jenq and Shah [1985], uses the three-point bending test with notched-beams and is based on the concept of the effective elastic crack. The fracture properties of concrete are described by 1. Crack-tip opening displacement (CTOD) and 2. The critical stress intensity factor at the tip of the equivalent crack length at peak load (K_{IC}) (Figure 2.21).

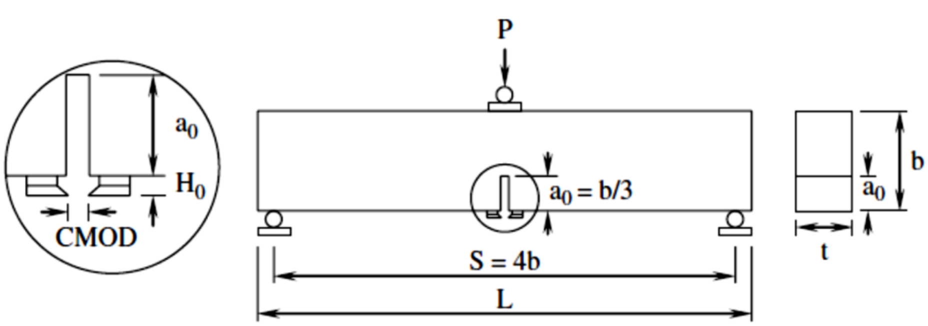

Figure 2.21: Three-point bending test setup for the two-parameter model [Li 2011]

The effective crack length is quantified by compliance measurements. By determining the initial compliance corresponding to the initial crack length (notch length), one can calculate the effective modulus of elasticity of the material. Using the effective modulus of elasticity and compliance at maximum load, the effective crack length can be obtained followed by determination of the critical stress intensity factor. It can be observed that after unloading from peak stress to zero stress, CMOD does not return to zero, showing that CMOD contains plastic deformation (Figure 2.22). However, when determining K_{IC} and CTOD parameters, the effective-elastic crack shows a compliance equal to the unloading compliance, which means that the plastic part of the total CMOD is disregarded and the critical fracture state is based on its elastic response; this may lead to an underestimation of effective crack length followed by overestimation of fracture toughness and material strength.

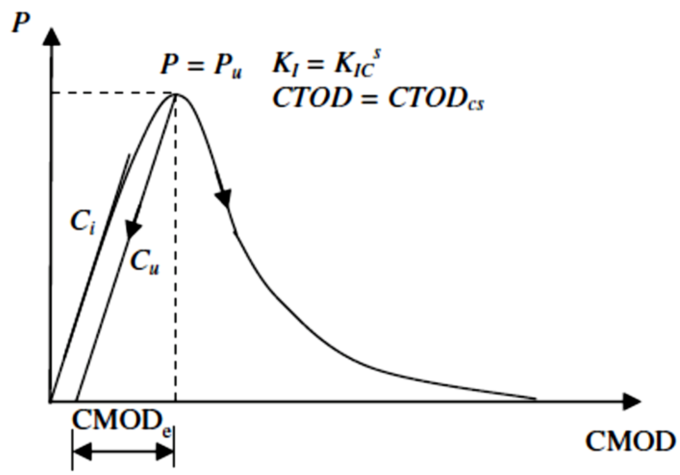

Figure 2.22: Typical load versus CMOD curve for TPFM [Kumar and Barai, 2011]

It was shown by Jenq and Shah [1985] that K_{IC} and $CTOD^e_c$ are constant for beams with different sizes made of the same material. Hence, they are material properties and can be used to predict the maximum load for a structure. The two-parameter fracture model has been extended to fiber reinforced concrete [Jenq and Shah, 1986]; the only difference is that load-slip relationship of fibers is required which can be obtained from pull-out tests on single fibers.

R-Curve Method

R-curve approach was first proposed in early 1960s based on energy balance [Krafft et al. 1961]. According to the concept of R-curve, crack propagation occurs when strain energy release rate (*G*) is equal to a material's resistance to crack extension (*R*). R-curves can be expressed in terms of either strain energy release rate (*G*), or stress intensity factor (*K*), vs. the corresponding crack extension, Δa.

Brittle and quasi-brittle materials exhibit different R-curve behaviors. Highly brittle materials have a flat R-curve where a single crack causes rapid failure. On the other hand, quasi-brittle materials have rising R curves as cracks go through slow stable extension (Figure 2.23). Ascending R-curve favors formation of several tiny cracks. In the case of cementitious materials, the crack initially grows, but will be hindered by the toughening mechanisms; this causes an increase in the required energy for crack extension.

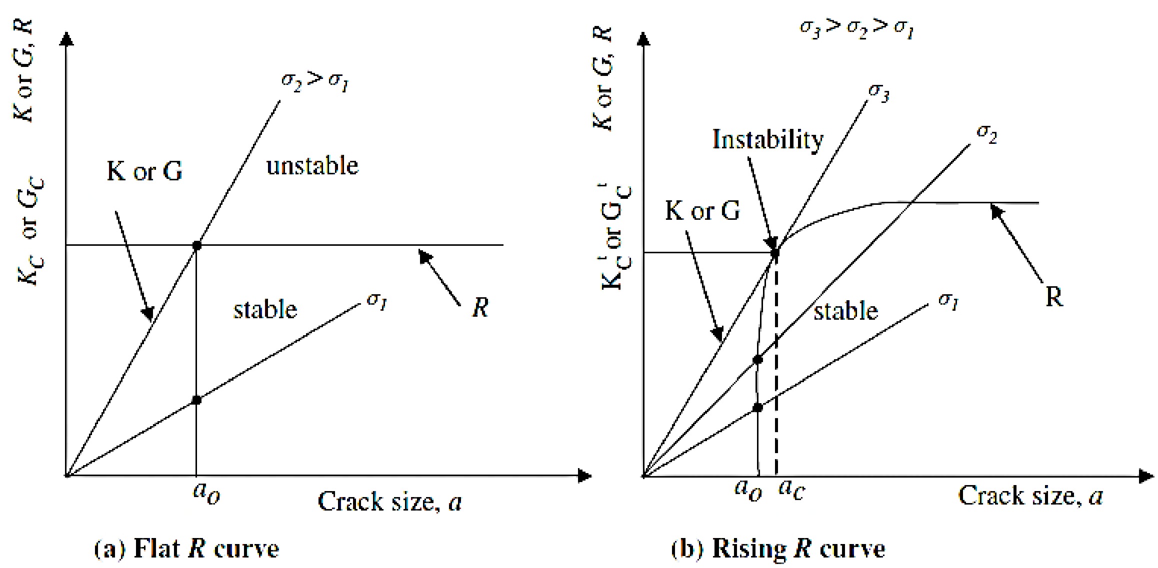

Figure 2.23: R-curves for different types of materials a) Brittle, b) Quasi-brittle [Kumar and Barai, 2011]

The R-curve for quasi-brittle materials represents the stable development of a process zone prior to critical state, known as the pre-critical or subcritical crack growth. Hence, linear elastic fracture mechanics (LEFM) is not applicable, except in the case of very small process zones.

Size Effect Model (SEM)

Nonlinear fracture of concrete and its nominal strength are affected by structural size. This might be due to the large and variable lengths of the fracture process zone (FPZ) at the crack tip. Strength criteria and LEFM size effect are at two extremes with respect to the size-effect law. The former disregards the size effect, while for the latter, nominal strength is inversely proportional to the square root of structural dimensions (Figure 2.24).

The size-effect law was proposed by Bažant [1984] to investigate fracture of quasi-brittle materials. In this approach, fracture behavior of any material is described by two parameters: the fracture energy (G) and the critical effective crack length (a_c) for an infinitely large test specimen. The fracture parameters are measured for geometrically similar notched specimens of various sizes. In the size effect model, the fracture energy is expected to be independent of specimen size and shape. This is due to the small size of the fracture process zone compared to specimen dimensions. The size-effect method is quite simple as the only required information for geometrically similar specimens is the maximum load values. Furthermore, there is no need for the post-peak softening response, crack length, and the use of a closed-loop test set-up.

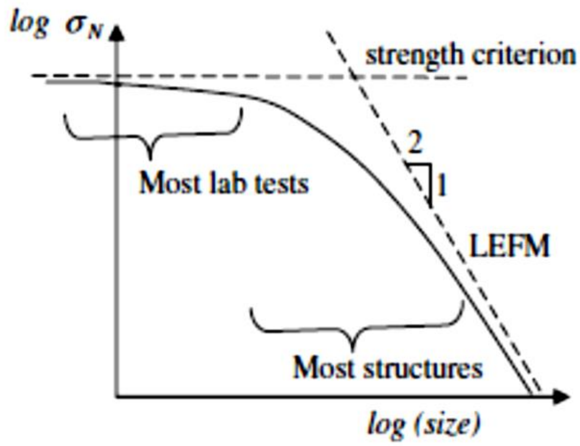

Figure 2.24: The size effect law versus the strength criterion and LEFM [Kumar and Barai, 2011]

Crack Band Model (CBM)

The crack band model (CBM) was developed by Bažant and Oh [1983]. Using this method, the fracture process zone is simulated as a system of parallel cracks that are continuously distributed (smeared) in the finite element (Figure 2.25). The width of the fracture process zone (h_c) is assumed to be constant. The behavior of the material is determined by the constitutive stress-strain relationship. The crack is modeled by modifying the isotropic elastic moduli to an orthotropic one where the stiffness in the direction normal to the cracking plane is reduced.

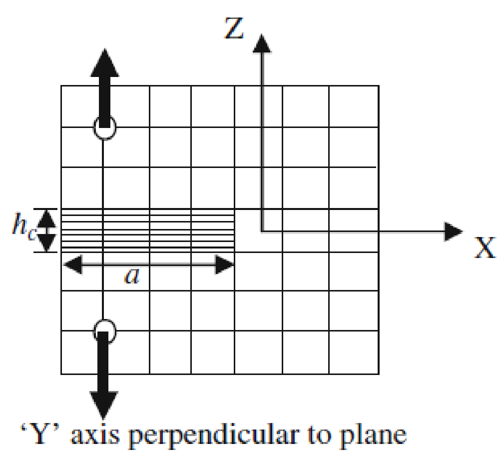

Figure 2.25: Crack band model in Cartesian coordinate system [Kumar and Barai, 2011]

The main drawbacks of CBM are as follows: 1. Special mathematical considerations are needed to investigate tortuous crack propagation; 2. Changes to cracking width and fracture energy cannot be addressed.

Effective Crack Model (ECM)

Effective crack model was introduced by Nallathambi and Karihaloo [1986] to assess critical crack extension. Using this method, the initial crack is substituted with a larger crack, known as the effective crack, in order to account for the impact of fracture process zone. In the effective crack model, fracture occurs when the stress intensity factor becomes critical, which happens at the critical crack extension. The effective crack extension can be determined by obtaining the midspan deflection from a standard three-point bending test using secant compliance.

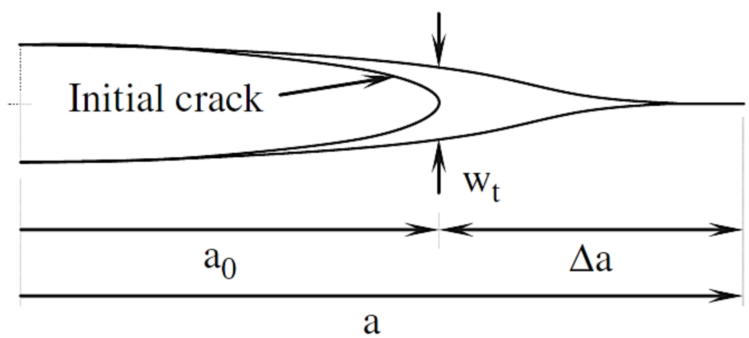

Figure 2.26: Representation of effective crack vs. initial crack [Li, 2011]

J-Integral Method

Rice [1968] proposed the concept of J-integral for investigating crack extension. The value of J-Integral is equal to the energy release rate in a nonlinear elastic cracked body. The critical value (J_c), which is considered as a material fracture parameter, indicates the initiation of a crack.

2.4 Modelling Interfacial Behavior of Cementitious Composite Systems

Different researchers have employed various approaches for modelling interfacial behavior of composite cementitious materials. These include algorithms to develop numerical models, employing specific theories to come up with analytical solutions, and running experimental tests to derive empirical expressions. Sometimes, two or three different approaches are used in a same study. In some cases, however, experimental and non-experimental results are not quite comparable due to various measuring errors occurring during the experiments, and lack of proper assumptions in numerical and analytical studies. This section reviews previous research on modelling interfacial behavior of cementitious composite systems under different loading regimes.

2.4.1 Numerical Models

Among numerical research studies, Qiao and Chen [2008] employed numerical simulation to evaluate cohesive fracture of fiber reinforced polymer (FRP)–concrete bonded interfaces. The interface cohesive process damage model was suggested as simulating the adhesive–concrete debonding, and tensile plastic damage model was used for cohesive cracking of concrete near the bond line. Concrete and FRP materials were simulated by plane stress elements and the interfaces were modelled by 2D cohesive elements. Moreover, the impact of various parameters including the interface cohesive strength, tensile strength of concrete, critical interfacial energy, and concrete fracture energy, on the modes of interfacial failure and load-bearing capacity was evaluated by means of parametric numerical finite element study [Qiao and Chen, 2008]. The behavior of concrete elements strengthened by sheets of carbon fiber reinforced polymer (CFRP) was investigated by Neto et al. [2004] employing the finite element (FE) method. The FE analysis was based on nonlinear fracture mechanics and discrete crack approach. The interface was modelled using linear elements with zero initial thickness. Required properties for numerical modelling were obtained through a parametric study on experimental data of pullout tests. The final numerical results fitted well with the experimental data.

Dias-Da-Costa and Julio [2012] developed a numerical model for the shear strength between two concrete layers. Various ratios of fiber reinforcement as well as the effect of elastic shear stiffness, internal friction angle, dilatancy angle, fracture energy, and bond-slip shape were investigated. Zero-thickness linear elements were inserted at the interface. Results from push-off tests were used for calibration purposes. Lampropoulos et al. [2016] used three-dimensional (3D) FE method for modelling the interfacial bond of ultra-high-performance concrete (UHPC)-concrete members with a well-roughened substrate under flexural loading. Special two-dimensional elements were employed to represent the rough interface between the original beam and the UHPC layer. The reliability of the proposed model was validated by experimentation. Another numerical study was done by Safdar et al. [2016]. They investigated the impact of tensile properties of ultra high-performance fiber reinforced concrete (UHPFRC) repair layer and yield strength of tension steel on the flexural response of repaired beams. Nonlinear FE method and 3D solid elements were employed. It was assumed that perfect bond develops at the interface of two layers. The assumption of a perfect bond was justified by applying a water jet to expose the aggregate in the concrete substrate which improved surface roughness and resulted in good bond strength between two layers. Post-cracking behavior of concrete substrate was modelled using discrete crack behavior, while for post-cracking behavior of UHPFRC, a fictitious crack model was employed. The results indicated that UHPFRC was able to improve stiffness and delay crack formation.

Sadouki et al. [2017] ran a two-dimensional (2D) FE simulation of composite UHPC–concrete beams and proposed a model for design prediction purposes for real repaired concrete infrastructure. The complicated cracking pattern of the composite system was numerically modelled using the nonlinear materials law and the smeared crack model in order to obtain more accurate prediction of the mechanical behavior. Their results were compatible with experimental data.

Al-Osta et al. [2017] employed nonlinear finite element and analytical models to predict the flexural behavior of reinforced concrete beams strengthened with ultra-high-performance fiber reinforced concrete. FE simulations were conducted assuming a perfect bond at the normal strength concrete (NSC)-UHPFRC interface which might result in the overestimation of failure load. A 3D finite element model of the beam specimens was employed and the nonlinear behavior of both concrete substrate and UHPFRC was modelled based on the Concrete Damage Plasticity Model (CDPM). Their results were in general agreement with experimental results and were able to anticipate the response of the composite beams with good accuracy. However, it was found that by increasing the volume of UHPFRC layer the accuracy of the FEM prediction decreased, which was attributed to the fibers' orientation and concentration.

Yin et al. [2019] used an improved finite element model to predict the structural behavior of reinforced concrete members with ultra high-performance concrete as a repair layer. The model was based on using equivalent beam elements at the interface between UHPC repair layer and NSC substrate. The model effectively and efficiently predicted the structural response of composite UHPC-NSC members.

2.4.2 Analytical Models

The other common approach for modelling interfacial behavior of composite systems is to use analytical models. Wu and Yoshizawa [1999] conducted analytical/experimental research on the behavior of composite reinforced concrete members strengthened with carbon fiber sheets. The impact of concrete strength, thickness of concrete layer, and various carbon FRP materials was studied. An analytical approach, based on fracture mechanics, was used to predict cracking deformation, and failure behavior of reinforced concrete–FRP composite systems and was adopted to predict behavior of carbon fiber sheet–reinforced concrete elements. The applicability of the proposed analytical method was compared with experimental data. Dai et al. [2006] published work on a unified analytical approach for determining shear bond characteristics of FRP-concrete interfaces based on pullout tests. A new nonlinear bond stress-slip model for analyzing shear bond distributions at the interface was developed. One of the main advantages of their proposed model was the incorporation of interfacial fracture energy and development of an interface ductility index, which could be obtained from pullout tests.

Building on the previous study, Zhou et al. [2010] developed a modified analytical model for the bond-slip relationship at concrete-FRP interfaces for adhesively-bonded joints. Their model is applicable to any externally bonded joint including joints externally bonded with steel mesh or plate and FRP. In their analytical model, the bond-slip relationship was derived from strain-slip responses that were measured at the loaded end from a pull-off test. Both finite and infinite bond lengths were evaluated. This stated that their analytical solution for concrete-FRC joints with an infinite bond length is not directly applicable to joints with a limited bond length. Shrestha et al. [2017] proposed bond-slip models for concrete-FRP interfaces under moisture exposure based on the analytical expression developed by Dai et al. [2006]. Various concrete-FRP systems were investigated, and the predicted ultimate loads were compared with experimental results.

Espeche and Leon [2011] estimated bond strength envelopes for old-to-new concrete interfaces employing an analytical approach and experimental pull-off and splitting tests. The proposed

Carol-type failure envelope is based on plasticity theory and assuming that concrete acts as a modified Coulomb material having three main parameters for tensile strength (f_t), cohesion (c), and friction angle (φ). It is assumed that the failure mechanism of the interface between two layers happens under a plane deformation field and a crack nucleates when the normal and tangential stresses reach the cracking failure envelope. Two different failure envelopes were proposed for cracking and post-cracking interfaces and are validated using experimental data.

Other research has been done by D'Ambrisi et al. [2012] where the bond between fiber reinforced cementitious matrix (FRCM) repair layer containing a poliparafenilenbenzobisoxazole (PBO) net and the concrete substrate was analytically analyzed in the context of an approach usually used for FRP materials, that is, based on the local-bond slip relation. Their results were calibrated based on the experimental results of double shear tests. Chalioris et al. [2014] studied the behavior of retrofitted reinforced concrete beams with self-compacting concrete jacketing and proposed an analytical model to study the full response of the jacketed members. The response curve of the rehabilitated specimens was estimated using dual section analysis procedure. Analytical evidence showed the applicability and effectiveness of thin reinforced concrete jacketing for repairing lightly reinforced concrete members.

Al-Osta et al [2017] investigated the response of strengthened reinforced concrete beams with UHPFRC under flexural stresses. Their analysis was based on the sectional stress-strain distribution and was used to calculate internal forces and to compute the predicted moment capacity. Bilinear stress-strain curves were used for UHPFRC in tension as well as steel reinforcing bars. Predicted results were presented and compared with the experimental results which show ed good agreement with differences of 10% or less.

An analytical solution was developed for determining the bond-slip model of FRCM–concrete joints based on longitudinal fiber strains [Zou et al., 2019]. This study was based on previous research by D'Antino et al. [2014]. The strain profile proposed by D'Antino et al. was used to calculate shear stress, however, it did not account for interfacial slip in a closed-form solution. In order to address strain profile and the bond-slip relationship, Zoe et al. fitted discrete strain profiles with a continuous function. Then the slip and shear stress along the bonded interface was calculated by integration and derivation of the strain profile. The debonding load and peak load from direct shear specimens were obtained. Finally, a continuous bond-slip relationship was derived based on the maximum shear stress and corresponding slip.

2.4.3 Experimental Models

Much research has been published over the last 60 years on empirical modelling of concrete interfaces. Although this research was focused on interfacial shear bonding, the modelling approaches and governing parameters are still relevant to the process and investigated properties of this study. As a result, a chronological literature review of experimental modelling of shear bonds is informative. Since the 60's, various milestones were achieved, and design philosophy has been dramatically improved. Such advances are embedded in various design codes. The resulting empirical models can be used not only for the interface between an existing substrate and a repair layer but also for the interface between a precast element and a cast-in-place part, the interface between two parts of an element cast at various times, and the interface between an element and a support.

One of the first design expressions to predict shear strength of cementitious interfaces was proposed by Anderson [1960]. Their expression (Equation 2.10) is based on two parameters derived from push-off tests (v_0 and k) and the reinforcement ratio (ρ). The proposed equation was calibrated for concretes of two different classes, with lower and higher compressive strengths.

$$v_u = v_0 + k\rho \qquad 2.10$$

where v_u is the ultimate shear stress at the interface. Later, this equation was calibrated for rough interfaces presenting different coefficients than those applicable to smooth interfaces.

The first linear expression for interfacial shear strength in cementitious composite systems was proposed by Birkeland and Birkeland [1966]. Their expression (Equation 2.11) is applicable to smooth and rough surfaces. The effect of surface preparation is accounted for by an empirically determined friction coefficient. Although the proposed equation has several advantages, including accuracy of results and simplicity, it is limited in terms of reinforcement ratio and compressive strength of concrete.

$$v_u = \rho.f_y.\tan\varphi = \rho.f_y.\mu \qquad 2.11$$

where f_y is yield strength of reinforcement and φ is internal friction angle.

The earliest nonlinear expression for predicting ultimate shear strength at the interface between concrete elements was developed by Birkeland [1968]. A parabolic function was employed to model experimental data from a previous study (Equation 2.12).

$$v_u = 2.78\sqrt{\rho f_y} \qquad 2.12$$

Mattock [1974] developed a new expression for shear bond by taking the normal stress at the interface (Equation 2.13) and orientation of the reinforcement (Equation 2.14) into consideration. This equation was limited in terms of maximum ultimate shear strength.

$$v_u = 2.76 + 0.8\,(\rho f_y + \sigma_n) \qquad 2.13$$

$$v_u = 2.76\sin^2\theta + \rho f_s\,(0.8\sin^2\theta - 0.5\sin(2\theta)) \qquad 2.14$$

where σ_n is the normal stress at the interface, θ is the angle between the reinforcement and the shear plane, and f_s is experimentally determined for different reinforcement orientations. These expressions were later modified by adding a reduction factor to be used in cyclic loading regimes. For the first time, concrete density was included in a design expression (Equation 2.15) in Raths' research [Raths,1976]. By including the effect of concrete density in design expression, they could differentiate between normal and lightweight concrete and assign different density-related impact factors to them.

$$v_u = C_s 3.11\sqrt{\rho f_y} \qquad 2.15$$

where C_s is a constant value related to the concrete density.

The first researcher who explicitly included concrete strength in his model was Loov [1978] who proposed a non-dimensional expression to predict interfacial shear bond strength (Equation 2.16).

$$\frac{v_u}{f_c} = k\sqrt{\frac{\rho f_y+\sigma_n}{f_c}} \qquad 2.16$$

where f_c is the compressive strength of concrete.

Later, Walraven et al. [1987] developed a power function for interfacial shear strength including the reinforcement ratio, the yield strength of the reinforcement, and the concrete compressive strength (Equation 2.17-2.19).

$$v_u = C_1(\rho fy)^{C_2} \qquad 2.17$$

$$C_1 = 0.822\, f_c^{0.406} \qquad 2.18$$

$$C_2 = 0.159\, f_c^{0.303} \qquad 2.19$$

This design equation is based on considering the interface as the weakest zone and the site of crack nucleation.

Randl [1997] also made progress in developing design expressions. he explicitly addressed the contribution of cohesion, friction, and dowel action (Equation 2.20). Cohesion is due to interlocking between aggregates; friction is the result of relative slip between two concrete layers; and dowel action is caused by the flexural resistance of reinforcement crossing the interface. While cohesion and friction are related to the Coulomb shear friction criteria, dowel action results shear reinforcement deformation.

$$v_u = \tau_{coh} + \mu\sigma_n + \alpha\rho\sqrt{f_c f_y} \qquad 2.20$$

where τ_{coh} is the concrete cohesion as a result of aggregate interlock, μ is friction coefficient, and α is a coefficient representing the flexural resistance of reinforcement. Surface preparation is addressed by assigning different coefficients of friction and cohesion to smooth versus rough surfaces (Table 2.1).

Table 2.1: Constant values for coefficient of cohesion and friction proposed by Randl [1997]

Surface preparation	Surface roughness R (mm)	Coefficient of cohesion c (-)	Coefficient of friction (μ)	
			($f_{ck} \geq 20$ MPa)	($f_{ck} \leq 35$ MPa)
High-pressure water-blasting	≥ 0.3	0.4	0.8	1.0
Sandblasting	≥ 0.5	0.0	0.7	0.7
Smooth	-	0.0	0.5	0.5

Papanicolau and Triantafillou [2002] developed an experimental expression to study interfacial shear transfer capacity in composite concrete systems. The novelty of this work was including interface size effect in the expression. In addition to interface length, compressive/tensile strength of concrete, density of concrete, ratio of shear reinforcement, surface preparation, lateral confinement, and loading rate were addressed as well (Equation 2.21).

$$v_u = \mu\,(\rho f_y + \sigma_n)^{\,b} + C \qquad 2.21$$

where *C* is a generalized cohesion term which takes into account the interface size effect (table 2.2).

Table 2.2: Coefficient of cohesion and friction proposed by Papanicolau and Triantafillou [2002]

Size – surface preparation ($b \approx 1$; $d \approx 0.5$)	Coefficient of friction μ	Coefficient cohesion c
Small – smooth	0.33	3.63
Small – rough	0.45	2.97
Large – smooth	0.33	2.33
Large – rough	0.45	1.90

Although many studies indirectly address the impact of surface preparation, Gohnert [2003] considered the actual value for surface roughness and explicitly included it in his design equation. Various degrees of surface roughness, geometries, and concrete compressive strengths were included in his study. Results indicated that ultimate shear strength at the interface had a stronger correlation with surface preparation rather than concrete compressive strength, thus, the proposed model was based on a roughness parameter (Equation 2.22). Surface preparation was represented by the roughness parameter R_Z defined as the difference between the average height of peaks and the average height of the valleys from an arbitrary baseline.

$$v_u = 0.209R_Z + 0.7719 \qquad 2.22$$

Although Equation 2.22 includes surface roughness, it does not provide an explicit relationship between cohesion, friction, and surface preparation. To separately investigate the impact of surface texture on cohesion and friction, Santos and Julio [2011] developed empirical power functions encompassing five different surface conditions ranging from left as-cast to hand scrubbing (Equations 2.23 & 2.24).

$$c_d = \frac{1.062 R_{vm}^{0.145}}{\gamma_{coh}} \tag{2.23}$$

$$\mu_d = \frac{1.366 R_{vm}^{0.041}}{\gamma_{fr}} \tag{2.24}$$

where c_d is the design coefficient of cohesion, μ_d is the design coefficient of friction, R_{vm} is the mean valley depth, γ_{coh} is the safety factor for the coefficient of cohesion, and γ_{fr} is the safety factor for coefficient of friction. They also assessed and provided recommendations for the effect of curing conditions, age difference between two layers, and compatibility in terms of shrinkage and stiffness.

Most of the empirical models for interfacial bonds in cementitious materials are devoted to mode II or shear failure. There are some studies focused on tensile behavior of composite systems where concrete is bonded to other materials, however, there is no research study applicable to an experimental model for FRC-concrete behavior under mode I, or tensile stresses.

Tudjono et al. [2017] investigated the impact of surface preparation on interfacial tensile bond strength between concrete and synthetic wraps. Various surface preparation methods were explored, and pull-off tests were performed to evaluate tensile bond strengths. Results showed that in comparison to shear bond, tensile bond was less sensitive to surface preparation. Tamulenas et al. [2017] tested tensile concrete members bonded to carbon fiber reinforced polymer sheets (CFRP). Direct tensile tests were performed on two composite systems with two different CFRP sheets and their deformation and crack patterns were compared.

Wang and Petru [2019] investigated mode I fracture of CFRP-concrete interfaces under aggressive environmental conditions. Long-term durability of CFRP-concrete interfaces exposed to freeze-thaw cycles, acid attack, and alkali attack were investigated. The wedge driving test (WDT) method was used to quantify fracture energy release rate of composite specimens. They noted that environmental conditions had a strong adverse affect on bond properties of FRP-concrete specimens. More freeze-thaw cycles and longer soaking times led to lower fracture energy [Wang and Petru, 2019]. Moreover, environmental exposure changed the failure mode from slower cohesive-adhesive failure to rapid pure adhesive failure along the interface. Additionally, test results showed the effectiveness of a silane coupling agent at mitigating adverse effects of environmental exposure. Specimens treated with coupling agent exhibited higher fracture energy and greater tendency towards cohesive failure compared to untreated specimens. Finally, Zanotti et al. [2014] and Kabiri Far and Zanotti [2019] performed multiple CDCB tests on FRC-concrete interfaces to investigate the effect of different fiber classes and contents on mode I fracture of cementitious interfaces. Although the beneficial effects of fibers on tensile bond and mode-I fracture were confirmed, none of the studies arrived at a design equation.

2.5 Cementitious Interfaces at the Microscale

Concrete and other cementitious materials have a complex structure. In order to gain a comprehensive knowledge of the behavior of these complex systems, investigation at various length scales are required. In other words, cementitious materials cannot be studied at a single level of scale. The structure of concrete and cementitious interfaces is multiscale in nature, ranging from nanometer scale, to the micrometer scale, and the millimeter scale. The traditional term "microstructure" is used for the microscopically magnified portion of a macrostructure [Li, 2011]. The microstructure of a material is a descriptor to define its properties. Therefore, any change of the microstructure affects material's response at various levels. Understanding the cause of a change and its effects helps us determine the suitability of any specific alteration of materials' properties and control for it. For example, it has been demonstrated through microscopy of concrete that lower w/c ratio will lead to less capillary porosity [Christensen et al., 1979]. Table 2.3 shows different levels of the structure of concrete and their corresponding magnification range.

Table 2.3: Different levels of cementitious structure [Diamond, 1993]

Level	Optimal Magnification Range	Usual Method of Observation	Structures to be Revealed
Visual	1×–10×	Unaided eye or hand lens	Details of coarse aggregate and air voids
Petrographic	25×–250×	Optical microscope	Fine aggregates, air voids, some paste details, and some cracks
Intermediate SEM	250×–2000×	SEM backscatter mode on plane polished surfaces	Arrangement and juxtaposition of cement paste particles, sand, capillary voids
High-magnification SEM	2000×–20,000×	SEM secondary electron mode on fractured surfaces	Details of the internal structure of individual cement particles and masses
Nanostructure	1,000,000×	AFM, TEM	Some details of C–S–H

At the millimeter scale, or visual level, concrete is considered a homogenous two-phase material consisting of coarse aggregate and cement paste bonded together. At higher magnifications, however, the cementitious structure is clearly not homogeneous, and the hydration products also exhibit a heterogeneous structure. The complex heterogeneous nature of cementitious materials was the subject of various microscopic studies by means of scanning electron microscopy (SEM), transmission electron microscopy (TEM), image analysis etc. [Diamond, 2004; Richardson, 1999]. These variations in microstructure of cementitious materials depend on various factors including:

1. Type of cementitious material
2. Particle size distribution

3. Mix proportion
4. Curing condition (temperature, humidity, and age)
5. Admixtures
6. Degradation mechanisms

These factors define the microstructure of the solid and porous phases which in turn control the general properties of cementitious material.

Figure 2.27 shows the structure of concrete at different levels of magnification. The properties at microlevel can be averaged and used as a homogeneous single value representing the macroscale properties of cementitious materials.

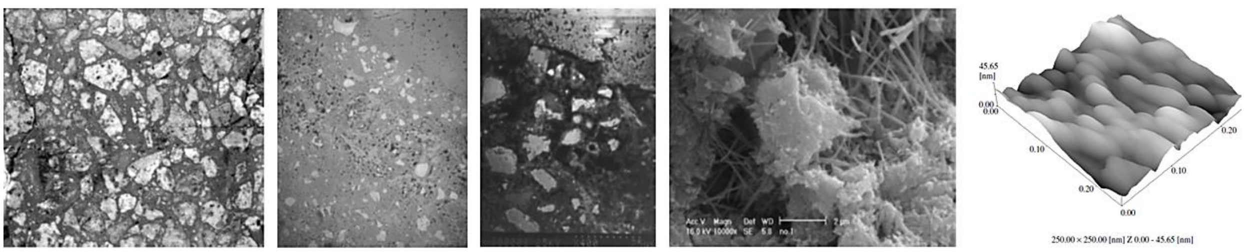

Figure 2.27: Concrete at different levels of magnification from visual to nanostructure level showing heterogenous nature of concrete structure and cement hydration products [Li, 2011]

2.5.1 Hydration Process and Microstructural Development

The hydration process of cementitious materials has been investigated extensively for many years [Lea, 1970; Taylor, 1964]. Hydration is a process during which the water-cement mixture transforms into a stone-like material which serves as the matrix phase. This process occurs through various chemical and physical reactions leading to phase change and spatial distribution of hydration products. The final hydration product is a porous material governing mechanical properties and durability of the system [Ye, 2003].

2.5.1.1 The Clinker of Portland Cement

The clinker of Portland cement mainly contains calcium, silicon, and oxygen. The dominant oxides in clinker are CaO, SiO_2, Al_2O_3, and Fe_2O_3. The four principal constituents in the sintered clinker are tricalcium silicate $3CaO.SiO_2$ (C_3S), dicalcium silicate $2CaP.SiO_2$ (C_2S), tricalcium aluminate $3CaO.Al_2O_3$ (C3A), and calcium ferro aluminate 4CaO, $Al_2O_3.Fe_2O_3$ (C_4AF). Moreover, gypsum $CaSO_4.2H_2O$ (CSH_2) is added as a reaction controller agent. X-ray diffraction (XRD) or energy dispersive spectroscopy (EDS) techniques can be employed to quantify the amount of oxides in the composition [Struble, 1991; Lin et al., 1997].

2.5.1.2 Development of Solid Phases

The development of concrete microstructure comes from the hydration products, that is solid phase, and a network of pores distributed throughout the solid phase. The main hydration products are calcium silicate hydrates (CSH), calcium hydroxide (CH), and ettringite (AFt), in addition to several other minor products (Figure 2.28).

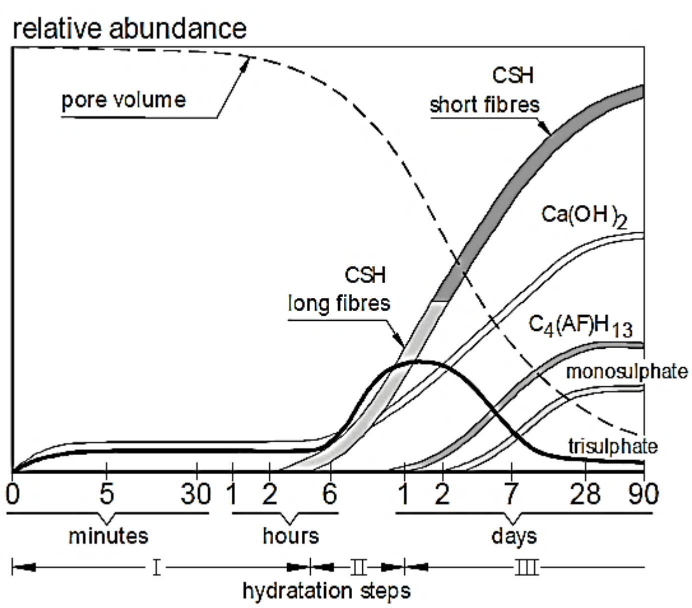

Figure 2.28: Development of cement hydration products [Locher et al., 1976]

In the first stage, C_3A is the most active phase and cement particles are covered with an aluminate-rich gel and short ettringite rods. During second stage, C_3S begins to react causing the formation of CSH on the ettringite rods. This is followed by secondary C_3A hydration which generates long ettringite rods and initiation of inner CSH formation [Scrivener, 1988]. Various morphologies have been reported for CSH gel including acicular, honeycomb, small disks, spheres, and long fibers [Locher, 1976]. CH also precipitates form the solution and crystallizes in empty pores with hexagonal plate-like shape [Figure 2.29]. Ettringite is usually observed as thin needles. Ettringite needles, unlike CSH, do not have branches.

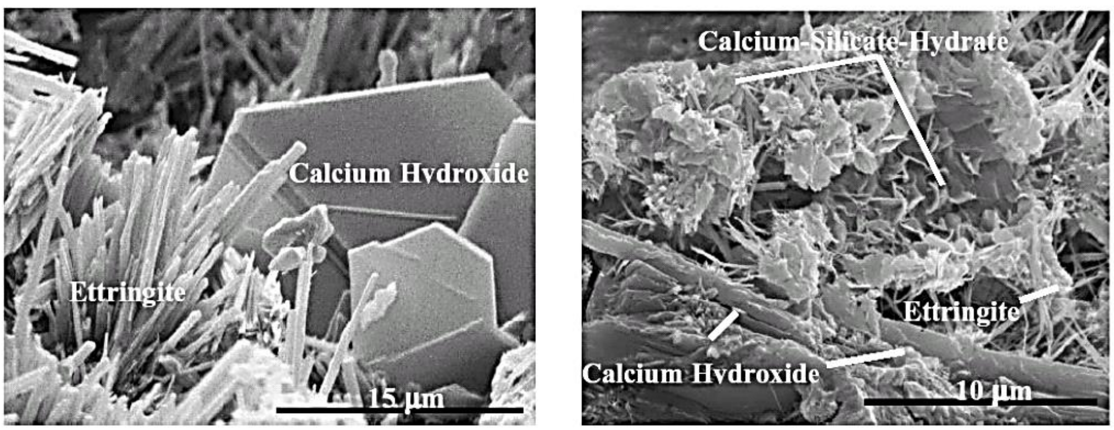

Figure 2.29: Morphology of CH , CSH, and ettringite [Stutzman, 2001]

Figure 2.30 represents evolution of hydration products and pore structure. Upon mixing cementitious material with water, the cement particles separate. With the initiation of the hydration process, calcium hydroxide forms from solution into the pores, and the CSH fibers develop on the surface of cement grains connecting cement grains to each other. Further formation of CSH and crystallization of CH leads to the solid phase. Eventually, all hydration products are connected to each other. This stage can be considered as an indicator of the hardening state.

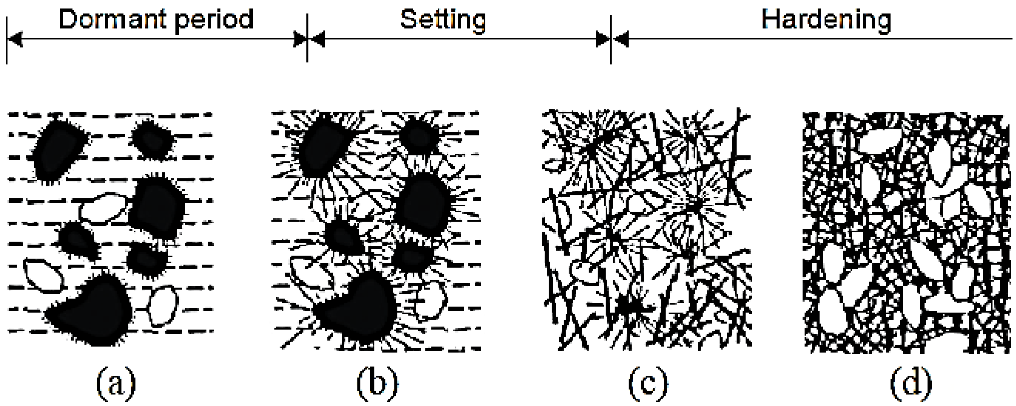

Figure 2.30: Evolution of hydration products and pore structure in cement showing gradual formation of CH and CSH particles, which lead to formation of the solid phase [Ye, 2003]

2.5.1.3 Pore Structure

Hardening cement paste is a permeable material. Development of pore structure is mainly governed by the hydration process and w/c ratio. Pores can be classified into gel pores, capillary pores, and air voids. Table 4.2 classifies pores based on their dimensions. It must be taken into consideration that the size division between capillary and gel pores is quite arbitrary due to continuous spectrum of pore sizes. However, capillary pores are mainly responsible for water absorption [Mindess and Young, 1981].

Table 2.4: Classification of pores in hydrated cement paste [Mindess and Young, 1981]

designation	diameter	description	affected
Capillary pores	50 nm to 0.5 μm	Large capillaries	Strength, permeability
	10 to 50 nm	Medium capillary	Strength, permeability, shrinkage at high humidities
Gel pores	2.5 to 10 nm	Small capillaries	Shrinkage to 50% RH
	0.5 to 2.5 nm	Micropores	Shrinkage, creep
	<0.5 nm	Micropores (interlayer)	Shrinkage, creep

2.5.1.3.1 Gel Pores

These are very small pores which are an intrinsic part of the CSH and cannot be easily observed by scanning electron microscopy (SEM). Large gel pores (diameter ≈ 5 *nm*) exist in the outer CSH gel, while small gel pores (d < 0.5 *nm*) exist in the inner CSH gel [Bonen Diamond, 1992].

2.5.1.3.2 Capillary Pores

Capillary pores form due to the inability of hydration products to fill all spaces. These pores tend to be larger than gel pores, hence, they can get detected by SEM more easily than gel pores. They are governed by degree of hydration and w/c ratio. Higher w/c ratio gives more and larger capillary pores, as mentioned above. As the hydration reaction continues, the amount and size of these pores decreases. Figure 2.31 shows SEM photographs of pores in hardened cement paste (left) and schematically (right)

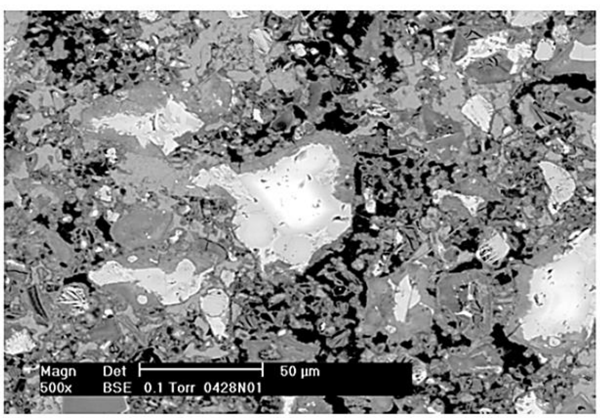

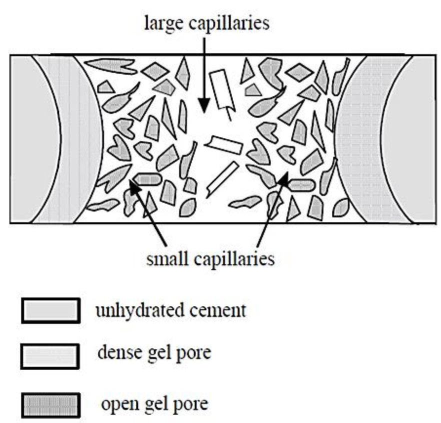

Figure 2.31: Pores in hardened cement paste [Ye, 2003]

Pore volume fraction and pore size distribution can be used to characterize pores in concrete. These parameters are useful for deriving a relationship between porosity and strength, as well as porosity and transport properties of concrete.

2.5.1.4 Microstructure of the Interfacial Transition Zone

Modern concretes have various interfaces, including the one between aggregates and bulk material, fibers and bulk materials in FRCCs, and the one between old and new layers in composite systems. In monolithic systems, microcracks tend to nucleate at the interface between aggregate and matrix. There are two major components of the microstructure in this transition zone. First, there is a thin layer of hydration products (a micron or so) on the aggregate surface. Around this, there is a region of paste with lower density where the packing of cement grains is affected by the presence of aggregates (around 50 microns). The significant variations from the bulk material occurs within the first 20 microns and very often the weakest part lies within 5 to 10 microns of the aggregates and not immediately at the interface [RILEM, 1996]. The space around the aggregate is less effectively filled with hydration products and it contains more CH and ettringite and less CSH. In this interfacial zone, the connectivity of pore structure increases which can govern transport properties and durability of concrete. Thus, microcracks tend to build at the aggregate interface due to insufficient packing, porous media, and effects of bleeding and segregation [Hemalatha et al. 2013]. As a result, interfacial transition zone between aggregates and matrix is the weakest zone and the most vulnerable element to cracking.

In fiber reinforced cementitious materials, the micromechanical properties of fiber-bulk material have a critical role in determining the mechanical properties of the matrix. This fiber-bulk interfacial zone is very similar to the interfacial zone around the aggregates. It contains large amount of CH close to fibers and is more porous than the bulk material. Figure 2.32 schematically represents the microstructure of the interfacial zone around steel fiber.

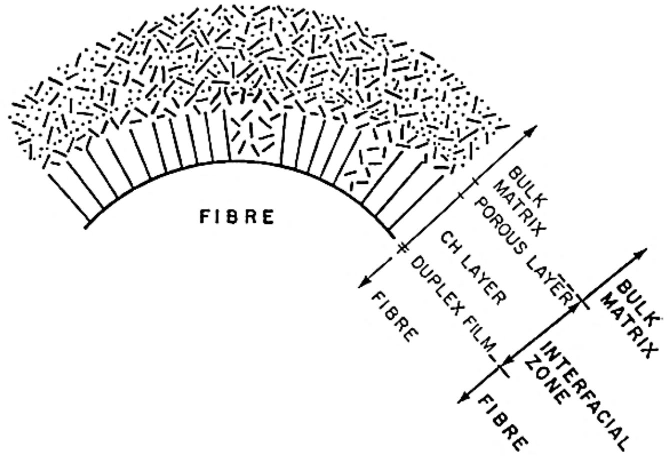

Figure 2.32: Schematic representation of the microstructure of the interface between steel fiber and bulk material [Bentur et al., 1986]

Although many studies have focused on the microstructure of the interfacial zone in monolithic specimens, there has been little research on the microstructural characterization of interfacial transition zone in repaired specimens. In composite systems, the transition zone between two layers serves as a bridge between repair and substrate materials. This region has a different microstructure and chemical composition than the bulk material. Although the volume of the interfacial transition zone is only a few percent of the total, its influence on repaired system is significant and exerts a strength-limiting effect. Higher porosity, less CSH, more CH, lower stiffness, and lower strength are some of the generally accepted features of the interfacial transition zone [Trtik and Bartos, 1999]. As a result, the mechanical properties of cementitious composites are considered to be a function of properties of repair-substrate interface, the weakest link in the system.

Moreover, the pore structure, which is recognized as the key to a wide range of various mechanical properties such as strength, fracture energy, toughness, and elastic properties, exhibits different pattern at the interface. Higher porosity at the interface causes strain localization, leading to further cracking. Higher stress levels lead to gradual spread of localized cracks and failure. This transition zone also affects long-term behavior and durability of repaired system. The existence of voids and microcracks at the interface makes concrete more vulnerable to aggressive environmental effects [Lukovic et al., 2012]. Various harmful materials, as well as moisture, can penetrate microcracks and adversely affect the whole system. There are different methods to improve microstructure of the interface, including lower w/c ratio which helps create a denser microstructure and mechanical behavior, incorporating chemical admixtures to help with the dispersion of cement particles, using supplementary cementing materials such as silica fume to improve packing efficiency, and introducing microfibers to the repair layer to mitigate early-age interfacial cracking. All these modifications can be used to create a microstructural system with desirable characteristics.

Additionally, as pointed out in Chapter 1, the durability of concrete structures has recently become of pressing concern. The increasing focus on the durability of structures and materials requires a more comprehensive understanding of the microstructure formation of cementitious materials. In line with this, repair of concrete infrastructure needs to meet specific details set out in various standards. For example, European standard EN 1504 [2010] asks for the nature and causes of defects to be identified and the extent and rate of increase of defects to be assessed in order to estimate when the affected element will no longer perform without repair measures or with a new repair layer. Thus, microstructural analysis may have a more central role as diagnostic method for new, damaged, and retrofitted concrete structures.

Better knowledge of the microstructural properties of cementitious composite interfaces is required in order to understand the composite's behavior at higher scale levels. Microstructural analysis can be employed as a tool for quality control of repair works as well (Figure 2.33). It can provide useful qualitative and quantitative information on the initial quality of concrete and repairs, the cause of deterioration, and the degree of deterioration. With such investigations, it is feasible to develop up-scaled predictors of macro-mechanical properties.

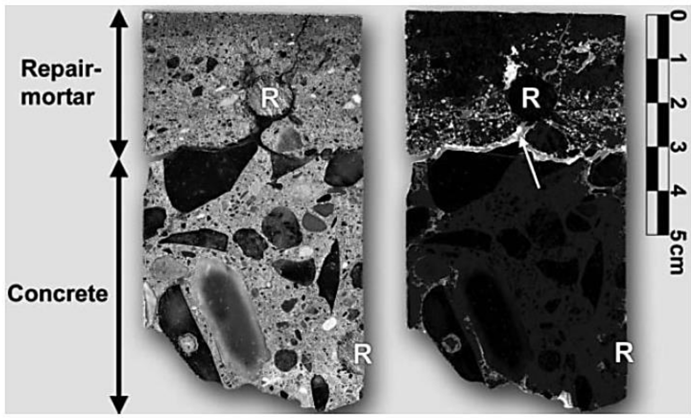

Figure 2.33: Fluorescein impregnated section of a core taken from the exterior part of a reservoir wall in a water tower. A crack at the surface can be followed to a corroded reinforcement bar [Hansen and Frederiksen, 2012]

However, due to small size and heterogeneous nature of the interfacial zone, interpretation of these structures is quite challenging and requires advanced equipment. In addition, considering the limited volume of samples and variation of the concrete from one area to another, the sampling and the subsequent investigation must be done properly to provide representative results and to create a solid basis for correct conclusions.

2.5.2 Evaluation Techniques

Various testing methods can be employed for microstructural investigation of cementitious materials. These tests can be used for different purposes including investigation of microstructural constituents, pore structure, and mechanical properties. Scanning electron microscopy can be used for 2D material and pore characterization. CT-scanning is helpful for 3D evaluation of the specimen. Mercury Intrusion Porosimetry (MIP), magnetic resonance relaxation analysis (MRRA), and complex impedance spectroscopy give detailed information on pore structure. Micro and nano indentation techniques are used for studying mechanical properties at the microscale. X-ray diffraction is useful for material characterisation. Electron spectroscopy for chemical analysis (ESCA) and secondary ion mass spectrometry (SIMS) are among other surface analysis methods [RILEM, 1996]. In this section, the principles of the methods used in this study are explained.

2.5.2.1 X-ray Micro-computed Tomography (CT-scanning)

CT-scanning can be used to investigate the void content and pore connectivity along the interface and inside the repair layer. This technique makes it possible to observe the internal structure at a relatively high resolution. It also facilitates the characterization and measurement of internal features such as cracks and pores. CT images are maps of X-ray beam absorption in a material. When a concrete specimen is irradiated with X-rays, the X-rays are attenuated as a result of the interaction with a material. This attenuation can be due to the scattering of X-ray beam and absorption by material [Lukovic, 2016]. This attenuation behavior can be quantified by the Beer-Lambert law [Landis and Bolander, 2009]:

$$I = I_0 e^{-\mu d} \qquad 2.25$$

Where μ is the attenuation coefficient, d is the thickness of the specimen and I_0 is the incident intensity. Attenuation causes a transmitted intensity of I. A detector visualizes intensity levels as grey scale values (GSV) which can be later used for the thresholding of images [Roels and Carmeliet, 2006]. During each scan, multiple x-ray images of a sample are taken. By aligning all of these slices on top of each other, 3D images of the internal structure of a specimen can be constructed. By thresholding dark pixels, which represent voids, in the original image, the image with only pores in the system can be obtained. CT techniques have been previously used for concrete characterization by many researchers [Kaufmann et al., 2014] [Trainor et al., 2013] [Landis and Bonaldo, 2009].

Lukovic [2016] used CT-scanning to evaluate the effects of moisture exchange on the microstructure of the repair system. Suzuki et al. [2017] employed CT-scanning for evaluating cracking damage in freeze-thawed concrete. They used both acoustic emission and X-ray CT parameters and correlated results of these two methods. Trainor et al. [2013] used CT-scanning for the measurement of energy dissipation in the fracture of fiber-reinforced ultra-high-strength cement-based composites. They identified fracture surfaces, fiber volume fraction, fiber orientation, fiber debonding, and pullout and crack area. These results were correlated with energy dissipation mechanisms. Cui et al. [2017] used dual CT-scans for the porosity characterization of aggregate-bulk hydrated cement interfacial transition zone. A novel method was proposed to calculate the width and the average porosity of the interface based on computer tomography (CT). they concluded that the dual-scan method can mitigate the shortcomings of the traditional CT scan.

2.5.2.2 Gravimetric Water Absorption Test

In composite cementitious systems, the overall durability of the repair material and the interface between substrate and repair layers is significantly influenced by the water absorption of the system. If too much water is absorbed by the substrate and passes through the interface, the durability of the repaired system can be compromised. Thus, for a repaired system to have acceptable long-term performance, better understanding of moisture exchange between the repair and substrate layers is needed. In order to evaluate and compare the water absorption of different repaired systems, gravimetric water absorption test have been performed according to NEN-EN 480-5 [2005]. This test is based on the increase in the mass of a specimen due to water absorption over time. The substrate is immersed in water up to 5 *mm* below the interface between the substrate and repair layer. Capillarity causes water to enter the repair layer and increase the mass of specimen.

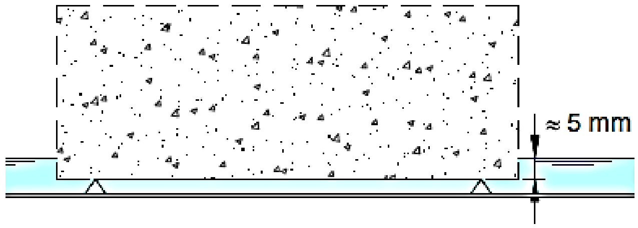

Figure 2.34: Schematic diagram of the gravimetric capillary absorption test for single layer concrete [Bogas et al., 2015]

The gravimetric test has been employed in many studies. Bogas et al. [2015] used this absorption test for an investigation of capillary absorption of lightweight aggregate concrete. Specimens were monitored for 72 hours and the influence of various parameters including the volume and initial water content of light weight aggregate were measured. This method has also been used for modelling water penetration into concrete [Wang and Ueda, 2011], capillary transport of water through textile-reinforced concrete [Lieboldt and Mechtcheine, 2013], non-invasive estimation of moisture content of bricks [Agliata et al., 2018], and capillary water absorption in cracked and uncracked mortar [Van Belleghem et al., 2016].

The gravimetric water absorption test provides values for cumulative water absorption, penetration depth of waterfront, and water absorption rate of repaired systems. The test is used in this chapter to examine the influence of different fibers, volume fraction of fiber, and curing condition are on water absorption. Moisture transport between the repair material and concrete at an early stage has already been investigated in previous studies [Lukovic., 2016] [Faure et al., 2005] [Kazemi et al., 2012] [Brocken et al, 1998]. Hence, this area is not addressed in this study.

2.5.2.3 Micro-indentation Test

Having comprehensive knowledge on micromechanical properties of interfaces is crucial, however, there is still a lack of information in this area, which can be attributed to limited availability of appropriate testing techniques. The micro-indentation test is particularly useful for evaluating the local mechanical properties of concrete at the microscale. Hardness and modulus of elasticity can be obtained based on the indentation load and displacement measurements. This test method has been used in various research studies. Moser et al. [2013] employed a nano-indentation technique to characterize impact damage in ultra-high-performance concrete, and Guruprasad and Ramaswamy [2018] used micro-indentation for the micromechanical analysis of concrete and reinforcing steel after the material was exposed to high temperature. Research was also performed by Shah and Kishen [2010] on nonlinear fracture properties of concrete-concrete interfaces using micro-indentation and scanning electron microscopy. Sakulich and Li [2011] employed a micro-indentation technique to evaluate the mechanical properties of the matrix-fiber interface. This technique has also been used to measure the properties of the interface in glass fiber reinforced cement [Zhu and Bartos, 1997], interfacial characterisation of steel fiber reinforced mortar [Wang et al. 2009], and evaluation of interfacial transition zones in recycled aggregate concrete [Xiao et al., 2013].

Although the micro-indentation test has some limitations due to its high sensitivity to surface preparation methods [Sakulich and Li, 2011] [Trtik et al., 2009], it is one of the few techniques which provides local micromechanical properties of the interface zone. As a result, this technique is employed in this chapter to investigate the interfacial properties of concrete-FRC composite systems. The local mechanical characteristics of the indented points can be obtained from the indentation load and displacement [Oliver and Pharr., 2004]. Hardness (H) can be determined from the following equation:

$$H = \frac{Pmax}{Ac} \qquad 2.26$$

where P_{max} is the peak indentation load [gf] and A_c is the contact area [μm^2]. The reduced modulus of elasticity (E_r) can be calculated from the load-displacement slope and can be correlated to the elastic modulus of the sample (E_s) using equation (2.27):

$$\frac{1}{Er} = \frac{(1-\nu s)^2}{Es} + \frac{(1-\nu t)^2}{Et} \qquad 2.27$$

where v_s is the Poisson's ratio of the sample, v_t is the Poisson's ratio of the diamond tip and E_t is the modulus of elasticity of the diamond tip. A series of indents were used here on randomly selected areas at the interface, substrate layer, and repair layer of concrete-FRC composite systems.

2.5.2.4 Scanning Electron Microscopy (SEM)

In order to characterize porosity, authentic images of pores need to be produced and analyzed. SEM has two common modes of operation: secondary electron (SE) and backscattered electron (BSE). While former mode allows for the observation of individual particles and pore structure, latter provides more information on composition of hydrated material. To properly employ SEM techniques for characterization of pore structure, sample preparation, image acquisition, and data interpretation need to be done with care.

In SEM, the emitted electrons are accelerated by an electric field at energies of 1 – 30 kV. The beam is focused at the surface of the sample by aid of electromagnetic lenses. Deflecting coils empower the electron beam to look over a specific part of the surface.

Scanning electron microscopy is a very common technique used in various fields of study for material characterization at the microscale. It has been employed in many research works on concrete, FRC, and cementitious composite systems. Diamond and Huang [2001] employed SEM to investigate the interfacial transition zone between bulk hydrated cement and aggregates. Wang et al. [2005] used SEM to characterize the microcracks in concrete at different temperatures. It has been widely used in conjunction with the indentation method to characterize materials. Moser at al. [2013] used SEM and nano-indentation tests to characterize impact damage in ultra-high-performance concrete. Hrbek et al. [2017] used SEM and indentation tests to evaluate the micromechanical performance recycled cementitious composite. Lukovic [2016] employed both techniques to investigate the influence of the addition of blast furnace slag (BFS) on the interface and the bulk material microstructure, as well as on the fracture properties of cementitious composite systems.

SEM suffers form some problems and limitations including:

1. SEM only provide two-dimensional images for a three-dimensional specimen. Thus, information on pore paths will be missing.
2. The resolution of pores' images is restricted by depth of field and magnification issues. Higher magnification levels lead to a smaller field of observation and larger number of fields must be evaluated.
3. The high energy of electron beams can damage the microstructure of specimen [Lukovic, 2016]. In addition, samples are highly vulnerable to microstructural damage during sample preparation.

Chapter 3: Interface Performance under Mode-I Loading

In order to extend the service life of deteriorating reinforced concrete structures, and to ensure safety in the case of increased loading demand, interventions of repair and rehabilitation have become of frequent practice worldwide [Guide to concrete repair, 2015]. Nevertheless, poor compatibility and debonding of the repair material can jeopardize these interventions. In a repaired system, the interface between the concrete substrate and the new repair layer is typically weaker than the materials on either side. Due to this weakness, combined with stress concentrations (emphasized in case of poor substrate repair compatibility), the interface is much more vulnerable to cracking and failure. As a result, the performance of repaired systems and, thus, their safety and durability, are highly dependent on the properties of the interface [Sadowski, 2017]. Fiber reinforced concrete (FRC) is recognized as a promising option for improving concrete durability. These benefits become even more relevant in repaired structures, where fibers can help improve compatibility with the substrate or, at least, reduce the extent of damage arising from poor compatibility [Banthia et al., 2014].

It has been shown that fiber reinforcement can improve the bond of a repair concrete layer to an existing substrate, though this is highly dependent on several factors including substrate preparation and roughness, fiber bonding, size, aspect ratio, and stiffness, type of stress applied at the interface, etc. Lim and Li [1997] investigated the bond strength, failure mode, and cracking behavior of Engineered Cementitious Composites (ECC) and introduced the concept of interface crack trapping. Their test results indicate that the ECC repair system has higher strength, more ductile behavior, and better crack width control [Li, 2003]. Wagner et al. [2013] studied the interface between strain hardening cementitious repair layers and concrete substrate. The researchers concluded that bond strength was highly affected by surface roughness, and added the qualitative observation that the beneficial effect of fiber reinforcement was impacted by the amount of repair material that remained attached to the substrate after failure (in other words, by the deviation between failure and bond plane). Slowik et al. [2017] characterized the behavior of strain-hardening cement-based composite systems aimed at enhancing the overall durability of structural retrofits, by addressing both interfacial behavior and drying shrinkage. Zanotti et al. [2014a; 2014b] studied the interface behavior under both tensile and shear loading. Their results showed the effectiveness of fibers at enhancing the quality of the interface both in tension and in shear. Further studies investigated the effect of fiber properties and surface preparation on the shear bond strength of substrate-repair interfaces in mixed modes of fracture [Zanotti et al., 2018]. It was found that surface preparation has a strong effect on crack deviation from the interface followed by fiber activation and gradual cracking before failure. A study by Banthia et al. [1994] explored the suitability of fiber reinforced cementitious composites with high volume fractions of microfibers for thin repair applications. Results of tensile tests indicated a significant enhancement of the repair bond strength from the introduction of micro-fibers to repair layer.

Although various studies indicated the potential effectiveness of fiber reinforcement in improving interface performance, the exact governing mechanisms are neither well understood nor quantified for the different concurring contributing factors, so accounting for these effects in the design and analysis of a repair application can be challenging. For instance, knowledge gaps pertaining to the collaborative effect of surface preparation/roughness and fiber reinforcement for different fiber types need to be addressed, as does the distinction between the impact of fibers on interfacial transition zone (ITZ) quality (early-age damage prevention such as drying shrinkage [Slowik et al. 2017]) and the contribution to fracture mechanisms such as crack deviation, kinking, or trapping [Zanotti et al., 2018] [Zanotti et al., 2014b] [Wagner et al. 2013] [Lim and Li, 1997].

The main objective of the work presented in this chapter is to provide a contribution towards the understanding of complex mechanisms involved with the interfacial cracking in cement-based bi-material systems. The study is focused on testing and characterization of fracture in Mode-I for steel and PVA fiber reinforced concretes (the repair materials) and, especially, their bond to an older, unreinforced concrete (the substrate). Beyond the plain, unreinforced control condition, volume fractions of 0.5% and 1% with three types of fibers were considered for the repair material, namely: (i) 8 mm long Poly-Vinyl-Alcohol (PVA) fibers, (ii) 12 mm long PVA fibers (to compare the effects of different fiber lengths), and (iii) 13 mm long steel fibers (to compare fibers with similar lengths but different materials, matrix bonding, and stiffness). Both PVA and steel fibers were selected because these reinforcements can be very effective at enhancing the mechanical performance of concrete and especially its fracture toughness and have potential for strain hardening behavior in tension [Zanotti et al. 2014; Banthia and Nandakumar, 2003]. In addition, both PVA and steel fibers can be very good at preventing or mitigating cracking related to volume changes such as shrinkage, a crucial property in repair applications where optimum compatibility between old and new concrete needs to be achieved to prevent damage acceleration. Previous studies have shown that both PVA and steel fibers can enhance concrete-concrete bond [Zanotti et al. 2018] [Slowik et al. 2017] [Zanotti et al. 2014a] [Lim and Li, 2003], although most of the information available is focused on shear bond and very limited information is available on progressive debonding in Mode I. Studies also indicate that steel fibers can be more effective than PVA fibers at lower volume fractions while, conversely, PVA fibers can be more effective at higher volume fractions. PVA has also proven more effective than steel fibers in shear bond tests with minimum interfacial roughness (i.e. smooth interface, no sandblasting) [Zanotti et al., 2018]. In this study, Mode-I crack propagation was investigated through Contoured Double Cantilever

Beam (CDCB) tests [Zanotti et al., 2014a], supported by imaging techniques for stress-strain analysis. Fracture parameters were computed based on a classic Modified Linear Elastic Fracture Mechanics (MLEFM) approach. No bonding agent was applied but the substrates were sandblasted to enhance interfacial roughness before applying the repairs. Interfacial roughness and crack deviation were quantified through laser scanning; correlations between surface topography and fracture parameters were analyzed.

3.1 Methodology

3.1.1 Materials and Specimen Preparation

The mix proportions of substrate and repair materials are shown in Table 3.1. General use hydraulic cement and class F fly ash were used. The employed cement complied with ASTM C150 type I and included Portland cement clinker, calcium sulfate, limestone, inorganic and organic processing additions based on the recommended proportions in ASTM C150. The fine aggregate was a natural sand and the coarse aggregate was crushed limestone rock with maximum size of 10 mm. Particle size distribution of cement and aggregates can be found in Figure 3.1. For the repair materials, beyond the plain control condition without fibers, three types of fibers with volume fractions V_f = 0.5% and 1% were considered, namely: (i) 8 mm long Poly-Vinyl-Alcohol (PVA) fibers, (ii) 12 mm long PVA fibers (to compare the effects of different fiber lengths), and (iii) 13 mm long steel fibers (to compare fibers with similar lengths but very different materials, matrix bonding, and stiffness). As described above and discussed in the introduction, short fibers can be more effective than longer fibers with respect to bonding especially because their effectiveness depends upon the relative size of the fiber compared to the interface roughness. The technical information on the fibers is shown below in Table 3.2.

Table 3.1: Mix proportions of substrate and repair layers adopted (from suppliers)

	Cement	Fly Ash	Sand	10mm Aggregate	Water	Fibre Volume Fraction
Substrate	1	0.25	2	0.48	0.5	----
Repair	1	0.25	2	---	0.5	0%, 0.5% & 1%

Table 3.2: Technical information about PVA and steel fibers adopted (from suppliers)

Type of fiber	Diameter [mm]	Cut Length [mm]	Tensile Strength [MPa]	Young's Modulus (GPa)	Specific gravity
8 mm PVA	0.04	8 ± 0.1	1600	40	1.3
12 mm PVA	0.10	12 ± 0.2	1100	28	1.3
13 mm Steel	0.20	13 ± 0.4	2750	210	7.85

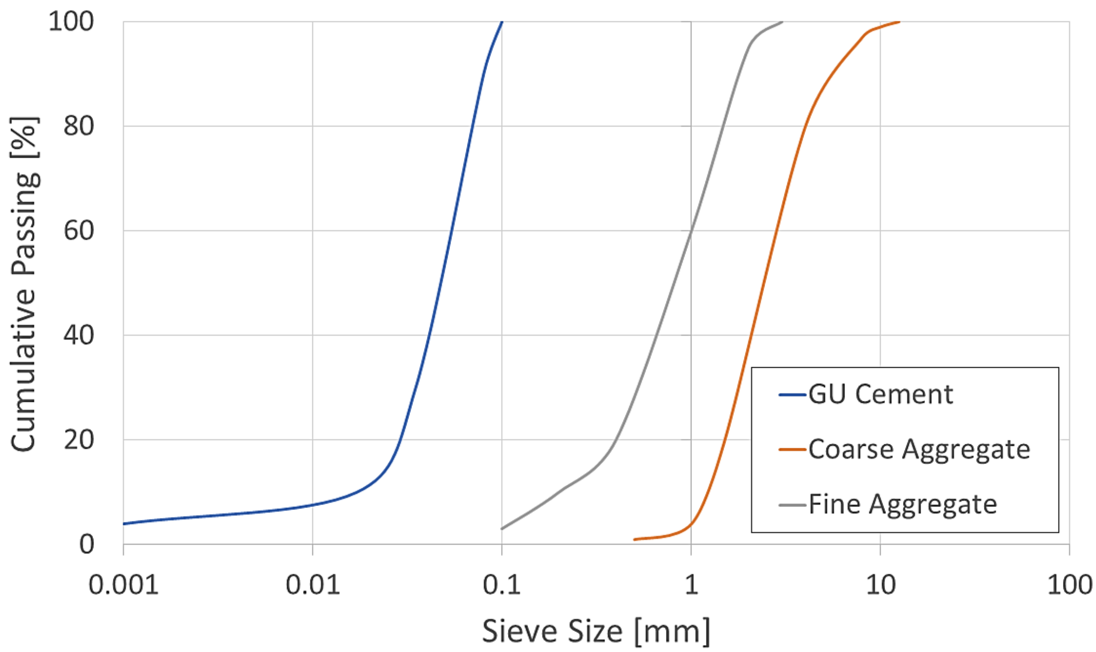

Figure 3.1: Particle size distribution of general use (GU) cement and aggregates adopted (from suppliers)

For the composite substrate-repair samples, concrete substrates were cast in pre-formed moulds designed to cast only half of the final specimen. Substrates were covered with plastic sheets immediately after casting, demoulded after 24 hours, and cured at a standard temperature of 20°±2° and humidity 95±5% [ACI 308]. After 28-day curing, the substrates were sandblasted. Afterwards, concrete substrates were put back into the moulds in optimum Saturated Surface Dry (SSD) condition [Momayez et al., 2005], and the repair mortar was poured against the substrates. It is important to mention that in this work, unlike in other studies, the mortar was cast parallel to the substrate. Although the mortar was well vibrated and compacted, this casting direction could reduce compaction at the interfacial transition zone with the substrate and affect fiber orientation near the bond plane (especially for steel fibers, which are stiffer). The repaired specimens were cured using procedure described above. When casting the substrate and repair components for specimens used for bond testing, monolithic specimens of the repair materials were cast in similar CDCB molds and cured together with the bond samples, in order to characterize fracture properties of the repair materials as well. Three replicates were tested for each of the seven repair materials and each of the seven corresponding concrete-repair interfaces.

3.1.2 Experimental Methods and Testing Set-up

Contoured Double Cantilever Beam (CDCB) tests were conducted to analyze Mode-I substrate-repair debonding and to assess crack growth resistance of the repair materials. 3D surface scans were conducted to obtain substrate roughness profiles. Modified Linear Elastic Fracture Mechanics (MLEFM) theory was employed investigating fracture toughness vs effective crack length response curves. In addition, an imaging technique for displacement analysis was employed with the purpose of visualizing crack and displacements during the test. This is further explained in Section 3.1.2.1.

3.1.2.1 Contoured Double Cantilever Beam (CDCB) test

In general, tensile bond tests can be subdivided into direct and indirect methods. The main flaw of direct tensile tests is their high sensitivity to the specimen anchoring system and to slight eccentricities, which might lead to bending effects at the interface or premature material failure rather than bond failure [Austin et al., 1995]. Indirect tensile tests, such as flexural and splitting methods, on the other hand, can help overcome some of these issues, although the indirect nature of the stresses applied may introduce some computational challenges. There is a long tradition of splitting fracture tests to determine the fundamental mechanical behavior of materials and of bi-material systems [Wagner et al. 2013] [Momayez et al., 2005]. The technique using a Double Cantilever Beam (DCB) specimen was first developed for structural adhesives and eventually adapted to studying fracture properties of monolithic materials [Genois., 1995] as well as interfaces in cement-based bi-material systems [Zanotti et al., 2014a]. The DCB test consists of applying a splitting load to propagate a crack in a pre-notched specimen while recording the applied load and the opening displacement of the crack faces, with the major benefit that several fracture parameters can be investigated. In addition, more reliable compliance measurements are possible (as described in the following sections) as the test geometry promotes application of smaller splitting loads and larger displacements compared to other test setups [Genois, 1995]. Further studies suggested tapering the samples in order to make the rate of strain release theoretically independent of the crack length, hence leading to a more stable crack propagation [Mostovy et al., 1967]. This specific condition can be achieved by shaping the sample so that the rate of change of the compliance is theoretically constant during the crack growth (as detailed in the following sections). The resulting geometry was re-named Contoured DCB (CDCB) test (Figure 3.2), also known as the linear compliance test [Genois, 1995].

Geometrical proportions and size of the specimen tested are shown in Figure 3.2 and accord with those described by [Zanotti et al., 2014a]. A side groove along the desired crack plane promotes crack growth and hinders any unfavorable crack deviation in monolithic specimens (Figure 3.2 a). In this study, however, the test was also adapted to allow fracture analysis of interfaces, with the specimen subdivided into two symmetrical parts, that is, the concrete substrate on one side, the repair material on the other side, and the bond plane in between, running exactly along the CDCB middle section (Figure 3.2 b). For these bi-material tests, the interface represents a plane of weakness by itself, and to avoid excessive damage during handling, the side groove was removed from the middle line (Figure 3.2 b). This aspect is computed in the back-calculations described below.

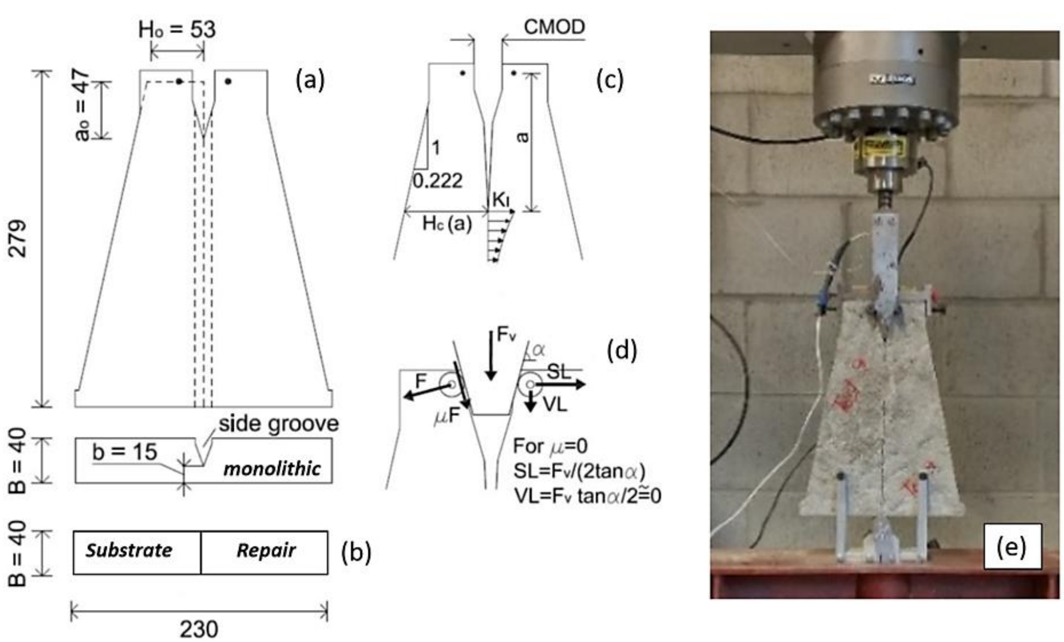

Figure 3.2: (a) CDCB specimen geometry and (b) adaptation for testing of bi-material systems, (c) parameters for crack growth resistance analysis [Zanotti et al., 2014a], (d) calculation of forces applied [Zanotti et al., 2014a], and (e) test set-up

Tests were performed using a servo-hydraulic Instron universal testing machine (Figure 3.2 e). Specimens were supported by a hinge fixed to the lower plate of the testing machine, while the upper part was supported by a steel profile with two identical wedges, which was used to apply the splitting load. Each wedge was positioned between two low-friction bearings mounted on both sides of the CDCB sample using steel rods passing through the section (and placed above the crack so that this would not be affected, Figure 3.2 d). The steel profile was connected to a load cell, which was connected to the cross-head of the machine. Although each specimen was subjected to a vertical load in addition to the horizontal splitting load (SL), the vertical component can be ignored by keeping the angle of the wedge, $\alpha = 15°$ (Figure 3.2 d), small and by employing low friction needle bearings so that the coefficient of friction, μ, between wedge and bearings can be reasonably neglected. Displacement rate was 0.02 *mm/min*, to promote more stable crack propagation.

During the test, load and Crack Mouth Opening Displacement (CMOD) were recorded continuously. The CMOD (Figure 3.2 c) was measured with a gauge transducer that recorded relative displacement near the base of the notch and was also monitored by means of 2D Digital Image Correlation (DIC) technique (Figure 3.3) [Dai et al., 2019] [Tekieli et al., 2017]. The values obtained with the sensor and with DIC were consistent. For the data acquisition using DIC, a high-speed 9-megapixel mvBlueFox camera in combination with the GOM SNAP software were used; the collected data was processed using GOM Correlate software. The camera was placed at a distance of 1.7 m from the specimen. Beforehand, a speckle pattern of black dots over a white background was applied on the surface of specimens by using a can of black spray paint. Various patters were applied on trial specimens and the best pattern was adopted for the tests. The light was adjusted for each test to guarantee even illumination of the specimen and to avoid over-exposure. Because crack propagation tests need to be performed at slow displacement rate to allow stable crack propagation, the maximum acquisition frequency was set to 0.5 *Hz*.

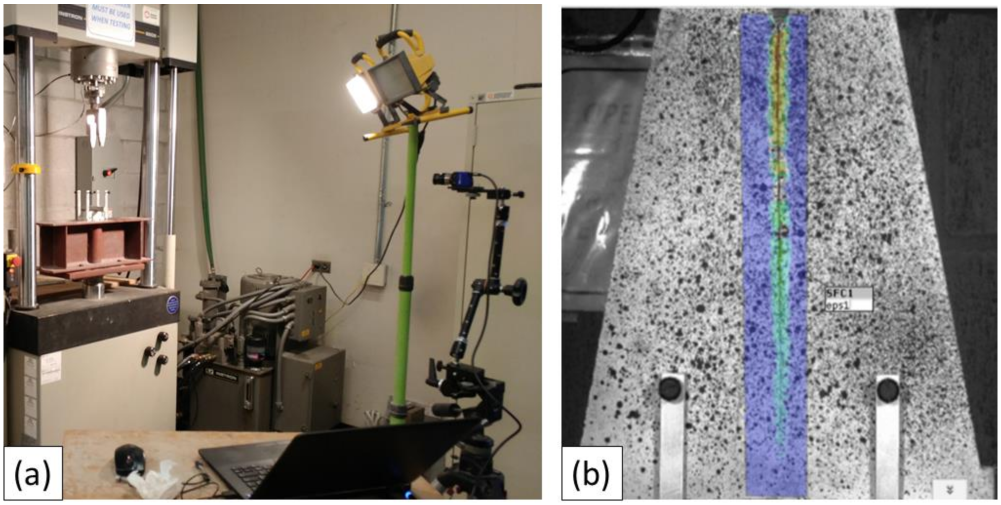

Figure 3.3: (a) Camera setup (b) Representative black dot pattern, with location of the region of interest (ROI) around the interface for Digital Image Correlation

3.1.2.2 Roughness profiles and quantification of crack deviation

Surface roughness analysis was performed for two reasons, namely: (i) to assess crack tortuosity of monolithic material samples after failure; and (ii) to assess the roughness of the substrates after sandblasting (prior to casting the repair material) the composite samples for interfacial bond studies.

The topography of the sandblasted substrates was quantified using a 3D laser scanner (Figure 3.4 a). This system consisted of a Nikon – 3D Cross Scanner with an accuracy of 8 μm and inspection/scan software (Focus 10.0). Full topography curves were obtained (Figure 3.4 b), and several parameters have been used to quantify surface roughness [Santos and Julio, 2013]. In this study, the mean peak height (S_{pm}) and the average roughness (S_a) parameters were selected [CAN/CSA A23.3, 2004] [Eurocode 2, 2004] [ISO 4287, 1997]. These parameters have been suggested as reliable roughness parameters [Mohamad and Ibrahim, 2015] [Santos and Julio, 2014]. S_{pm} was calculated as the average of the maximum peak height (p_i) for each sampling length where sampling length is equal to 1/5 of the total length, while S_a was calculated using arithmetic mean of the absolute values Z(x,y) within sampling length (*l*) and sampling width (*b*).

$$Spm = \frac{1}{5}\sum_{i=1}^{5} pi \qquad 3.1$$

$$Sa = \frac{1}{lb}\int_0^l \int_0^b |Z(x,y)|\, dxdy \qquad 3.2$$

In order to quantify crack deviation in the materials tests (monolithic specimens) and to reduce the computational load, 2D image analysis of the crack profiles was performed. To this end, 2D images of the crack profiles were taken after the failure and processed with a commercial image processing software (Web Plot Digitizer) with accuracy of 70 μm to calculate the area below the deviated crack with respect to the mid-line. This area represents a quantification of crack deviation.

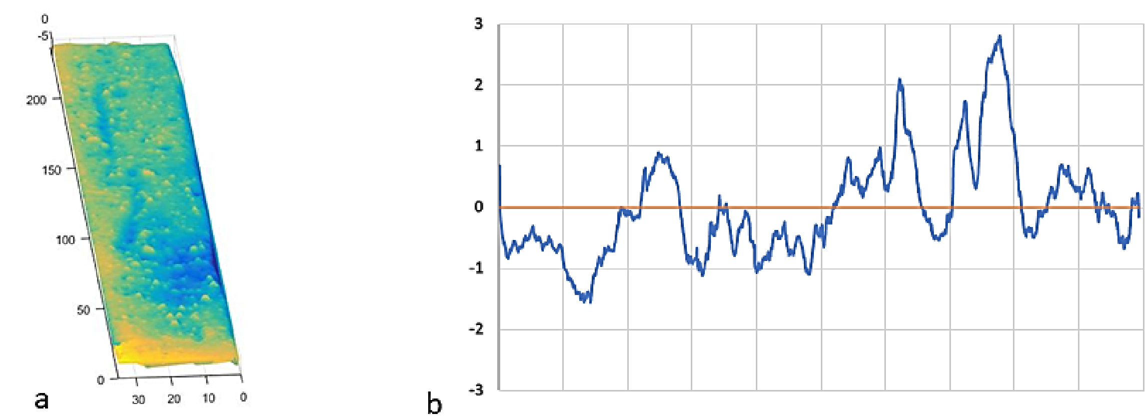

Figure 3.4: (a) Representative 3D topography of a substrate profile after sandblasting and prior to the repair application and (b) surface roughness profile [dimensions in *mm*]

3.1.2.3 Calculation of Fracture Parameters

Ideally, brittle materials are ones that can be characterized by the propagation of a single crack with the elastic zones near the crack. For fracture analysis of such materials, linear elastic fracture mechanics (LEFM) theory can be applied. LEFM indicates that the fracture instability of brittle materials in Mode-I or opening mode can be defined by only one parameter, i.e., the critical stress intensity factor (K_{IC}) or the specific fracture energy (G_f) [Zanotti et al., 2014a].

Back to Griffith [1920], a crack propagates unstably when the rate of change in the elastic energy released by the system for a unit crack extension (*U*), is equal or higher than the energy required for the crack to propagate within the material, for a unit crack extension (*W*):

$$G_{IC} = \frac{\partial U}{\partial a} = \frac{\partial W}{\partial a} = R \qquad 3.3$$

where G_{IC} = Mode-I critical strain energy release (or specific fracture energy G_f), a = crack length and R = crack growth resistance. The stress intensity factor, K_I, that defines the elastic stress field intensity ahead of the crack is then sufficient to characterize the whole stress field around the crack. K_I reaches K_{IC} (critical value) when enough energy is supplied to the system and unstable crack propagation occurs.

The LEFM theory is applicable to materials when the zone around the crack that undergoes inelastic deformations remains small and is therefore neglected. However, in the case of cement-based materials (typically referred to as quasi-brittle materials), a large zone of damaged material, known as fracture process zone (FPZ), subject to high stress concentration, develops around the crack tip. Micro-cracking along the FPZ improves the energy absorption capability of the system because it causes less energy flux released into the crack tip and increased area of cracking surface [Bazant, 1992]. The extension of FPZ affects toughness of quasi-brittle materials as well as tortuosity and bridging effects of aggregate and unbroken ligaments [Mindess, 1991] [Van Mier, 1991].

There are various, well-calibrated classic methods for analysing the behavior of the FPZ, including fracture models proposed by Bažant and Cedolin [1979], Hilleborg [1980], de Borst [1984], Rots [1988], Rots and Blaauwendraad [1989], Bažant [1992], and Reinhardt and Cornellisen [1994]. In the analysis of the CDCB test, a methodology was developed [Zanotti et al., 2014a] [Genois, 1995]

[Sorelli et al., 2014] for the computation of crack growth resistance curves based on the effective crack model. With this approach, the effect of the FPZ is accounted for by treating the quasi-brittle material as a brittle material with an increased, fictitious crack length, called effective crack length (a_{eff}). By treating the material as brittle, Modified Linear Elastic Fracture Mechanics (MLEFM) equations based on adaptation of LEFM [Van Mier, 1991] can be still utilized. The typical crack-growth-resistance curves of brittle and quasi-brittle materials (or interfaces, in case of bi-material systems) are represented in Figure 3.5 a. In brittle systems, the crack propagates unstably since formation and, hence, its resistance to propagation (here represented by the stress intensity factor) is a straight, horizontal line, unrelated to crack extension. In the case of quasi-brittle systems, the toughening mechanisms occurring after crack nucleation allow for a stage of stable (nonlinear) crack growth, represented by an initial rising trend (BOP-B), followed by a flat branch of unstable propagation after critical crack length and critical stress intensity factor are reached, point B of Figure 3.5 a.

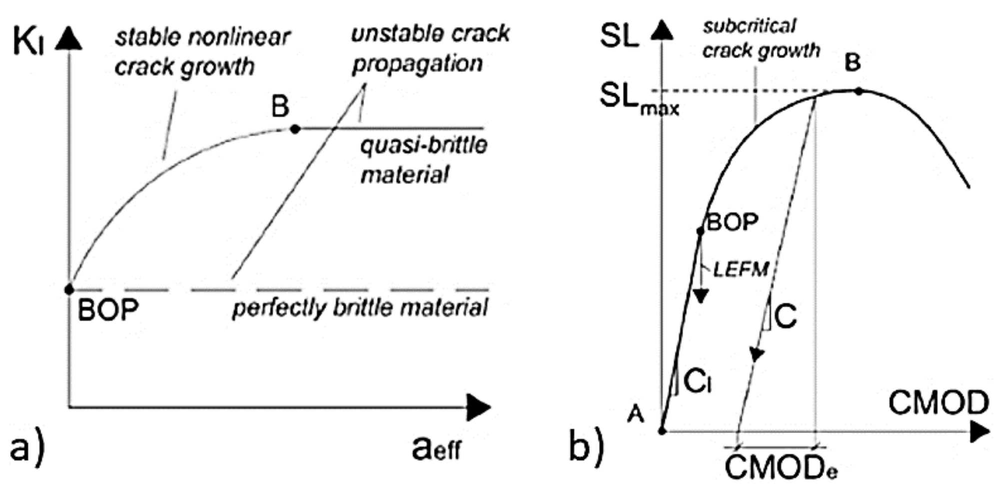

Figure 3.5 (a) Typical crack-growth-resistance curves of brittle and quasi-brittle materials and (b) typical response of quasi-brittle materials under CDCB test [Zanotti et al., 2014a]

A typical Splitting Load (SL)-Crack Mouth Opening Displacement (CMOD) response curve obtained from CDCB test of quasi-brittle materials or bi-material interfaces (for bond tests) is represented in Figure 3.5 b. Three main stages can be identified, namely: (i) initial linear elastic behavior (A-BOP), (ii) stable, subcritical crack growth (BOP-B) upon crack formation, here identified at the curve Bend Over Point (BOP), and (iii) unstable crack propagation (after the critical crack length is achieved at point B). These stages are related to the aforementioned stages depicted in Figure 3.4 a. In order to compute the crack growth resistance curves (Figure 3.4 a) from the experimental curves (Figure 3.4b), a procedure based on experimental and theoretical compliances [Visalvanich and Naaman, 1981] was employed. Compliance (C) is defined as the ratio between the elastic component of the CMOD ($CMOD_e$, Figure 3.4 b) and the corresponding splitting load (SL):

$$C = \frac{CMOD_e}{SL} \tag{3.4}$$

To calculate the experimental compliance based on experimental CMOD and SL data, it is possible to neglect the permanent deformation during the subcritical crack growth ($CMOD_e$ = CMOD, Figure 3.5 b), by assuming a return to the origin upon unloading.

Considering MLEFM, each specimen arm at one of the crack sides can be considered as a simple cantilever beam made of a perfectly elastic material. With reference to the strength-of-materials approach, the theoretical compliance can be calculated as follows by considering bending and shear deformations of the beam:

$$C_{th} = \frac{2\Delta}{SL} = \frac{CMOD}{SL} = \frac{24}{EB}\int_0^a \frac{x^2}{H^3}dx + \frac{6(1+\nu)}{EB}\int_0^a \frac{1}{H}dx \tag{3.5}$$

where E = Young's Modules, Δ = arm displacement, B = beam width (specimen depth), ν = Poisson's ratio and a = crack length. Since the beam height is variable, a constant equivalent height equal to the mean height is considered:

$$H_c = \frac{H_o + H_a}{2} = H_o + \frac{ma}{2} \qquad 3.6$$

where H_o is the width of the top of the beam and H_a is the beam height at distance a from the loading point.

Equation 3.5 was written based on the assumption that the end of the cantilever beam is fixed. However, the actual rotation of the bottom edge around the supporting hinge (Figure 3.2) needs to be considered. Based on the findings by [Mostovy et al., 1967], this can be accommodated by increasing the beam length by adopting an equivalent, increased crack length equal to $a + 0.6H_c$. As a result, Equation 3.7 can be re-written as follows:

$$C_{th}(a) = \frac{24}{EB}\left\{\frac{[a+0.6H_c(a)]^3}{3H_c^3(a)} + \frac{0.3a}{H_c(a)}\right\} \qquad 3.7$$

By equating the initial experimental compliance to the initial theoretical compliance prior to BOP (Figure 3.5 b), the effective modulus of elasticity (E_{eff}) is determined. The initial experimental compliance ($C_{exp,i}$) is calculated at the BOP, that is the first point of nonlinearity. Considering that the crack length before the BOP is equal to the length of the notch (a_0), the initial theoretical compliance is given by:

$$C_{th,i} = C_{th}\,(a_0) \qquad 3.8$$

Once E_{eff} is known, the effective crack length (a_{eff}) is calculated be equating the experimental compliance to the theoretical one at each point of the SL-CMOD curve. Hence, the Mode-I SIF (K_I) for a CDCB sample is determined from:

$$K_I^2 = \eta^2 S L^2 B^{-2} H_a^{-3} (a^2 + 1.4 a H_a + 0.5 H_a^2) \quad 3.9$$

where η is a function of the slope and here is equal to 3.1for *m* = 0.222 [Mostovy et al., 1967].

Considering that one *B* parameter in B^{-2} stands for beam depth and one for crack depth, when crack depth and beam depth are not equal to each other (in case of monolithic specimens, Figure 3.2 a) one of the *B* parameters has to be changed to *b* (crack depth, Figure 3.2 a). Hence, equation 2.18 is re-written as follows for monolithic specimens with side-groove:

$$K_I^2 = \eta^2 S L^2 (Bb)^{-1} H_a^{-3} (a^2 + 1.4 a H_a + 0.5 H_a^2) \quad 3.10$$

Based on this approach, crack growth resistance curves of repair materials and substrate-repair interface bond were computed using the software Matlab.

3.1.2.4 Sandblasting and Surface Preparation

Sandblasting was done by a Xstream pressure washer at 4000 *PSI* (27.6 *MPa*) using a commercially available glass abrasive product. The size of the particles ranges from 0.150 to 2 *mm*. The chemical composition of the abrasive product can be found in Table 3.3.

Table 3.3: Chemical composition of the abrasive product

Chemical Oxide	**Weight (%)**
Silica	93.2 – 93.6
Alumina	3.6 – 4.6
Iron	0.30 – 0.35
Calcium	0.25 – 0.65
Magnesium	0.08 – 0.15
Sodium	0.75-0.85
Titanium	0.1 maximum

The nozzle was kept at a distance of 10-20 *cm* from substrate surface up to the point the aggregate was visible on the substrate surface and desired roughness was obtained. Figure 3.6 demonstrates the surface roughness as a function of sandblasting time over the area of 25 cm^2.

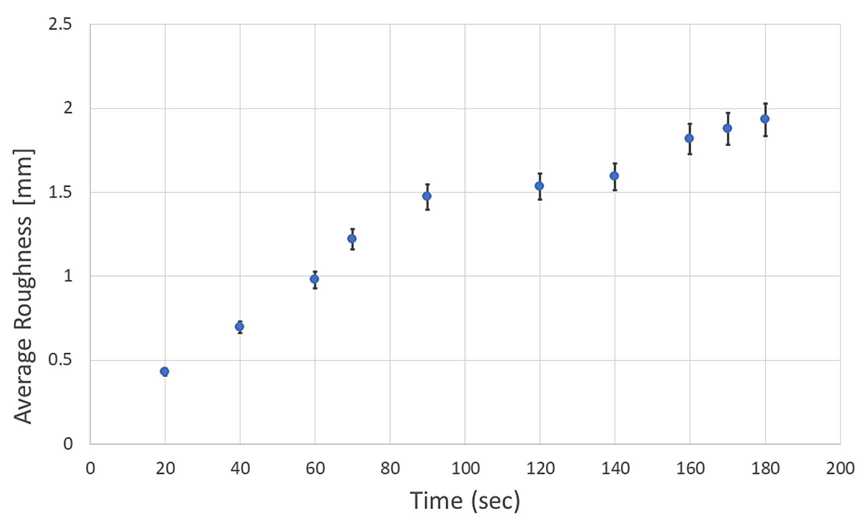

Figure 3.6: Relationship between average roughness (R_a) versus the duration of sandblasting

3.2 Results and Discussion

3.2.1 Mode-I Crack Growth Resistance of the Repair Materials

As anticipated, plain mortar specimens exhibited brittle, abrupt failure soon after initial crack nucleation, while more controlled, steady crack propagation was observed in the fiber reinforced mortars overall at both pre-peak crack nucleation and post-peak crack propagation. Failure occurred along the groove at the mid section as desired.

Experimental Splitting Load (SL) versus crack mouth opening displacement (CMOD) curves obtained with 8 *mm* PVA fibers are shown in Figure 3.7 a, where the curve of the plain repair material is also plotted for comparison. Only one type of fiber is shown here for sake of conciseness. The allowable maximum crack width for durability of FRC structures ranges from 150 to 300 μm, with the most stringent requirements specified by American Concrete Institute (ACI) 224R [2001]. According to ACI 224R the maximum crack width at the tensile face of reinforced concrete structures is specified as 150 μm for exposure to seawater, seawater spray, wetting, and drying, and 180 μm for deicing chemical exposure. The FRCs here achieve these crack opening values within the stable stage of subcritical crack growth prior to achieving the peak of the response curve and the unstable crack propagation in most cases, or otherwise exhibit significant residual stresses (Figure 3.7 a).

Average values for the peak splitting loads of the different repair materials (representing the onset of unstable crack propagation, point B of Figure 3.5) are plotted as a function of fiber type and content (V_f) in Figure 3.8 a. As expected, a consistent increase of the peak SL is observed for increasing fiber contents, with steel fibers reaching the highest values. With V_f = 1% of the steel fiber, SL is increased from 0.8 *kN* to 2.8 *kN* (around 250%). Similar contents of 8 *mm* and 12 *mm* long PVA fibers provide 175% and 87.5% SL increments, respectively. With a lower V_f, the SL increment is 75%, 62.5%, and 50% with steel, 8 *mm* PVA, and 12 *mm* PVA fibers. Therefore, the incremental benefit from 0.5% to 1% V_f is much higher than the one from 0% to 0.5% V_f.

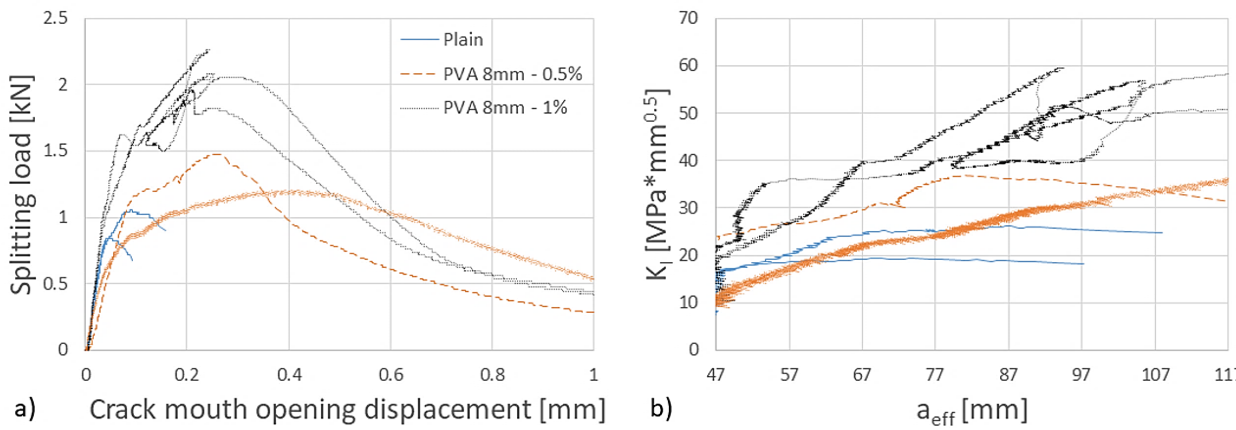

Figure 3.7: (a) Splitting load (SL) vs. crack mouth opening displacement (CMOD) curves of 8 *mm* PVA FRC and (b) crack growth resistance curves (in terms of SIFs, *KI*, vs. effective crack length, a_{eff}) of 8 *mm* PVA FRC

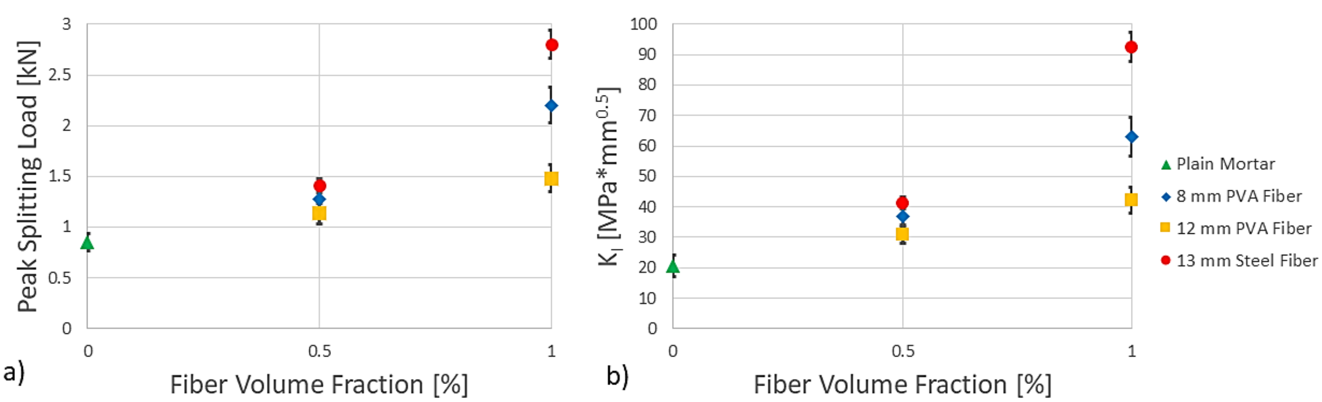

Figure 3.8: (a) Peak splitting loads (SL) and (b) and critical stress intensity factors (K_I) obtained for various fiber types and volume fractions

Crack growth resistance curves in terms of stress intensity factor (K_I) and effective crack length (a_{eff}) were calculated following the procedure described in Section 3.1. Also in this case, only one representative fiber type is shown in Figure 3.7 b and compared to the plain repair mortar, while the full curves for the other fiber types are available in the Appendix. Compared to the plain repair material, fiber reinforced concretes exhibited greater subcritical crack growth branch (BOP-B, Figure 3.5) before the onset of unstable propagation. The critical stress intensity factors (K_{IC}), which represent the initiation of unstable crack propagation, are plotted in Figure 3.8 b for different fiber types and contents. Consistently with the trends observed for the peak SL, K_{IC} increased for increasing fiber contents and highest increment were obtained with 1% V_f steel fibers.

Microcracks encounter greater crack growth resistance and increased toughness in the presence of fibers. Some fibers develop chemical bond with the cementitious matrix that causes stress redistribution around crack tips, promotes crack blunting, and bridges the cracks. This favors the tortuosity of the crack and causes directional deviations. It is expected that larger crack deviation leads to greater crack growth resistance [Zanotti et al., 2014a].

Quantitative correlations between crack deviation, shown in Figure 3.3 b (Section 3.1), and peak splitting load is examined (Figure 3.9 a). It can be observed that higher values for splitting load correspond to greater crack deviation. This is due to the ability of fibers to blunt cracks and cause them to deviate. In this way, more energy is dissipated and higher of splitting loads can be obtained. As crack deviation increases, the enhancement of splitting load becomes more significant. Figure 3.9 b shows dissipated energy (G) versus crack deviation. G corresponds to the area under SL-CMOD curve beyond the peak splitting load up to the crack width of 1 *mm*. While Figure 3.9 a represents the ability of fibers to mitigate subcritical crack growth, Figure 3.9 b demonstrates the effectiveness of fibers in controlling unstable crack propagation beyond the peak splitting load. For example, plain mortar shows slight subcritical crack growth resistance, however, it cannot hinder unstable crack propagation beyond the peak splitting load. By comparing Figure 3.9 a with Figure 3.9 b, one can also observe at which stage of crack propagation each solution is more effective. For instance, increasing the 8 *mm* PVA fiber content from 0.5% up to 1% affects the subcritical crack growth (peak SL, Figure 3.9 b), but the post-peak behavior remains unchanged as similar G values are obtained for the two V_f values (0.5% and 1%).

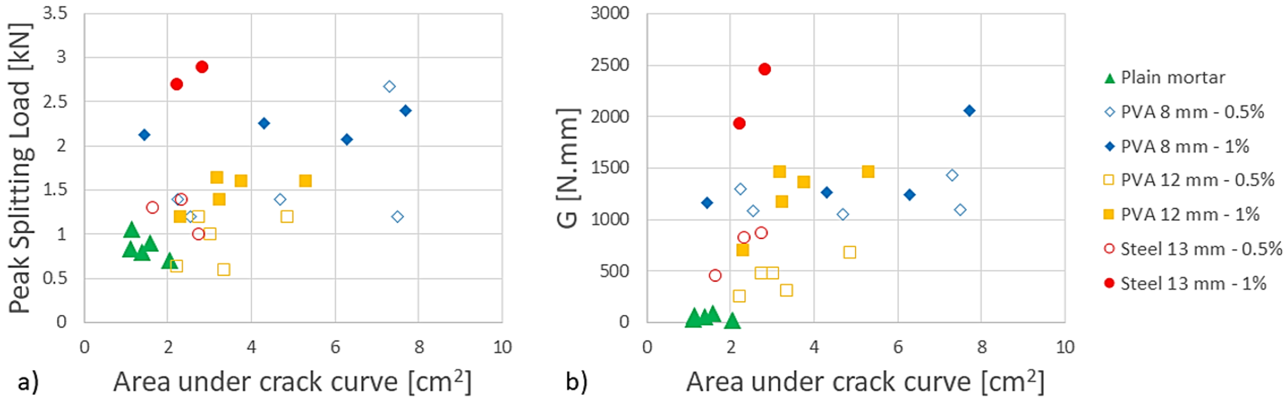

Figure 3.9: (a) Peak splitting load and (b) post-peak fracture energy vs. crack deviation with respect to the midline

3.2.2 Mode-I Crack Growth Resistance of the Substrate-Repair Interfaces (bi-material systems)

The bi-material specimens failed at the interface as expected, with the failure plane passing through and nearby the bond plane. Given the interfacial tortuosity achieved through substrate roughness treatment (sandblasting), some slight deviation of the failure plane from the bond plane was expected and, in fact, desired, as this is a known toughening mechanism in interfacial cracking [Li, 2003] [Zanotti et al., 2014a]. Similar to the material result discussion, the experimental response curves (SL-CMOD) obtained for only one representative type of fibers (8 *mm* PVA) are shown in Figure 3.10 a, while the bond response curves obtained with other fibers are available in Appendix. Some of the crack growth resistance curves obtained using the MLEFM approach described in Section 3.1 are shown in Figure 3.10 b for 8 *mm* PVA fibers. Similar to the FRC materials discussed above, although for smaller values of Splitting Load and Crack Mouth Opening Displacement, concrete substrate-FRC repair interfaces still exhibited stable, subcritical crack growth (Figure 3.10).

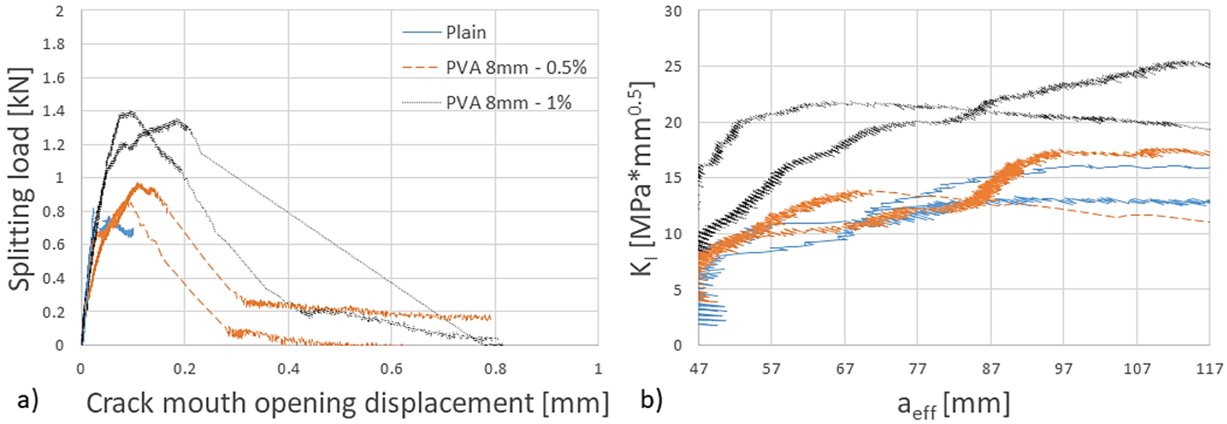

Figure 3.10: (a) Splitting load (SL) vs. crack mouth opening displacement (CMOD) curves of concrete-FRC interfaces and (b) Crack growth resistance curves in terms of stress intensity factor, K_I, vs. effective crack length, $a_{eff.}$

Crack propagation after peak splitting load, however, was quite different. Two main types of post-peak crack propagation were identified, namely: (i) Quick failure along the interface followed by sample split-up in two parts along the concrete – concrete interfaces (Figure 3.11 a), and (ii) micro-crack deviations from the interface followed by slower failure and slight residual splitting load (Figure 3.11 b).

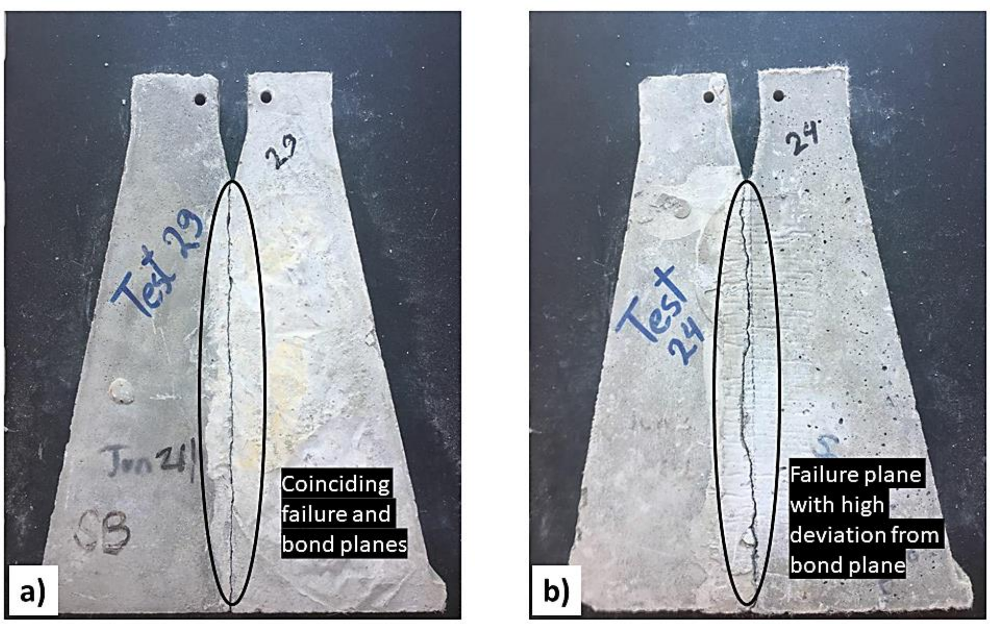

Figure 3.11: Representative failures of the interface for (a) lower crack deviation (plain repair) (b) higher crack deviation (PVA fiber repair)

Figure 3.12 a reports average Mode-I strength values and corresponding fiber volume fractions for three different types of fiber reinforcement. Mode-I bond strength of repair mortars reinforced with 8 *mm* long PVA fibers ranges from 1.1 to 1.5 *kN*. It ranges from 0.8 to 1.1 *kN* for 12 *mm* long PVA fibers and from 1.2 to 1.4 *kN* for steel fibers. Although most of the samples exhibited bond failure, in some specimens, partial material and bond failure was observed.

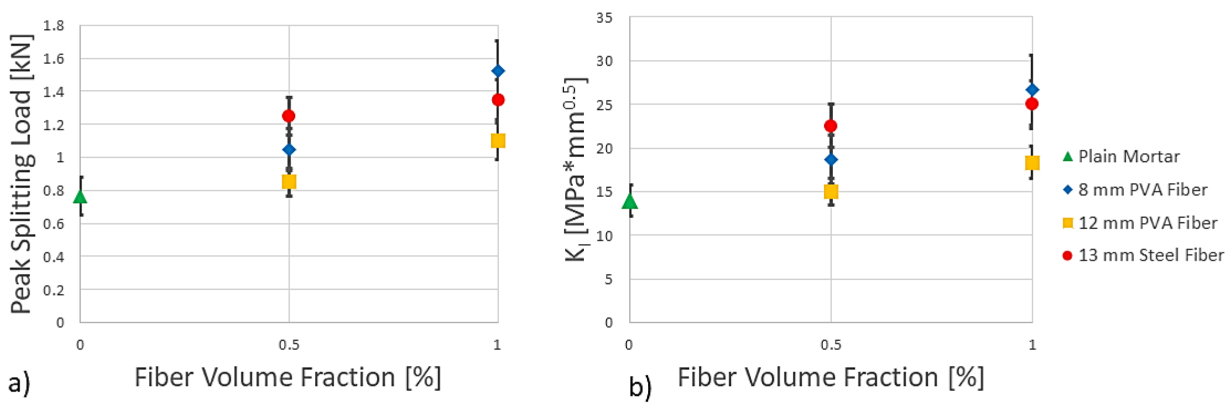

Figure 3.12: a) Peak splitting load (SL) and b) critical stress intensity factor (K_I) of substrate-repair interfaces for various fiber types and volume fractions

3.2.3 Substrate-repair interface cracking: comparison and discussion

Peak values for bond splitting load and the critical stress intensity factor, corresponding to the stress intensity factor at the crack tip prior to the start of unstable cracking, are plotted in Figure 3.12 as a function of fiber type and content. A steady increase was observed as the fiber content (V_f) was increased. With $V_f = 1\%$, peak splitting load and critical stress intensity factor are twice as high as those of the plain concrete. However, while steel fibers outperformed PVA fibers in the material fracture tests (Figure 3.8), quantitative differences between steel and 8 *mm* PVA fibers are negligible when it comes to concrete-FRC interfaces (Figure 3.12). This may be due to the different mechanisms involved in the failure of the material versus the failure of the interface.

In the case of concrete-FRC bond, the beneficial effects of fibers can be classified into two main categories as follows:

1. Fibers reduce interfacial damage, help compatibility, reduce shrinkage and bleeding [Banthia et al., 2014] [Zanotti et al., 2014b] [Banthia and Gupta, 2006];
2. Fibers can provide additional toughening mechanisms for the interface. This is highly dependent on mode of fracture, fiber bonding, size relative to the interface roughness, stiffness, and orientation with respect to the bond plane, and overall deviation of the failure plane from the bond plane [Zanotti et al., 2018] [Li, 2003] [Lim and Li, 1997].

With respect to point 2., it is informative to investigate how many fibers were intersected by the failure plane during crack propagation. An optical microscope was used to measure the number of fibers along the interface. This information is plotted against the peak Splitting Load in Figure 3.13 for the different fibers considered. One can observe that there is a consistent trend between the number of PVA fibers that remained attached to the substrate and were crossed by the failure plane (mixed adhesive-cohesive interfacial failure). No significant correlation was found for the number of steel fibers. This may be due to different fiber sizes, stiffness, and bonding of the two fiber types. Nevertheless, steel fibers had a favorable contribution to bond, comparable or superior to that of PVA fibers, thus confirming that, for different fibers, different mechanisms are involved. For PVA fibers, instead (due to their smaller size and different bonding), the number of fibers crossed at failure can be interpreted as an indication of the amount of cohesive rather than purely adhesive splitting occurring close to the interfacial area.

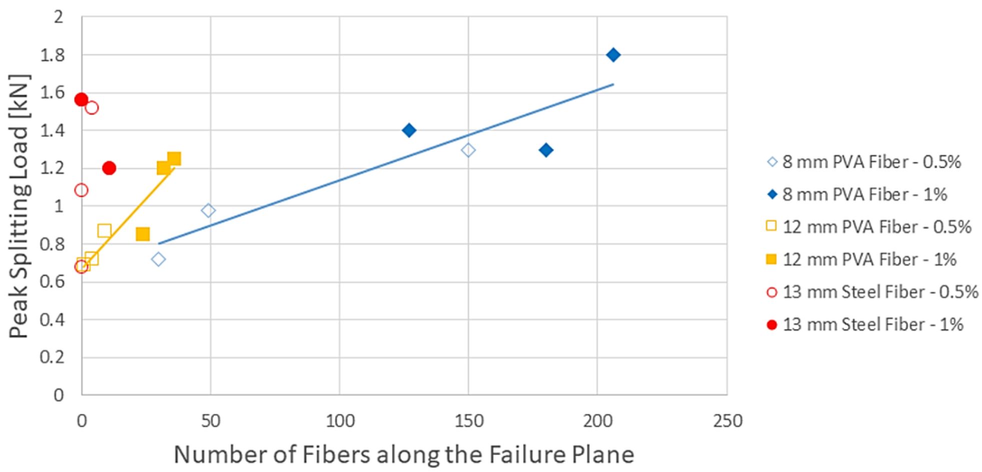

Figure 3.13: Peak splitting load vs. number of fibers along the failure plane after substrate-repair splitting

Because of the good correlation found in Figure 3.13 for PVA fibers, the analysis is extended to investigate possible correlations between the number of fibers crossed by the failure plane and the roughness of the interface. Although sandblasting was performed in the same manner for all the specimens, differences in the roughness parameters obtained (especially when calculated on a relatively small interface area) are inevitable. Based on the 3D surface scanning procedure and analysis described in Section 3.1, roughness quantification parameters were obtained. To author's knowledge, there is no other work that investigates the correlation between quantitative roughness parameters and concrete-FRC bond parameters under Mode-I fracture tests. Hence, the correlation between quantitative roughness parameters and Mode-I crack growth resistance parameters were investigated. The average roughness (*Sa*) exhibited the best correlation with the splitting load (Figure 3.14 a). However, this finding cannot be generalized and other bond strength/cracking parameters (e.g., in Mode II) may be better correlated to other roughness parameters. Interestingly, the peak splitting laod-*Sa* trends are not as clear as the ones depicted in Figure 3.13 for peak splitting load vs number of PVA fibers attached to the failure plane. While peak SL was best correlated to Sa, the number of PVA fibers crossed by the failure plane was found to be best correlated to S_{pm}, a parameter that depicts the maximum topographical gaps in the roughness profile (Figure 3.14 b).

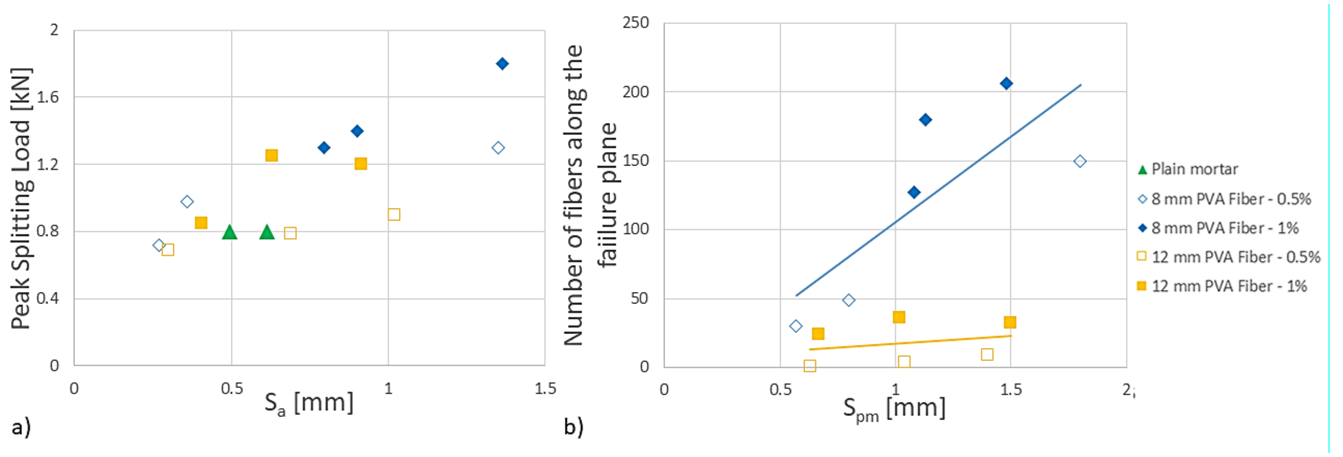

Figure 3.14: (a) Peak splitting load vs. S_a and (b) number of PVA fibers along the failure plane after testing vs. S_{pm}.

3.3 Conclusion Remarks

In this chapter, the effects of different fiber reinforcements and surface treatment on substrate-repair debonding in Mode-I were examined. The main results can be summarized as follows:

1. Significant enhancement of Mode-I crack growth resistance was observed in the repair materials and in the substrate-repair bond after introducing steel and PVA fiber reinforcement to the repair.
2. In the repair materials, a significant enhancement of the overall crack growth resistance curves, peak splitting load, and critical stress intensity factors were observed for increased fiber contents, as anticipated. For example, peak splitting load increments of 50-75% & 87-250% were achieved at 0.5% & 1% V_f, respectively, with steel fibers providing the highest increases. Consistent correlations were found between the Mode-I crack growth resistance of the repair materials and quantified crack deviation, confirming the ability of fibers to

promote crack tortuosity as one of their different contributing mechanisms to crack growth resistance.

3. For the concrete-FRC interfaces, 8 *mm* PVA fibers exhibited the best performance at $V_f = 1\%$, while, in case of $V_f = 0.5\%$, 13 *mm* steel fibers reached the highest fracture load values. This finding may be due to a number of contributing factors, including the stiffness and size of the fibers with respect to the roughness of the interface (as far as failure mechanisms are concerned), the bonding of the fiber to the matrix, as well as the effect of fibers on compaction near and at the interfacial transition zone, the different ability of the various fiber types and contents to mitigate or prevent shrinkage/thermal cracking and bleeding. Some of these aspects are further investigated in Chapter 4.
4. Substrate roughness and interfacial tortuosity had a significant effect on Mode-I crack growth resistance. Minor changes, within the investigated range, in quantified substrate roughness parameters affected fracture parameters (such as the peak splitting load) and, for PVA fibers, also affected the amount of fibers intersected by the failure plane during splitting.
5. For PVA fibers, a correlation was also found between fracture parameters and number of fibers intersected by the failure plane. This was not the case for steel fibers, possibly due to their different stiffness and diameter. Regardless, the beneficial effect of steel fibers on concrete-concrete interfacial crack growth in Mode-I confirms that other bond enhancing mechanisms are in place.
6. The aim of this study was to provide a better understanding of complex mechanisms involved with the interfacial cracking in concrete-FRC composite systems. This information can be used to help the design of repairs and retrofits with fiber reinforced

concrete while striving to optimize stress transfer and durability along the substrate-repair bond, a parameter that is essential to the effectiveness and durability of the retrofitted structure. Finally, the investigation of the failure mechanisms provides information for subsequent modeling of concrete-FRC debonding in Mode I.

Based on these results, the following conclusions can be drawn:

1. Steel and PVA fiber reinforcement can improve mechanical behavior of concrete-FRC interfaces (within the investigated fiber content), and it should be considered as an effective repair material for deteriorated concrete structures.
2. Further toughening effects can be provided by increasing steel and PVA fiber content (within the investigated fiber volume fractions). This can improve load bearing capacity and crack resistance of the concrete-FRC interfaces.
3. Steel and PVA fibers differently affect the behavior of composite systems. Hence, same contents of two different fibers cause different responses.
4. In repair of concrete structures, surface preparation should be done prior to applying repair material. Surface roughness quantification can be done using mean surface roughness and the average of the maximum peak height parameters.
5. Considering surface roughness and fiber reinforcement together is highly recommended for repair of concrete elements. This can provide further toughening mechanisms and cause further improvement of the repaired structures.

Chapter 4: Modelling Tensile Failure of FRC-Concrete Interfaces

As the number of failing concrete infrastructure rapidly increases all around the world, there is an urgent need for durable repair and retrofit techniques. Considering the larger investment required for the maintenance and rehabilitation of failing structures, the effectiveness of these interventions is of vital importance. As mentioned previously, one of the most common techniques for repairing concrete structures is to apply a Fiber Reinforced Concrete (FRC) layer on cracked concrete surfaces. The suitability of employing FRC in repair projects can be mainly attributed to their ability to decrease bleeding, bridge microcracks, improve crack growth resistance, and reduce the extent of damage arising from poor compatibility. Zanotti et al. [2014a] and Kabiri Far and Zanotti [2019] studied the interface behavior of repaired systems under tensile and shear loading. Suitability of using FRC as repair material to improve the quality of the interface in both modes has been demonstrated. Another study by Banthia et al. [1994] investigated the effectiveness of fiber reinforced cementitious composites containing high volume fractions of micro-fibers for thin repair layers. Their results indicate a remarkable improvement of the repair bond strength due to the use of micro-fibers in the repair layer. The overall performance of repaired composite systems is governed by quality of interfacial transition zone , known as the weakest part of the composite system. Among the various factors affecting the interfacial behavior of repaired composite systems, surface roughness, strength of repair material, and compatibility of two adjacent layers play crucial roles.

The first efforts to model concrete-concrete interface behavior go back to the 1960s. Various milestones were reached over six decades of modelling cementitious interfaces. Birkeland and Birkeland [1966] were the first researchers who proposed a linear design expression to assess the ultimate shear stress of concrete interfaces. Mattock and Hawkins [1972] and Loov [1978] were the first researchers to consider compressive strength of concrete as a factor affecting interface strength. Walraven et al. [1987] proposed a non-linear function comprising the effect of reinforcement ratio, the yield strength of the reinforcement, and the concrete compressive strength. Tsoukantas and Tassion [1989] considered the effect of surface preparation and proposed different expressions for smooth and rough surfaces. Randl [1997] presented a design expression which explicitly included the contribution of cohesion, friction and dowel action. Finally, Santos and Julio [2011, 2010] performed a quantitative evaluation of surface roughness and explicitly included a roughness value in their proposed design expression.

As far as the influence of surface roughness on the interfacial behaviour is concerned, a number of research papers have been published. Santos and Julio [2014, 2011] investigated the effect of surface preparation on longitudinal shear strength between concrete layers cast at different times. Various surface preparation methods were employed, and a non-destructive *in-situ* method was developed to perform a quantitative assessment of roughness of a concrete surface [Santos and Julio, 2011]. The results indicate that the roughness of the concrete substrate has a significant influence on the bond strength of substrate-repair interfaces. The bond strength of the interface increased with increasing roughness. Another study was done by Lukovic et al. [2014, 2013] where various surface profiles were used in numerical experiments. Extensive debonding occurred in the case of smooth interfaces. However, rough interfaces encouraged distributed cracking and a trend towards cohesive failure. The other important point highlighted in the literature is that there is a certain threshold value for the roughness of interfaces beyond which, a further increase in roughness will no longer improve bond strength [Wagner et al., 2013] [Silfwerbrand et al., 2011].

The other governing factor of the composite system is the strength of the repair material. Hofbeck et al. [1969] and Mattock and Hawkins [1972] were among the first researchers to investigate the role of repair material strength on concrete-concrete interface strength. Their results indicated that there is a limit below which concrete strength does not affect interface strength. Above this limit, however, stress transfer is affected, and interface strength is increased by increasing concrete strength. Loov [1978] was the first researcher who explicitly included the concrete strength in an expression to predict interface strength. His non-dimensional expression for a concrete with a compressive strength equal to 30.9 *MPa* accords with other research works where concrete strength was not considered. For other types of concrete, however, the outcomes were different. Later, more general non-linear functions for predicting the shear interface strength were proposed, which considered concrete strength as an input [Walraven et al., 1987] [Mattock, 1987]. In another paper, Lin and Chen [1989] mentioned that previously proposed expressions are not valid for concretes with low compressive strength. As a result, a new design expression was proposed for concretes with high compressive strength. Finally, Mattock [2001] and Mansur et al. [2008] proposed design expressions applicable to concrete with different strengths, from low to high strength.

The other governing factor for composite behavior in repaired systems is the compatibility (e.g. thermal and mechanical) between old and new layers [Emmons, 1994]. Unlike surface texture and strength of the repair layer, compatibility is not well-addressed in previous studies. In most of studies to-date, the issue of compatibility is limited to employing repair layer which is more compatible with the substrate rather than using various compatible/incompatible repair materials and comparing outcomes. Compatibility can be defined in terms of mechanical behavior, dimension, and thermal response. Highly incompatible materials might not work properly together. The incompatibility can cause additional stress concentration leading to failure of the system.

Good quality repaired systems need to be able to withstand the effects of environmental conditions, applied loads, as well as maintain their level of performance during their service life. In this context, substrate-repair bond and fracture properties of composite systems are both of critical importance. A composite system with higher critical stress intensity factor exhibits higher resistance to crack propagation under certain load, less exposure to severe environmental conditions during the service life, and higher durability. Also, the maximum load bearing capacity of composite systems is important for both short-term and long-term responses of repaired systems. The higher the bond strength, the lower probability of nucleation of microcracks and failure of the composite system.

Although there are various proposed models for predicting interfacial behavior of concrete-concrete composite systems, most of them are focused on ultimate shear strength of the interface. To the best of author's knowledge, research on modelling failure behavior of concrete-FRC interfaces under tensile stresses taking into account the impact of repair layer strength, surface roughness, and ductility is not adequately addressed in the literature. This chapter aims to develop a design expression, based on experimentation, to predict mechanical response of concrete-FRC interfaces under Mode-I loading. This design expression model is not only capable of predicting maximum load bearing capacity of composite systems but also gives a predictive model for crack growth resistance curve which is relevant to the durability of the system.

4.1 Methodology

Various concrete-FRC interfaces are evaluated using contoured double cantilever beam tests. Load-displacement response curves and crack growth resistance curves are obtained from collected experimental data. In order to study the impact of surface preparation, all substrates are scanned prior to casting repair layers. Predictive models are developed based on semi empirical crack growth resistance curves and load-displacement response curves for different repair/substrate layers and surface preparation. Some data was obtained from a previous study [Kabiri Far and Zanotti, 2019]. Additional experiments using the same methodology were performed, including additional materials and roughness levels, so as to attain a comprehensive dataset.

4.1.1 Contoured Double Cantilever Beam Test

CDCB test is thoroughly explained in Chapter 3. It is a splitting fracture test used to quantify mechanical properties of materials and bi-material systems under tensile stresses. This technique was first employed for structural adhesives and later adapted for evaluation of fracture properties of monolithic materials and cement-based interfaces. The test is based on applying a splitting load to propagate a crack in a pre-notched specimen. The applied load and the opening displacement of the crack faces are monitored during the test which can be used for determination of fracture properties. Due to specific geometry of the specimens, which allows application of smaller splitting loads and larger displacements, more reliable compliance measurements are feasible. Tapering the samples helps to make the rate of strain release theoretically independent of crack length and more stable crack propagation.

For monolithic specimens, a side groove was placed along the desired crack plane to foster desired crack growth and avoid any adverse crack deviation. In the case of composite specimens, where each specimen was subdivided into two symmetrical parts with the concrete substrate on one side, the repair layer on the other side, and the interface in between, the interface represents a plane of weakness. Hence, to reduce damages during handling, the side groove was removed. This difference between monolithic and composite specimens is accounted for in the back-calculations of fracture analysis.

These tests employed a servo-hydraulic Instron universal testing machine, using the method described in Section 3.1.2.1. To obtain fracture parameters and the crack growth resistance curves, a procedure based on Modified Linear Elastic Fracture Mechanics (MLEFM) was employed. Details of MLEFM and back-calculations can be found in Section 3.1.2.3.

4.1.2 Materials Selection

Table 4.1 presents the mix proportion of substrate and repair layers. Two different types of specimen were employed: monolithic and composite. While the first type was used for material characterization of the repair layer, the second type was used for evaluation of interfacial behavior of FRC-concrete composite specimens. For the repair materials, in addition to plain concrete condition without fibers, two types of fiber with volume fractions $V_f = 0.5\%$ and 1% were used including: (1) 8 *mm* long Poly-Vinyl-Alcohol (PVA) fibers and (2) 12 *mm* long PVA fibers. In order to address the effect of ductility, two different substrates were investigated where substrate A had higher modulus of elasticity and more brittle behavior compared to substrate B.

To prepare composite specimens, concrete substrates were cast, covered by plastic sheets after casting, demoulded after 24 hours, and finally cured at a standard temperature of $20 \pm 2°C$ and relative humidity $95 \pm 5\%$ for 28 days. Before casting repair layers, the substrates were sandblasted, using the method described in Chapter 3. Sandblasted surfaces were scanned, as above, for roughness quantification prior to casting repair layers. Afterwards, substrates were put back into the moulds under an optimum Saturated Surface Dry (SSD) condition [Momayez et al., 2005] and the repair layer was cast against the substrate. The composite specimens were cured for another 28 days under the same condition. Monolithic specimens were also cast at the same time as of casting of repair layers and cured for 28 days in a curing room. Further details of sample preparation can be found in Kabiri Far and Zanotti [2019].

Table 4.1: Mix proportions of substrate and repair layers

	Cement	Fly Ash	Sand	10mm Aggregate	Water	Fibre Volume Fraction
Substrate A	1	0.25	2	0.48	0.5	----
Substrate B	1	---	2.5	1.7	0.42	----
Repair	1	0.25	2	---	0.5	0%, 0.5% & 1%

4.1.3 Roughness Quantification

In order to assess the impact of surface preparation on mechanical properties of FRC-concrete interfaces, roughness evaluation is required. In this chapter, the topography of sandblasted substrates was assessed following a similar procedure to that described in Chapter 3. However, unlike in Chapter 3, a 2D profilometer was employed. In order to minimize the errors induced by limited variability range of a 2D scanner (compared to the 3D scanning technique), several linear profiles in different regions of the surface were collected and examined for each specimen.

4.1.4 Materials Characterization

Compressive strength of repair and substrate layers were investigated based on ASTM C39 standard using a Forney machine. At least three specimens with height of 20 *cm* and diameter of 10 *cm* were cast and cured for 28 days in curing room (temperature of 20 ± 2°C and relative humidity 95 ± 5%) and tested for each mix design. In order to obtain splitting tensile strength of repair and substrate layers, splitting tests were performed according to ASTM C496. Cylinders with a length of 20 *cm* and diameter of 10 *cm* were cast and cured for 28 days in curing room.

4.2 Results and Discussion

4.2.1 Materials Properties

Figure 4.1 shows compressive strength, splitting tensile strength and calculated elastic modulus of two substrates compared with the average for the repair materials used in this study. Compressive strength varies from 44 to 66 *MPa*, splitting tensile strength varies from 3.7 to 5.8 *MPa*, and the modulus of elasticity varies from 30 to 38 *GPa*. As expected, repair materials and substrate A exhibit similar average mechanical properties; however, substrate B has lower compressive and tensile strength as well as a lower elastic modulus. While substrates A and B as well as plain mortar tend to exhibit a brittle failure in compression and splitting tests, the failure mode of fiber reinforced repair materials was slower and more controlled. In addition, substrate B exhibits lower stiffness compared to substrate A and repair materials. This difference can affect the ductility of the system and provides us with an opportunity to study the effects of ductility on the overall response of the composite system.

Indirect tensile strength is quantified based on the following equation:

$$f_{ct} = \frac{2P}{\pi A} \tag{4.1}$$

and modulus of elasticity is quantified experimentally and also calculated from compressive strength using equation suggested by ACI 318-08:

$$E_c = 4700\sqrt{f_c} \tag{4.2}$$

Figure 4.2 compares experimental and calculated elastic moduli. Calculated *E* values are employed in the following sections due to their lower variability.

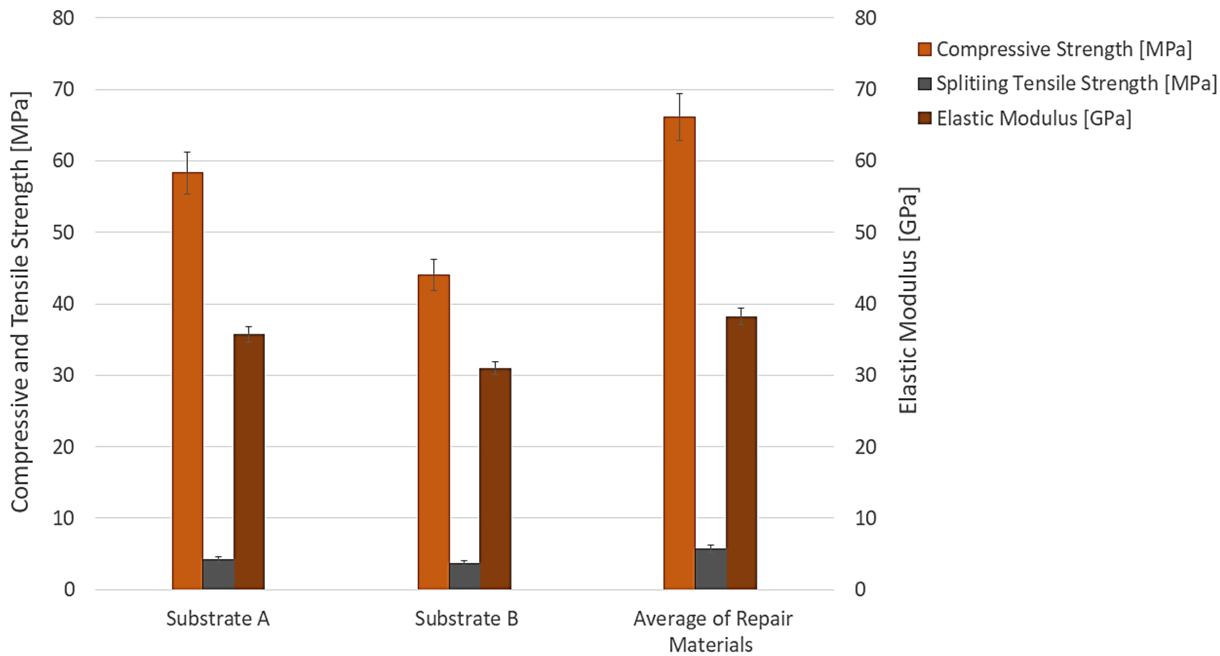

Figure 4.1 Compressive strength, splitting tensile strength, and elastic modulus of substrate and repair materials

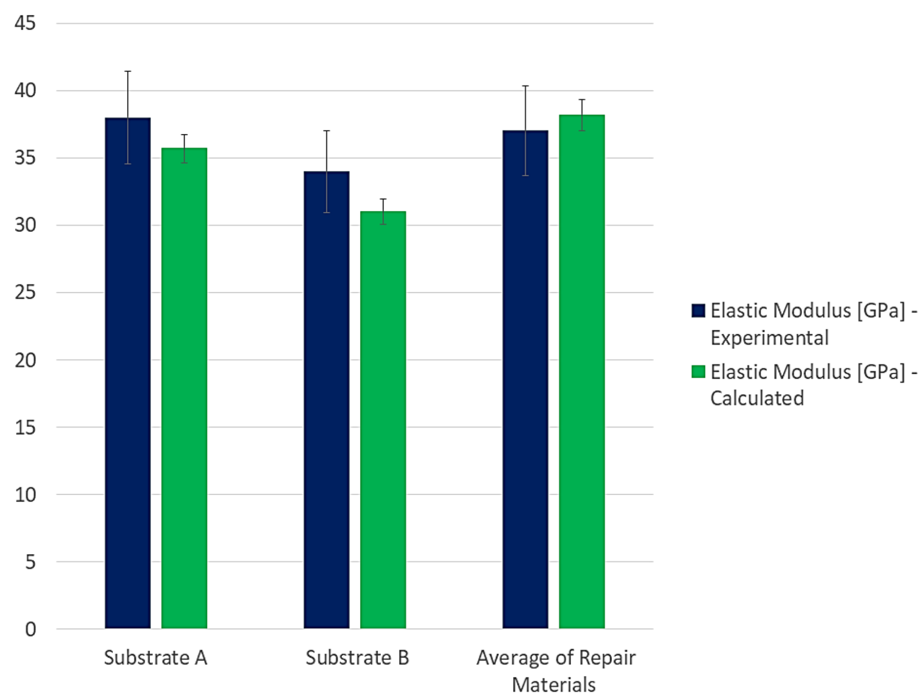

Figure 4.2 Comparison between experimental and elastic modulus of substrate and repair materials

4.2.2 Interfacial behavior in Mode-I: effect of materials' properties and surface roughness

In this section, semi-empirical models are provided based on experimental results and mechanical behavior of concrete-FRC interfaces. A concise summary of the primary governing factors - based on the experimental study presented in Chapter 3 and the literature reviews presented in Chapter 2 - is provided hereafter:

1. Interface roughness: Improved interface roughness can help with better mechanical response as a result of increased contact area and crack deviation. This has been demonstrated in Figures 3.11 and 3.12 as well. However, extra surface treatment will lead to interfacial microcracks and damages which explains the saturating behavior of mechanical response-surface roughness which can be observed in previous research works [Silfwerbrand et al., 2011] as well as results of this study.
2. Material strength and role of fibers: Having a repair material with higher strength can help with improved ITZ and composite behavior of the system. Furthermore, introducing fibers to the repair material can enhance interfacial response through increasing stability of the interfacial transition zone, avoiding pre-loading damages (both aspects will be further explored in Chapter 5), and providing further micromechanical mechanisms, such as crack bridging and crack blunting, to increase load-bearing capacity of the system. This has been demonstrated in Figure 3.10. On the other hand, a very strong repair material may increase brittleness of the system and decrease maximum strain capacity of the interface, which justifies a saturating trend of interfacial mechanical response versus material strength. This trend is further explained in this chapter and is compatible with previous research studies [Mattock and Hawkins, 1972].

3. Ductility of the composite system: To have a durable and long-lasting repaired structure, it is quite vital to consider ductility of new and old layers. Very brittle layers are not able to endure high strains. This would negatively affect the performance of the interface and increase likelihood of debonding. A very strong material increases the brittleness of the structure, while on the other hand, a weak material decreases the maximum stress capacity of the interface. As a result, ductility needs to be addressed very carefully. The results of this study, as well as previous research works, suggest that having a repaired element with slightly higher ductility may improve the overall response of the repaired element.
4. Synergistic effects of surface treatment and repair material: surface roughness and fibers within the repair matrix can intensify or decrease the effectiveness of each other. As presented earlier in Figure 3.12, higher surface roughness can get more fibers involved in the interfacial failure process. This can help with activating further micro-mechanisms, provided by fibers, and enhancing interfacial response. These mutual effects are thoroughly analyzed in Chapter 3.

In order to obtain an expression representing the relationship between maximum interfacial splitting load, surface roughness, and mechanical properties of repair and substrate layers, the relationship between interfacial tensile strength and tensile strength of repair layer and also the relationship between interfacial tensile strength and surface roughness are investigated separately. In this chapter, the same substrate (substrate A) is used for all specimens to remove the effects of substrate properties and compatibility variations on composite response, and to study the impacts of roughness and mechanical properties of repair layer.

Figure 4.3 shows interfacial tensile bond strength plotted against surface roughness. It is well known that interfacial behavior of composite systems is highly affected by surface preparation

[Kabiri Far and Zanotti, 2019; Santos and Julio, 2011]. One can observe that the trendline follows a similar saturating behavior for different types of repair material. The difference between curves is related to mutual effect of material properties and roughness values on the behavior of composite systems. This mutual behavior is shown in the following graphs. Increasing roughness results in better interfacial bond up to a certain point, beyond which further increase of roughness does not contribute to improvement in bond strength. This behavior is governed by the type of repair material. In other words, different types of repair material result in different rate loss, and accordingly, different level of improvement of interfacial bond. This trend accords with previous research. Silfwerbrand et al. [2011] mentioned that a specific threshold value exists for the roughness of the interface between substrate and repair layers. Beyond this threshold value, further increases in roughness do not enhance the bond strength. Work by Santos and Julio [Santos and Julio, 2010 & 2011] also examined the relationship between surface roughness, cohesion, and friction. Their expressions for cohesion and friction contain saturating power function for roughness. Further increase in roughness of the substrate surface, can increase damage at the interface. This damage can be in form of microcracks which can later coalesce creating macrocracks, which lead to failure. Such damage may explain the saturating behavior of the trendline between interfacial tensile bond strength and surface roughness. One must notice that the ascending fitted curve in Figure 4.3 has a low R^2 value. To address this issue, the mutual effect of repair material properties and roughness are investigated in Figures 4.4 and 4.5.

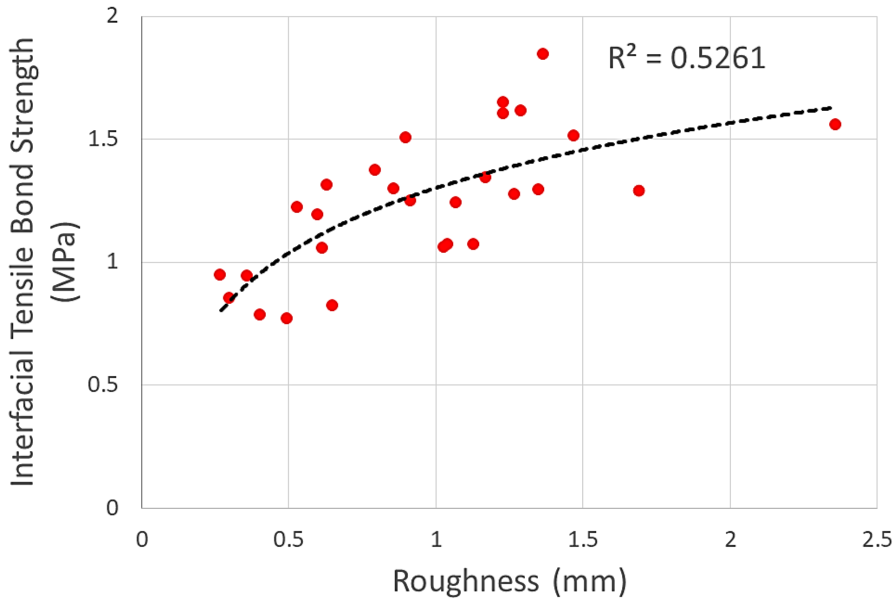

Figure 4.3 Interfacial tensile bond strength versus average surface roughness

In Figure 4.4, data points are categorized based on their level of roughness, where $0 < Ra < 0.5$ is considered as low roughness; $0.5 < Ra < 1$ as medium roughness; and $1 < Ra < 1.5$ as high roughness . Categorizing dataset based on a secondary variable (surface roughness) has a positive effect on fitting outcome and confidence level leading to higher R^2 values. It can be observed that employing stronger FRC repair layers (higher fiber volume fraction) improves interfacial tensile bond strength. Considering fracture mechanics, higher material strength corresponds to greater volume fraction of fibers; the enhancement of interfacial crack growth resistance can be explained by the beneficial effects of the addition of fibers. Fibers mitigate interfacial damage, shrinkage and bleeding [Banthia et al., 2014; Zanotti et al., 2014b]. Furthermore, they can provide additional toughening mechanisms by the interface [Lim and Li, 1991; Momayez et al, 2005]. The rate of this enhancement, however, is not constant and decreases as the strength of repair concrete increases. This behavior accords with results of previous research. For example, Mattock and Hawkins [1972] investigated the effect of concrete strength on the shear strength of concrete-

concrete interfaces and obtained a similar saturating curve. Also, Walraven et al. [1987] studied the shear friction capacity of concrete-concrete interfaces taking into account the compressive strength of concrete. Their proposed expression included a saturating power function between interfacial splitting strength and material strength. This behavior can be explained as a result of incompatibility between substrate and repair layers. As tensile strength of repair layer increases beyond a certain point, the incompatibility between two layers becomes more exaggerated and the mutual behavior of these layers in a composite system is adversely affected.

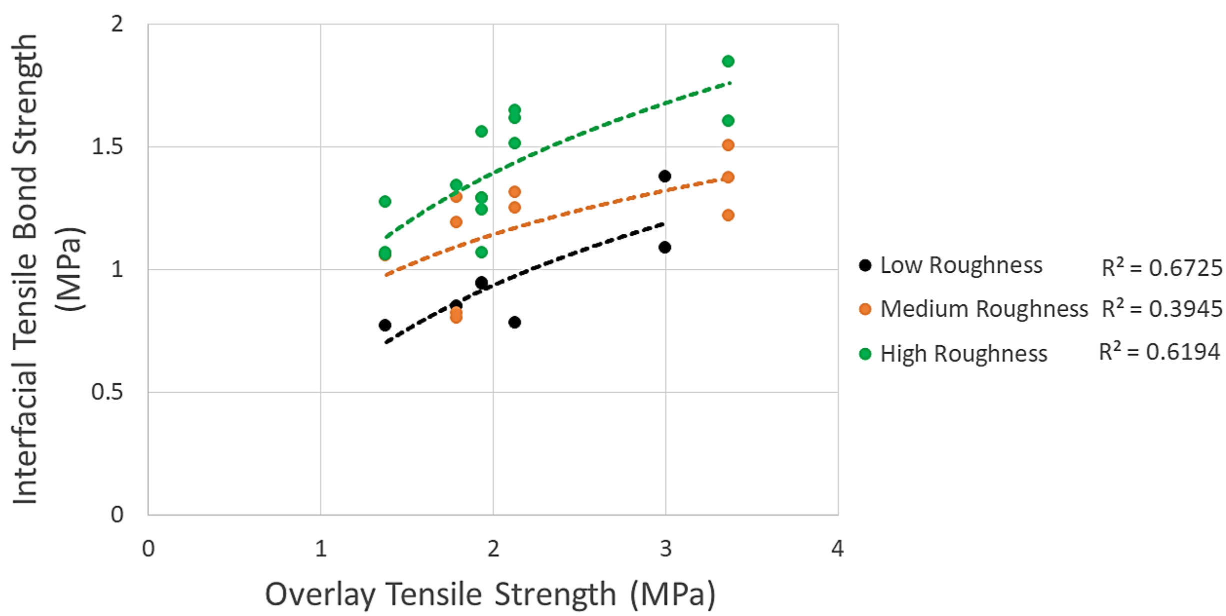

Figure 4.4 Interfacial tensile bond strength versus tensile strength of repair material for different roughness categories

The same approach was employed in Figure 4.5 where data points are separated based on their associated repair material. Once again, considering a second variable (type of repair material) leads to clearer final results with more consistent curves and higher confidence level. After comparing Figures 4.4 and 4.5 one can observe that the roughness-based model is giving more reliable outcome. One source of error in a repair material-based model is that since material properties and composite strength are derived from tests on different types of specimen, it is difficult to correlate data points one-by-one to each other. Any solution including averaging repair material strengths can introduce further errors in the model. As a result, it seems reasonable to consider roughness as the primary variable for a model while overlay tensile strength can be considered a secondary variable, which can be addressed later by applying a correction factor to the main model.

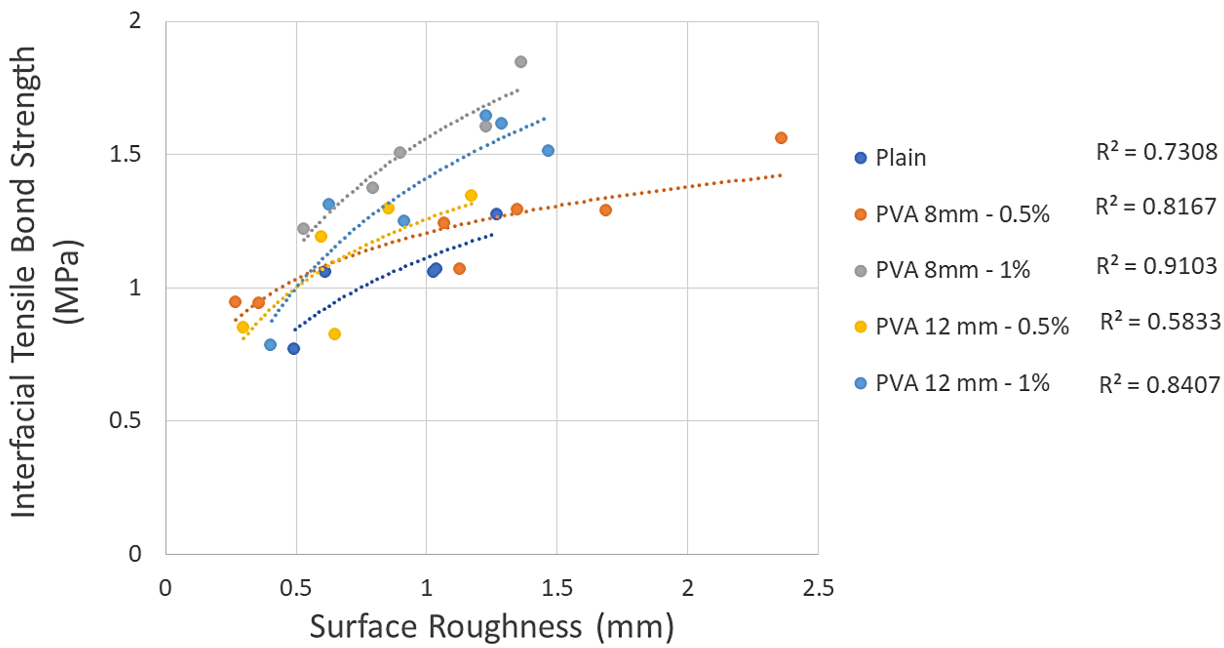

Figure 4.5 Interfacial tensile bond strength versus surface roughness for different repair materials

4.2.3 Proposed Expression for Load Bearing Capacity of Concrete-Concrete Interfaces under Tension

There are various factors that affect the behavior of composite repair systems including properties of repair material, characteristics of substrate layer, topography of the surface, adhesive materials applied on the substrate, curing condition, saturation level of substrate before applying repair layer, compatibility etc. (as described above). Considering that including all abovementioned factors in a single study is a formidable task and requires extensive experimental work, and that some of these factors have already been investigated in other research works [Lukovic, 2016], the focus of this study is on the three most dominant factors affecting the composite behavior, namely properties of repair and substrate materials, topography of the substrate surface, and ductility of two layers. These three factors have higher priority not only because of their direct effect on the final response of the system, but also because in practice, these three factors are easy to modify. This study can be divided into two parts where the effects of substrate properties and surface preparation are addressed first, and the ductility issue is then examined.

In order to obtain an expression representing the relation between interfacial properties (in terms of maximum tensile strength (f_t)), surface roughness, strength of repair material, and ductility criteria, experimental data are analyzed using Matlab's regression module. Regression used the least square method. This is a standard regression analysis approach where the sum of squares of the residuals corresponding to the results of every single equation is minimized in the overall solution.

$$r_i = y_i - f(x_i, \beta) \qquad 4.3$$

$$S = \sum_{i=1}^{n} r_i^2 \qquad 4.4$$

In these functions, r_i is the residual, y_i is a dependent variable, x_i is an independent variable, and f (x, β) is the model function. Various regression models are employed and compared with one another, including tangent hyperbolic, power, exponential, and logarithmic functions. Based on the results, the nature of the problem, and relevant research works available in the literature [Santos and Julio, 2014] [Mattock and Hawkins, 1972], the saturating exponential function is considered as the main model function.

$$y = a_1 (1 - e^{a_2 x}) \qquad 4.5$$

Figure 4.6 compares these models. Generally, these models can be categorized based on their saturating (Figure 4.6 a & d) or non-saturating behavior (Figure 4.6 b & c) as well as their intercepts. Figure 4.6 a represents tangent hyperbolic regression model with non-zero intercept. Although the saturating behavior is aligned with findings in the literature, the non-zero intercept overestimates bond strength of smooth surfaces. Figures 4.6 b & c represent power and logarithmic regression functions; however, both suffer from sharp ascending curves even beyond high roughness level which does not accord with previous research findings. Figure 4.6 b contains an exponential regression function which seems to be the best model due to it saturating behavior, zero y-intercept, and acceptable R^2 values. It should be acknowledged that bond strength of smooth surfaces is not quite zero, but due to its small value it can be conservatively considered to be zero [Santos and Julio, 2014]. Based on fracture mechanics, increased interfacial tortuosity achieved through the substrate surface treatment (sandblasting), which can promote slight deviation of the failure plane from the bond plane causing further toughness increases [Li, 2003]. Higher roughness values promote greater subcritical crack growth as well as more stable crack propagation. In the case of FRC as repair material, crack deviation and cohesive failure can activate toughening mechanisms provided by fibers in the repair material. The concept has been described more fully in Chapter 3. However, extensive surface treatment might not be beneficial. This saturating behavior is attributed to possibility of inducing microcracks at the interface as a result of extensive sandblasting which results in higher surface roughness. This behavior is well-supported by other studies in the literature as explained in Section 4.2.3.

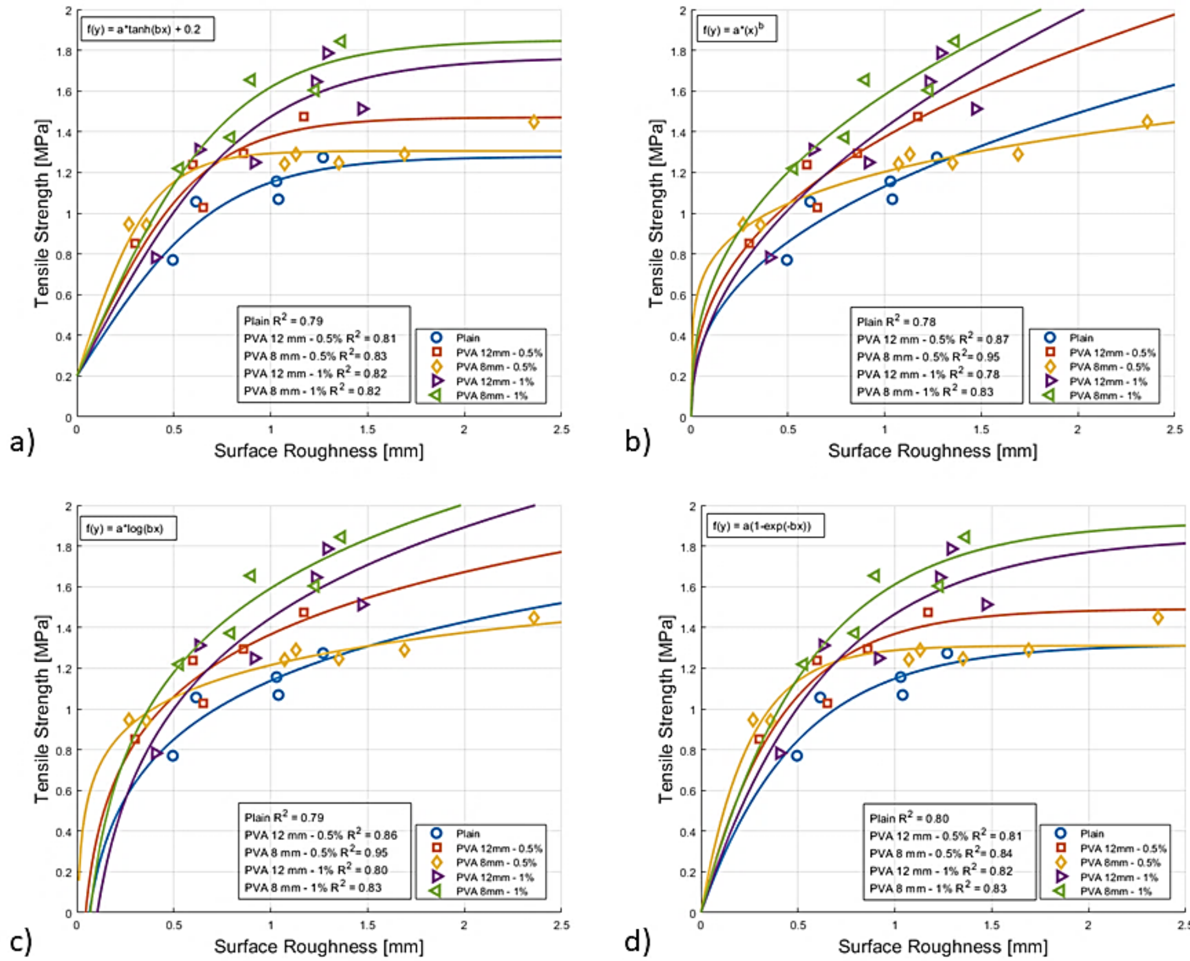

Figure 4.6 Different regression functions to model tensile bond strength as a function of surface roughness and mechanical properties of repair material a) Tangent hyperbolic, b) power, c) logarithmic, d) exponential regression models

Hence, following exponential function can be considered as the main model to predict behavior of composite system with plain repair material.

$$f_{tc} = 1.32\ (1 - e^{-2.05Ra}) \qquad 4.5$$

where f_{tc} is tensile bond strength of composite systems in MPa and R_a is average roughness in mm.

Table 4.2 shows correction factors for four other types of repair material and R^2 values for each material. The confidence level of the proposed design equations is 95%. In general, adding fiber to repair material avoids nucleation of microcracks during curing and prior to loading stage, and also provides further toughening during loading via crack blunting and crack bridging. These positive impacts are amplified with higher fiber content which explains why the repair material with 1% fiber ratio exhibited better bond strength compared to the material with 0.5% fiber ratio or the plain repair material. Some of these positive impacts, however, are also influenced by surface texture. In other words, some toughening mechanisms will be activated only if minimum surface roughness is provided. That is why bond strengths of different repair materials at very low surface roughness were almost similar. All these aspects are more fully explained in Chapter 3.

This model can predict the behavior of composite systems with similar, but not identical, materials within specified range of surface roughness and material strength, which are common values relevant to practical use of repair materials.

Table 4.2 Model correction factors for different types of repair material

$\boldsymbol{f(y) = 1.32a\,(1 - e^{-2.05bx})}$	**a**	**b**	$\mathbf{R^2}$
Plain Repair	1	1	0.80
PVA 12mm 0.5%	1.12	1.21	0.81
PVA 8mm 0.5%	1.01	1.97	0.84
PVA 12mm 1%	1.4	0.76	0.82
PVA 8mm 1%	1.45	0.89	0.83

4.2.4 Effect of Ductility on the Composite System

While the previous section was concerned with concrete-FRC interfaces where repair and substrate layers are exhibiting same elastic modulus, the focus of this section is on concrete-FRC systems with a softer substrate. Employing a softer material can affect bond strength and crack growth resistance, as well as maximum strain capacity and overall ductility of the system. A new set of specimens were prepared using a new mixture design for the substrate layer (substrate B) and keeping the same repair layers used in the previous investigations reinforced (12 *mm* PVA fibers at V_f = 1*%* were selected). To quantify ductility of two adjacent layers, elastic modulus ratio is employed as the ratio of overlay elastic modulus to that of the substrate. Elastic modulus ration of 1 indicates that both substrate and repair layers exhibit same level of ductility. Higher values than 1, where elastic modulus of the substrate decreases, indicate softer and more ductile composite systems. However, higher values than 1 where elastic modulus of the overlay is increased, indicate stiffer composite systems.

$$\text{Elastic Modulus Ratio} = \frac{E_O}{E_S} \qquad 4.6$$

where E_0 is the elastic modulus of the overlay and E_s is the elastic modulus of the substrate. The average elastic modulus ratio for concrete-FRC interfaces with substrate A, addressed in Section 4.2.3, is around 1.05 and for the new concrete-FRC interfaces with substrate B it increased to 1.25 indicating that newly introduced concrete-FRC system is more ductile compared to previous ones.

The new set of specimens were tested and their associated regression model was compared to the regression model of previously tested specimens (Figure 4.7), which was already presented in Section 4.2.3, where same repair material (FRC with PVA 12 *mm* 1*%)* was employed for both specimens with two different substrates (substrate A & B). The same exponential regression model is employed as in Section 4.2.3. It can be observed that although the second set of specimens, where substrate B is employed, has a higher elastic modulus ratio, it has stronger tensile bonds between two adjacent layers. This suggests that the issue of ductility between two adjoining cementitious materials is more complicated than was previously thought. Although significant differences between properties of two layers is not suggested by previous researchers, small differences within a specific range may have positive effects. In the other research works, the same improvements are reported, provided that repair layer is stronger than the substrate. However, for the other cases where repair material is weaker than the substrate, load transfer is not adequate, and the two materials are considered as incompatible [Pattnaik and Rangaraju, 2007]. In other words, with a softer substrate, the composite system can exhibit higher ductility and improved mechanical performance. . This might be explained by the fact that a substrate with lower stiffness, here substrate B, exhibits more ductile behavior in comparison to the stiffer substrate here, substrate A. A more ductile substrate not only helps with increasing ductility of the whole system, but also may positively affect stress distribution among two layers, which can enhance load transfer to the repair layer. It also helps by taking advantage of ductile behavior of the repair material and increased cohesiveness of the failure. A low-modulus substrate material has higher deformation capacity [Pattnaik and Rangaraju, 2007] [Liu et al., 2016]. This helps with avoiding debonding due to thermal deformations where repair layer has high deformation capacity. Substrate materials that have limited deforming capacity can adversely affect mechanisms of load transfer as well as overall composite response. Further cohesive failure of repair material in the second type of specimens is represented in Figure 4.8. While repair material can be seen in various parts of substrate B, substrate A shows more adhesive failure.

Table 4.3 shows model variables for two classes of concrete-FRC interfaces. In Sections 4.2.3 and 4.2.4, various types of repair materials in addition to two different substrate layers are investigated. Based on fundamental similarities in mechanical behavior among different cementitious materials and considering the scale of this experimental study and number of tested specimens, one can suggest that similar model function would work for other repaired systems provided that appropriate calibration is applied. Two different approaches for calibration can be suggested.

General calibration, which is easier to do but less accurate than precise calibration, is based on strength class of repair materials. By having maximum tensile strength of repair material, one can come up with appropriate correction factors for a specific material based on models provided here. The shortcoming of this quick calibration method is that the way different fibers (or other agents like nanomaterials) affect fracture of the interface has not been addressed, but only final tensile strength of repair material is used for calibration. To consider the effect of different fibers (or other strengthening agents) on cracking behavior, which leads to slightly different correction factors for materials which exhibit same strength class by employing different fibers, at least two tensile tests on composite specimens need to be performed including both low roughness and high roughness substrates. This can help with obtaining quite accurate calibration factors based on model function suggested here.

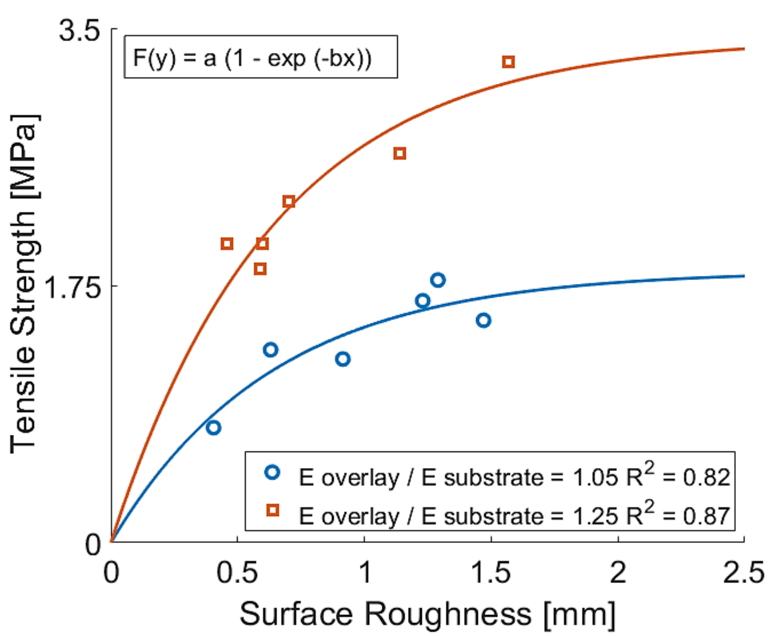

Figure 4.7 Comparison of regression models corresponding to different elastic modulus ratios

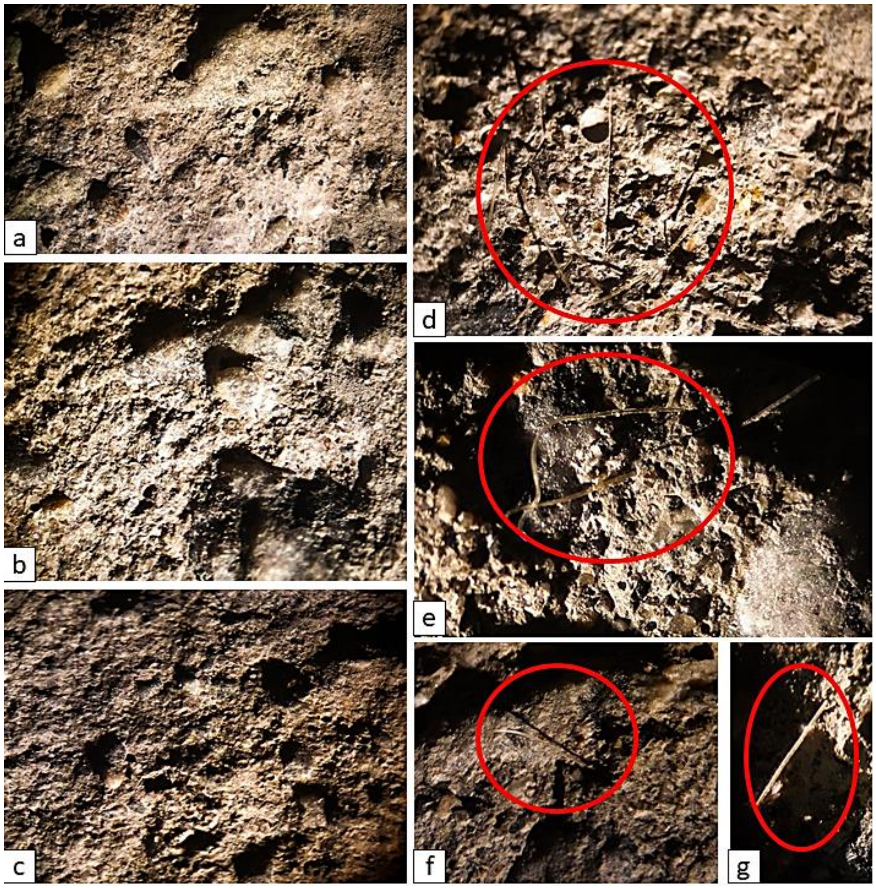

Figure 4.8 Failure surface of substrate A (a-c); failure surface of substrate B (d-g)

Table 4.3 Correction factors for two classes of composite systems with same repair material but different substrates and ductility

$f(y) = 1.32a\,(1 - e^{-2.05bx})$	a	b	R^2
Substrate A - PVA 12mm 1%	1.24	0.76	0.82
Substrate B - PVA 12mm 1%	2.59	0.75	0.87

4.2.5 Modelling R-curve under tensile loading regime

This section is focused on modelling long-term behavior of concrete-FRC interfaces subjected to tensile stresses. R-curve is not only a common way to evaluate durability of materials and their vulnerability to the penetration of dangerous substances but also provides further information on structural behavior of repaired system. A higher initial stress intensity factor indicates greater crack nucleation resistance, while the maximum stress intensity factor at the plateau of a material's or an interface's R-curve represents the material's resistance to crack propagation. In other words, beyond the maximum stress intensity factor, rapid, unstable development of macrocracks occur leading to the system's failure as explained in Chapter 3.

R-curves corresponding to different tested repaired systems are modelled using experimental data for CDCB tests and based on a saturating exponential function (Figure 4.9). Different models are proposed for different repair materials. In addition, roughness level (i.e. Low roughness: $R < 1$ *mm*, High roughness: $R > 1$ *mm*) and compatibility criteria (corresponding to substrate B) are addressed following previous discussions.

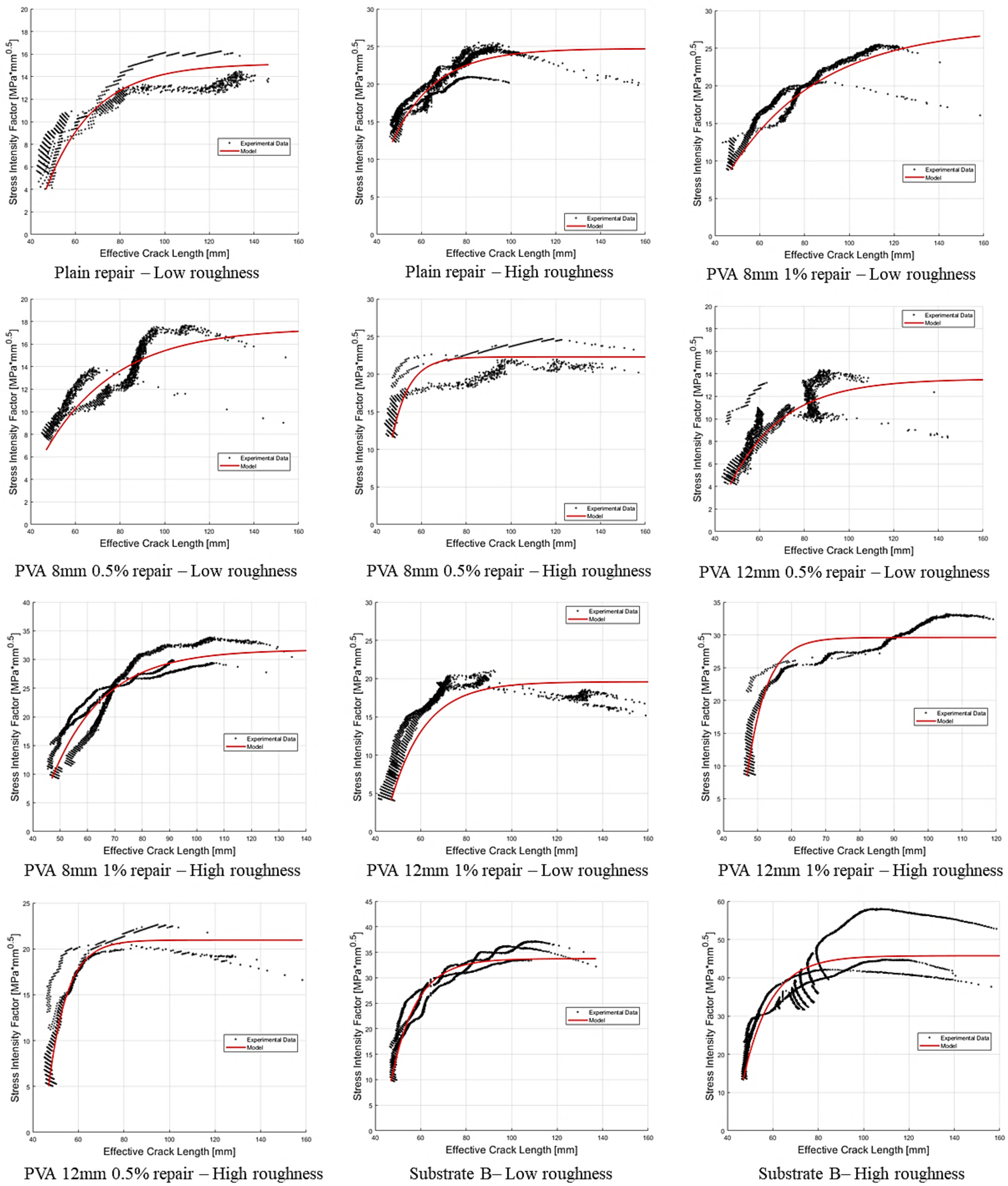

Figure 4.9 Comparison of proposed R-curve model vs. experimental data for various composite systems categorized based on level of surface roughness, type of repair material, and incompatibility criterion

The following exponential function can be considered as the main model to predict the behavior of composite system with plain repair material.

$$K_I = 11.1\left(1 - \mathrm{e}^{-0.04(a_{eff}-47)}\right) + 4 \qquad 4.7$$

where K is stress intensity factor of composite systems in $MPa.mm^{0.5}$ and a_{eff} is the effective crack length in *mm*. The value of 47 is a constant depending on the shape of the specimens and test setup. Figure 4.10 shows stress distribution at the crack tip and R-curve expression parameters including stress intensity (K) and crack length (a).

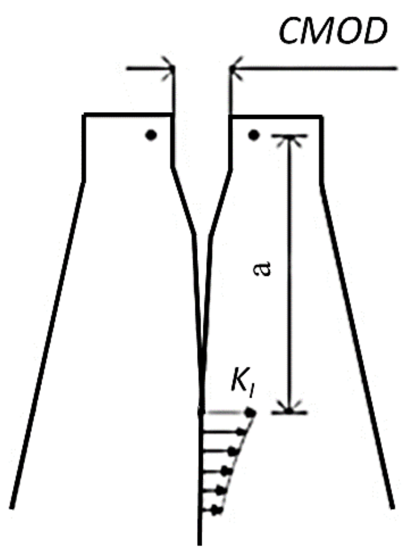

Figure 4.10 Parameters of crack growth resistance model expression, K and a

In order to thoroughly address the impact of repair material, surface preparation, and ductility, one should study changes in crack nucleation resistance (initial stress intensity factor, c), as well as maximum crack growth resistance (sum of a and c factors). Experimental and model results indicate that increasing surface roughness as well as volume fraction of fibers improves crack nucleation resistance. Moreover, maximum crack growth resistance tends to exhibit same trend where introducing fiber to repair material and further surface preparation increases maximum stress intensity factor. Considering overall crack growth resistance curves, composite systems with 1% fiber ratio in repair material and high roughness exhibit the best R-curves among tested specimens where compatibility criteria has not been changed. This is attributed to the ability of fibers to provide further resisting mechanisms both prior to and during loading including crack bridging, crack blunting, etc. Furthermore, higher roughness helps with further positive enhancement of these mechanisms specifically the ones activated during loading stage. Comparison between composite systems with different class of substrates (namely A and B) indicate that slightly different materials, in terms of modulus of elasticity, exhibit more resistance to crack nucleation and propagation. Suggested causes of this behavior have already been described in Section 4.2.4. These results can also be interpreted in terms of energy-based fracture mechanics. However, the trends would be the same considering the correlation between energy approach and stress intensity approach (Section 2.1.3). As a result, all the expressions here are only developed in terms of stress intensity factor. Correction factors for each case can be found in Table 4.4. The proposed equations have a confidence level of 95% based on T-test statistical approach.

Table 4.4 Proposed equations for R-curve models

$f(y) = 11.1a\left(1 - e^{-0.04b(x-47)}\right) + 4c$	a	b	c	R^2
Plain Repair – Low roughness	1	1	1	0.88
Plain Repair – High roughness	1.11	1.25	3	0.87
PVA 8mm 0.5% - Low roughness	0.97	0.75	1.65	0.78
PVA 8mm 0.5% - High roughness	0.96	3.25	2.9	0.73
PVA 8mm 1% - Low roughness	1.71	0.5	2.2	0.95
PVA 8mm 1% - High roughness	1.8	1.25	2.3	0.85
PVA 12mm 0.5% - Low roughness	0.84	1	1.05	0.76
PVA 12mm 0.5% - High roughness	1.43	3	1.26	0.74
PVA 12mm 1% - Low roughness	1.4	1.5	1	0.89
PVA 12mm 1% - High roughness	1.89	4.5	2.12	0.82
Substrate B – Low roughness	2.16	2.25	2.42	0.91
Substrate B – High roughness	2.91	2	3.33	0.84

Comparing the results of Sections 4.2.3-4.2.5, various similarities can be found among R-curve and tensile strength models. First, in both cases, higher surface roughness improves the response of composite systems. Rough substrates exhibit higher tensile load bearing capacity as well as improved R-curves. This suggests that surface preparation can directly and indirectly (through activating fiber-related mechanisms) enhance load bearing capacity, crack nucleation, and crack propagation resistance. Moreover, introducing fibers (especially at higher volume fractions), has positive impact on both models. These strengthening and toughening mechanisms have been described earlier. Surface preparation and fiber addition work strongly together in a way that rough surfaces with more fiber exhibit the best results while a smooth surface with plain repair material has the weakest interface. In addition, softer substrate helps with having a more ductile system and better stress transfer between two layers as discussed in Section 4.2.4. This not only improves overall strength of the system, but also leads to higher crack nucleation and propagation resistance. The R-curve models provided here can be used for other cementitious materials following the same calibration method explained in Section 4.2.4.

Section 4.2.3 – 4.2.5 provide semi-experimental models on progressive failure of concrete-FRC interfaces in Mode-I. Proposed models are given for tensile strength and crack growth resistance curves of concrete-FRC interfaces. These can be employed for practical design purposes considering both long-term and short-term behavior of the repaired systems. In addition, stress distribution at the interface can be characterized using stress intensity factors and effective crack lengths. This information can be used for numerical simulations of concrete-FRC interfaces in future works.

4.2.6 Comparison with existing research studies

Interfacial properties of concrete-FRC interfaces in Mode-I are investigated in various studies, however, none of them are comprehensive enough to yield a model which can be used for designing composite structures. In this section, results of these research studies are compared with the predictive models provided in this thesis. The main objective of this section is to verify the model equations proposed in Sections 4.2.3 – 4.2.5. The model equations which are developed in this thesis are employed and relevant variables are plugged in from the other research studies.

Predicted values are compared with the experimental values and the applicability of the proposed model equations is validated for different materials, surface treatments, and testing methods.

Zanotti et al. [2014] employed the same substrate (substrate A) and repair material (PVA 8 *mm* 1%) used in this work and described in Chapter 3; the authors investigated both tensile strength and crack growth resistance of substrate-repair interfaces. Figure 4.11 represents R-curves and tensile strength values obtained from their experimental tests and the results obtained by applying the model proposed in this work. For the R-curve, crack length values are taken from Zanotti et al. [2014] and plugged in the model equation for PVA 8 mm-high roughness (Table 4.4, Model equation for PVA 8 *mm* 1% - High roughness). Also, for tensile strength, since roughness data is not available, an average roughness of 1.5 *mm* is assumed, based on the R-curves which belong to the higher part of roughness spectrum (Table 4.2, Model equation for PVA 8 *mm* 1%). The slight discrepancy between the results may be explained by higher values of roughness employed in the study done by Zanotti et al. [2014]. However, the predictive curve and tensile strength are still close enough to be used as a fast tool for design purposes.

Table 4.5 Variables for verifying the predictive model versus the results of Zanotti et al. [2014]

Type of Material	PVA 8 mm V_f = 1% (Provided by Zanotti et al. [2014])
Surface Roughness	High Roughness, 1.5 *mm* (The value is based on the explanations and the results presented in the paper)
Effective Crack Lengths	Provided by Zanotti et al. [2014]
R-curve Model Equation	PVA 8 *mm* 1% - High roughness from Table 4.4
Tensile Strength Model Equation	PVA 8 *mm* 1% from Table 4.2

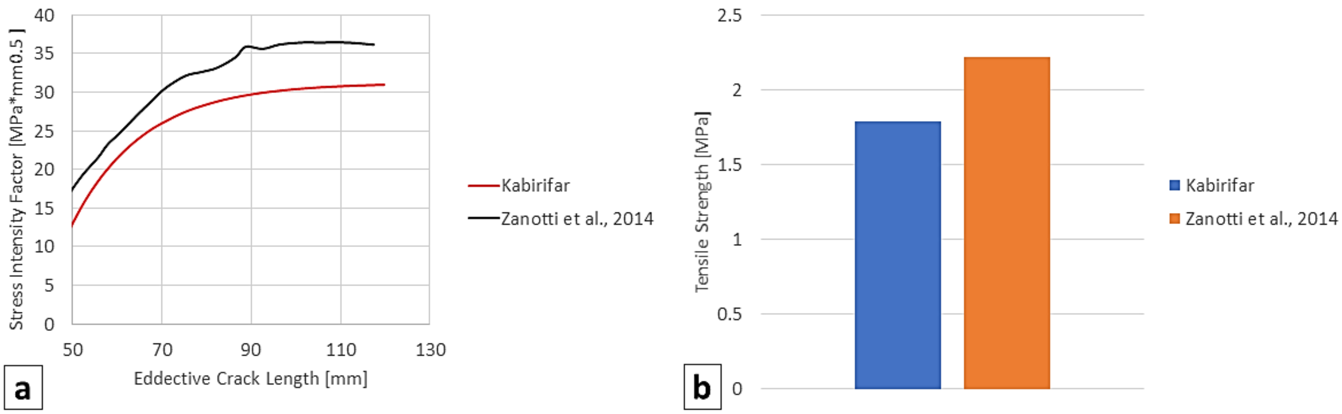

Figure 4.11 Comparison of results obtained by Zanotti et al. [2014] and predictive models

Zanotti and Randl [2019] conducted a study on comparability of different bond tests. The substrate adopted in this work is identical to substrate B adopted in this study (and described in Section 4.1.2). However, their repair materials are different, hence, this comparison can assess the suggested predictive models for different types of repair materials, as well as test setups. Figure 4.13 shows average tensile strengths obtained by different test setups and compares them with the predicted values. In this case, a roughness value of 1.35 *mm* is used, which is the value reported by Zanotti and Randl [2019], along with the model equation obtained for substrate B in Section 4.2.4 (Table 4.3, Model equation for Substrate B – PVA 12 *mm* 1%). As it was expected and is thoroughly discussed by Zanotti and Randl [2018] in their work, adopting different tensile test setups leads to different tensile strength values. The tensile strength predicted with our model is close to the average value of the different test methods (Figure 4.12). This suggests that model equations provided here might be extended to the results from different test setups and materials.

Table 4.6 Variables for verifying the predictive model versus the results of Zanotti and Randl [2019]

Type of Material	Substrate B (Provided by Randl and Zanotti [2019])
Surface Roughness	1.35 *mm* (Provided by Randl and Zanotti [2019])
Tensile Strength Model Equation	Substrate B from Table 4.2

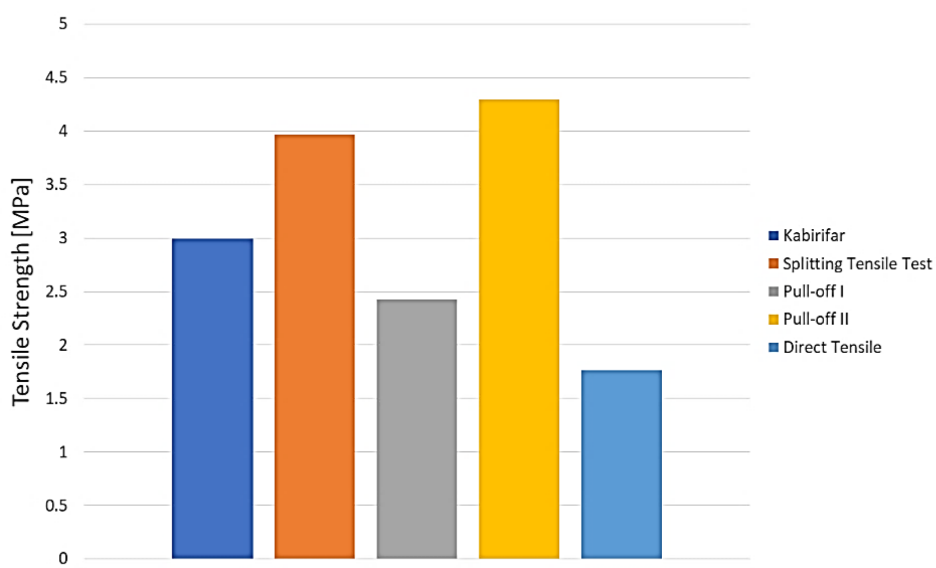

Figure 4.12 Comparison of results obtained by Zanotti and Randl [2019] and predictive model

Shah and Kishen [2010] studied maximum stress intensity factors in Mode-I of various cementitious interfaces using concrete mix designs with compressive strengths of 34 – 66 *MPa*. The mix designs and test setups are different from the ones employed in this thesis. Substrates were roughened but the roughness values are not provided. Due to the difference between the repair materials studied here and the ones in the paper, experimental results obtained by Shah and Kishen [2010] are compared with: (1) The model equation corresponding to plain concrete, which is the most similar material studied here to the one employed in the paper and (2) The average value obtained from R-curve equations in Table 4.4. The maximum limit of R-curve equation represents the critical stress intensity factor which is compared to the critical stress intensity factors reported by Shah and Kishen [2010]. Figure 4.13 depicts that the predicted stress intensity factors from proposed model are slightly less than the average critical stress intensity factor obtained by Shah and Kishen [2010]. In other words, the predictive values are slightly conservative yet applicable to the other test setups and mix designs.

Table 4.7 Variables for verifying the predictive model versus the results of Shah and Kishen [2010]

Type of Material	Plain concrete with different compressive strengths (Provided by Shah and Kishen [2010])
R-curve Model Equation	Average value from R-curve equations (Table 4.4) and Plain concrete with rough surface from Table 4.4

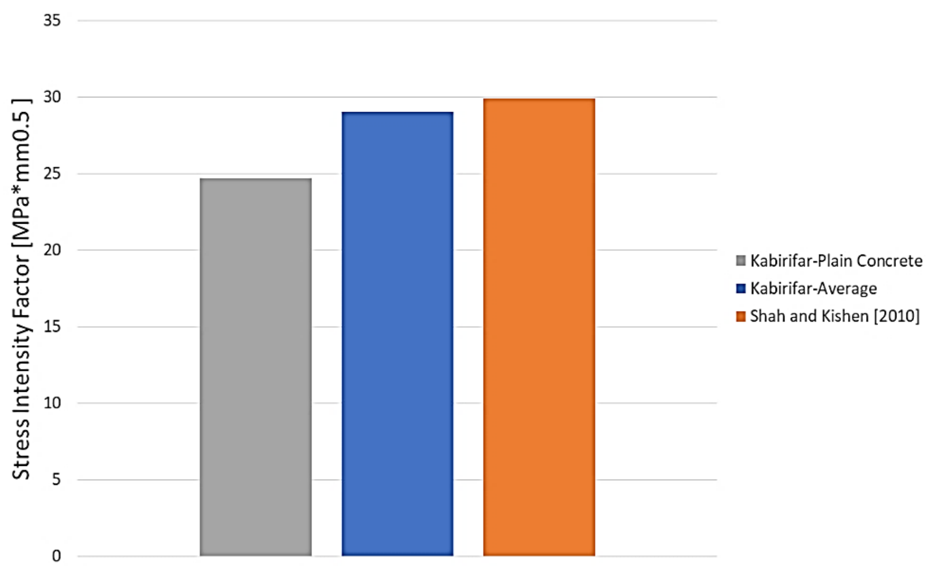

Figure 4.13 Comparison of stress intensity factors obtained by Shah and Kishen [2010] and predictive models

Wagner et al. derived tensile strengths of cementitious interfaces with various levels of roughness using slant shear tests with variable angles [2014] and wedge splitting tests [2013]. They have also compared their results with Mohr-Coulomb and Carol [1997] models. Figure 4.14 compares predicted values versus their experimental tensile strengths. The average roughness value of 0.45 *mm* is employed according to the values reported by Wagner et al. [2013]. The employed repair material is 8 *mm* PVA FRC with fiber volume fraction of 2% and compressive strength of 86 *MPa*.

Due to the difference between the mix designs used by Wagner et al. [2013, 2014] and the ones used in this thesis, experimental results obtained by Wagner et al. [2013, 2014] are compared to: (1) the model equation corresponding to the most similar material studied here to the one employed in their paper, which is PVA 8 *mm* with V_f = 1%, and (2) to the average predicted value from the tensile strength equations.

Table 4.8 Variables for verifying the predictive model versus the results of Wagner et al. [2013, 2014]

Type of Material	PVA 8 *mm* V_f =2% with compressive strength of 86 *MPa* (Provided by Wagner et al. [2013, 2014])
Surface Roughness	0.45 *mm* (Provided by Wagner et al. [2013, 2014])
Tensile Strength Model Equation	Average value from tensile strength equations (Table 4.1) and PVA 8 *mm* V_f = 1% from Table 4.1

The values obtained from the predictive models are slightly conservative compared to the experimental results. The difference can be attributed to the size effect and different interfacial lengths, as well as, different roughness evaluation techniques and different compatibility criteria among the experimental work done in this thesis and by Wagner et al. [2013, 2014]. In spite of that, predicted tensile strengths are close enough to the experimental values.

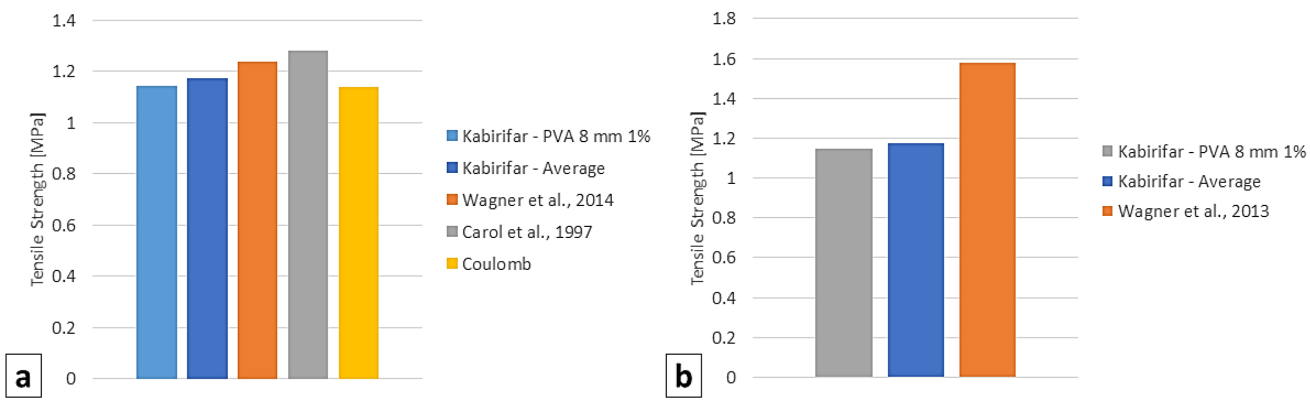

Figure 4.14 Comparison of tensile strengths obtained by Wagner et al. a) slant shear tests [2014] and b) wedge splitting tests [2013] with values from the predictive model

The other investigation is performed by Silfwerbrand [2003] on tensile bond strengths of cementitious composite systems using pull-off tests. His results are compared with the predicted values in Figure 4.15. Roughness values are not provided in the paper, however, due to employing various roughening techniques which can result in high roughness values, an average value of 1 mm is assumed. The repair material is cast-in-place concrete. Since the materials investigated in the paper are not identical to the ones studied in this thesis, experimental results obtained by Silfwerbrand [2003] are compared to: (1) the results of the model equation corresponding to the most similar material studied here to the one employed in their paper, which is plain concrete, and (2) the average predicted value from tensile strength equations in Table 4.2.

Table 4.9 Variables for verifying the predictive model versus the results of Silfwerbrand [2003]

Type of Material	Plain Concrete (Provided by Silfwerbrand [2003])
Surface Roughness	Assumed 1 *mm* based on surface treatment techniques employed in the paper
Tensile Strength Model Equation	Average value from tensile strength equations (Table 4.2) and plain concrete from Table 4.2

It can be seen that the experimental and predicted values are quite close to each other. As it can be observed, the models provided in this thesis can be used for the other testing methods as well.

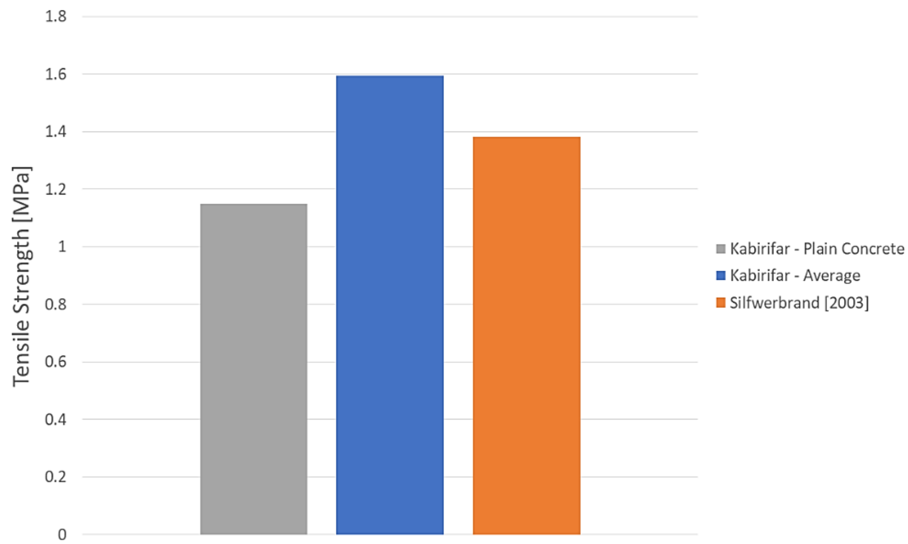

Figure 4.15 Comparison of tensile strengths from experimental work done by Silfwerbrand [2003] and model equations

As demonstrated in this section, the suggestive model is applicable to other cementitious repair materials and different test setups. In other words, these model equations are not limited to the materials and testing techniques which are used in this study. Nevertheless, it is not surprising that employing different materials, surface treatments, and evaluation techniques might result in slightly different outcomes. Although this difference is not significant in most of the cases, whenever higher accuracy is required, it is recommended to develop correction factors corresponding to the specific testing methods and materials.

The model provided here is a semi-empirical model which is based on a vast experimental investigation beside a profound study of the effects of every single variable, comparing various functions and choosing the best one aligned with the nature of the problem. The main strengths of this model are 1. Unlike all other previous works which deal with shear behavior, it is fully focused on Mode-I behavior, 2. Unlike many other models/codes which qualitatively address surface roughness, it has been quantitatively implemented in this model, 3. It does not require many different parameters as inputs unlike many other models and it makes it much more convenient to work with, 4. It does not only provide tensile strengths, but also fracture parameters in Mode-I which is a very new aspect not only for interfaces in tension but also compared to the studies on interfaces in shear.

4.3 Concluding Remarks

In this chapter, the mechanical behavior of concrete-concrete interfaces under Mode-I loading is investigated and a model is based on experimental data. The main results can be summarized as follows:

1. The main goal of this study was to obtain a convenient and comprehensive expression which can be used to estimate and model the failure progression of composite concrete-FRC repaired systems including high performance and fiber reinforced concrete. To the best of author’s knowledge, this has not been comprehensively addressed in any other study. The proposed expression is based on the most important factors, including surface roughness, material characteristics of the repair layer, and material elastic modulus mismatch – a property that can be easily adjusted in practical applications and projects.

2. Interfacial bond of concrete-FRC specimens under Mode-I is directly affected by the surface preparation and material characteristics. Below certain thresholds, higher roughness values and stronger repair materials lead to enhanced interfacial bond. The rate of this enhancement, however, decreases as higher roughness values and stronger repair materials are employed.

3. The curve representing interfacial bond-roughness and interfacial bond-strength of repair material exhibits a saturating trend. This suggests that excessive surface preparation and employing very strong repair materials, which are less compatible with the substrate layer, does not contribute to further remarkable improvement of interfacial bond.

4. Comparing roughness-based models with the models based on material properties, the impact of surface texture gives much more clear and consistent results. This suggests that surface topography has to be considered as the main variable, while material's mechanical properties can be addressed as a secondary variable by introducing correction factors corresponding to different repair materials.

5. The effect of elastic modulus mismatch has been investigated as well. Results suggest that within the investigated range of data, as long as the repair material has slightly stronger mechanical properties compared to the substrate layer, slightly lower elastic modulus of the substrate might help with the overall ductility and response due to higher deformation capacity and improved load transfer.

6. Suggestive models are provided for the full, progressive debonding response in Mode-I (crack growth resistance curves) considering different repair materials, surface roughness, and elastic modulus mismatch. Results indicate that higher roughness along with higher volume fraction of fibers can positively affect resistance to crack nucleation and crack propagation within the investigated range of material properties. Moreover, employing repair and substrate layers with slightly different elastic modulus might decrease vulnerability of composite repair systems to both crack nucleation and propagation.

Based on these results, following conclusions can be drawn:

1. The resulting model can be easily implemented in analytical and numerical design approaches. This expression is applicable to repaired systems where substrate concrete has the mechanical properties of a commonly used concrete in practical projects.

2. In repair of concrete structures, extensive surface roughening and repair layers with very large fiber contents should be avoided as they may negatively affect the behavior of composite structure.

3. Although mix design of repair material affects the composite response, the effect of surface preparation comes first. Hence, in designing repair for concrete structures, extra attention needs to be paid to surface treatment.

Chapter 5: Quantifying Material and Interface Properties at the Microscale

The complexity of concrete's microstructure comes from both the binder phase, the aggregate-binder interfaces, and the presence of voids. In the case of repaired systems, the interface between substrate and repair layers further contributes to the complexity of the system. This interfacial transition zone is the weakest part of the composite system and is the location of nucleation of microcracks due to a complex stress and strain state caused by the incompatibility between the substrate and repair layers, in addition to the inherent ITZ weakness. As a result, the overall performance of the composite system depends to a high degree on the properties of the interface.

Due to the limitations of available test techniques and the difficulty of quantifying parameters of the interface, there is still a knowledge gap in this area [Lukovic, 2016] [Zhou, 2011]. Most of the common test methods for the evaluation of interface properties are meso/macroscale bond strength tests. These meso/macroscale tests, however, do not provide detailed information on the failure mechanism. Moreover, failure can also occur in repair or substrate layers in which case the bond strength cannot be attributed solely to the interface. Considering these bond strength test shortcomings, further investigations are necessary to gain a better understanding of the failure process in concrete-FRC interfaces. Micro-computed X-ray Tomography (CT-scanning), micro-indentation, and Scanning Electron Microscopy (SEM) are some of the microscale methods that can be employed to investigate the microstructure and micromechanical properties of concrete-FRC interfaces. CT-scans provide 3D images of the repaired system which can be used for porosity evaluation and durability characterization. Micro-indentation and SEM results are also useful for characterizing the micro-properties of the interface and the bulk material.

Limited but useful information is available from previous studies of the state of the art [Sadowski, 2019] [Lukovic, 2016] [Moser et al., 2013] [Landis, 2009]. For the purpose of this work, some informative and relevant information was found in [Lukovic, 2016], where the influence of the following parameters on micromechanical properties of cementitious interfaces was investigated: w/c of repair material, saturation level of the substrate, duration of sealed curing and application of primer between substrate and repair layers. In this chapter, composite systems are evaluated at the microscale and the influence of adding steel and PVA fibers to the repair material on the micromechanical properties of the interface is investigated. Moreover, the ability of steel and PVA fibers to mitigate damages under harsh environmental condition is assessed.

5.1 Methodology

5.1.1 Materials and Specimen Preparation

The microscale properties of concrete-FRC interfaces are investigated in this chapter. The mix design of the substrate layer is the same as the one used in Chapter 3. For the repair layer, based on preliminary results, three mix designs were used (12 *mm* PVA and 13 *mm* steel fiber with and without superplasticizer, $V_f = 1\%$); these mixes were found to have the best performance in composite systems. In addition, a control without fibers (plain repair material) were examined. Small cubic substrates (100 x 50 x 50 mm^3) were cast, placed in the curing room for 28 days, and sandblasted afterwards. They were cut into smaller pieces (50 x 35 x 25 mm^3 and 100 x 35 x 25 mm^3) before casting repair layers. The average roughness value of substrate surfaces were consistent with those of Chapter 4. After sandblasting, a repair layer (50 x 35 x 25 mm^3 and 100 x 35 x 25 mm^3) was applied on the rough surface of the substrate. The moisture condition of the substrate at the time of repair casting was saturated surface dry (SSD), which is consistent with the preparation method in Chapter 3. In order to evaluate the influence of curing condition and shrinkage on the microscale properties of the concrete-FRC interfaces, two different curing conditions were used. The first condition was 7 days wet curing in a designated curing room (T = 20 ˚C and RH = 100%), and the second one was 7 days dry curing at 50˚C and 10% relative humidity (RH).

Prismatic specimens measured 100 x 50 x 35 mm^3 and 100 x 35 x 25 mm^3 were used for CT-scanning and gravimetric tests, respectively. For both tests, samples were dried in an oven at 105 ˚C until they reached a constant weight. This step is necessary to have consistent initial moisture content at the start of the experiments [Hall, 1989]. To mitigate probable microstructural changes in the material due to the high temperature in the oven, the duration of the high temperature drying process has to be minimized [Ye, 2003]. However, it must also be pointed out that the oven treatment took place 7 days after casting the repair. The specimens were later cut with a diamond saw into smaller samples for micro-indentation and SEM analysis. In addition to prismatic specimens, a set of cylinders were cast and cured for evaluation of the effect of curing condition on compressive strength.

5.1.2 Experimental Methods and Testing Set-up

5.1.2.1 X-ray Micro-computed Tomography (CT-scanning)

For CT scanning, small prismatic specimens (100 x 50 x 35 mm^3) were left in an oven and their weight were monitored (every 24 hours) until they reached a constant weight (that is, when weight measurement variations were below 0.5% as per [ASTM C642]. This was done to ensure that all water was removed from pores and the initial moisture content of the material was zero. Moreover, differentiating air-filled pores from bulk concrete in easier than differentiating water-filled pores.

Samples were scanned using a Scanco Medical μCT100 with voxel size of 25 μm. Parameters used in the setup of X-ray system were: tube voltage 90 kV, tube current 200 μA, spatial resolution 24.6 μm, and 28 minutes exposure time per data set. Projections obtained during scanning were reconstructed into slices with a thickness equal to the voxel size (25 μm). Each reconstructed 3D image contains 200 slices, representing 5 mm of the composite element. Image analysis and porosity evaluation were performed using ImageJ [Ferreira and Rusband, 2012].

By thresholding dark pixels which represent voids in the original image, a thresholded image showing only voids can be obtained (as described in Section 5.1.2.3.1). The void content in different places can be quantified. To evaluate the void content, a region of interest (ROI) was chosen and ratio of voids area to total area was calculated.

5.1.2.2 Gravimetric Water Absorption Test

In order to quantify capillary water absorption of the specimens, they were left in an oven (as above) to reach a constant weight. After that, they were placed in water, where the water level was set at 5 mm below the interface. The weight of the specimen was recorded at specific time intervals over 24 hours, and cumulative water – time curves were obtained.

5.1.2.3 Scanning Electron Microscopy (SEM)

For SEM, smaller specimens (30 x 30 x 20 mm^3) were cut from bigger samples using a saw. In order to avoid damage, specimens were placed in a desiccator under vacuum and submerged in a layer of epoxy prior to being cut. The epoxy was fed from outside of the vacuum to the top of the specimen. The upper part of the specimen was covered with epoxy and after 10 minutes, air was let gently into the desiccator to push the epoxy further into the pore system of the sample. The impregnated specimen was cured at atmospheric pressure for 24 hours. Afterwards, the cured specimens were cut, ground, and polished. The effectiveness of the grinding and polishing were verified using an optical microscope. Hitachi SU3500 Scanning Electron Microscope (SEM) was used to examine polished samples. The instrument used an accelerating voltage of 10 kV and the magnification varies between 50x to 500x. Repaired specimens were evaluated by scanning electron microscopy (SEM) to investigate the micro-features of the interface such as microcracks due to shrinkage and overall stability of the interface.

5.1.2.3.1 Image Segmentation by Thresholding

Image processing techniques have a critical role in characterising features of the pore structure and microcracks in a SEM images. Thresholding is a well-known technique in which a multi-level image is converted into a binary image [Sahoo et al., 1988]. In this binary image, each pixel value is defined by a single binary digit. In the simplest model, thresholding is a point-based process during which the values of 0 or 1 are assigned to each pixel of an image having some global threshold value, T. Thus, the thresholding process helps with data storage size reduction and provides binary images which are easier to analyze.

It is quite hard to find a boundary value between pore space and solid structure from an original grey scale image. However, a grey level histogram can be employed to define a threshold value and to segment pore space (Figure 5.1). This differentiation is possible due to the difference between the atomic number of cement hydration products and pores impregnated with epoxy. The threshold value of the pore structure corresponds to the left peak in the grey level histogram below (Figure 5.1).

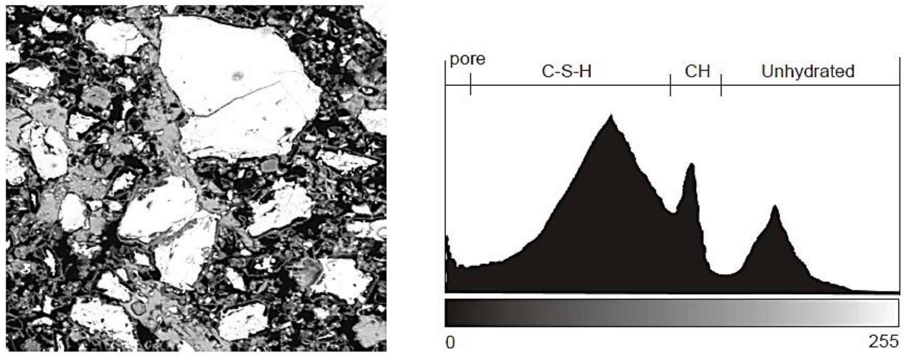

Figure 5.1: Back scattered electron image of concrete and its corresponding grey level histogram [Ye, 2003]

5.1.2.4 Micro-indentation Test

A Leco LM-310 micro-indenter with a diamond tip was used for micro-indentation tests. The indenter is a Vickers square-based pyramidal diamond indenter which is capable of producing geometrically similar impressions, irrespective of size; it is a highly polished, pointed, square-based pyramidal diamond with face angles of 136° 0’ [ASTM E92]. A standard test block, provided by the manufacturer, was indented prior to each test series to ensure its calibration. The local micro-hardness of different types of interfaces which correspond to different repair mix designs were evaluated. Local mechanical characteristics of the material can be quantified using indentation load and displacement. A series of indents was performed along the interface and inside the bulk material.

5.1.2.5 Compression Test

Compressive strength of repair and substrate layers were investigated based on ASTM C39 standard using a Forney machine. At least three specimens with height of 20 *cm* and diameter of 10 *cm* were cast and cured for 7 days in curing room and drying chamber and tested for each mix design.

5.2 Results and Discussion

5.2.1 Effects of Curing Condition on Material Properties

Figure 5.2 shows the compressive strength for various wet-cured and dry-cured repair materials. All four mix designs lost around 10 percent of their 7-days compressive strength when subjected to dry curing. This can be attributed to the negative impact of harsh environmental condition leading to disruption of the hydration process as well as shrinkage-induced damage within the material.

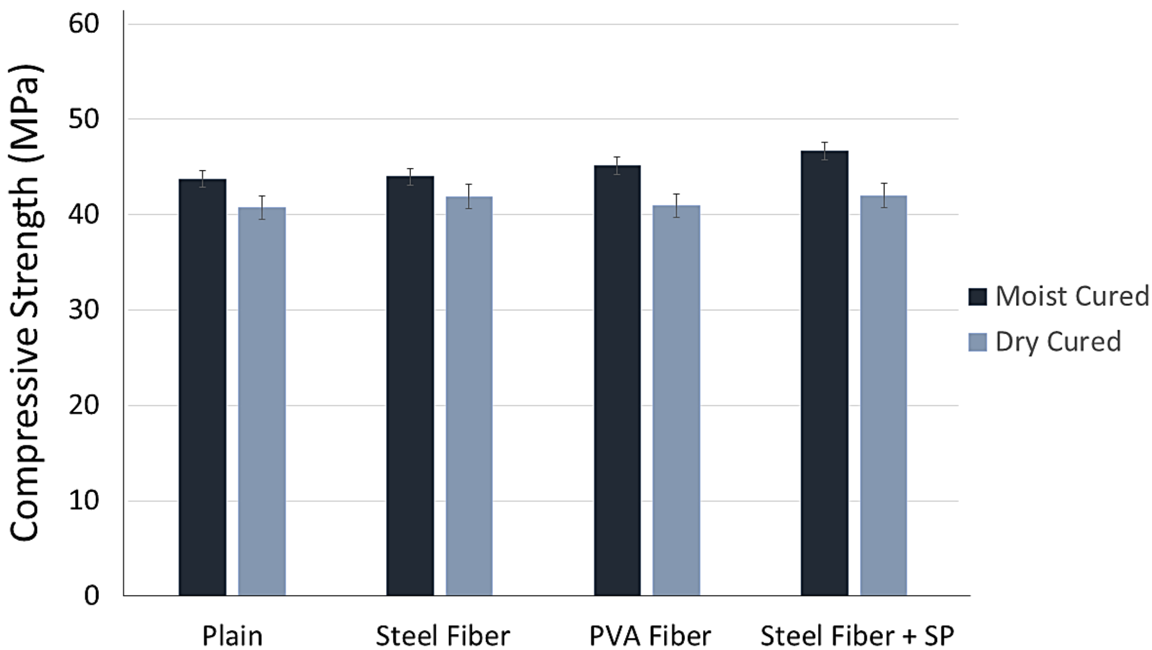

Figure 5.2: Compressive strength for wet-cured and dry-cured specimens

In addition, wet-cured and dry-cured repair materials exhibit different failure modes. In case of plain material, various diagonal cracks and detachments were observed prior to failure. However, dry-cured specimens exhibited more cracks at the edges suggesting that specimens were not properly cured. For specimens with steel fiber, dry-cured specimens showed more cracks prior to failure. While diagonal and circular cracks were observed in specimens subjected to both curing regimes, dry-cured specimens showed extra weakness at their edges. Dry-cured PVA fiber specimens and steel fiber specimens with superplasticizer were more likely to have an extra damaged zone at the two edges compared to their wet-cured counterparts. Specimens with higher compressive strength in wet environment seemed more likely to undergo higher strength loss and greater damage at their edges. The cracked zones can be observed in Figure 5.3.

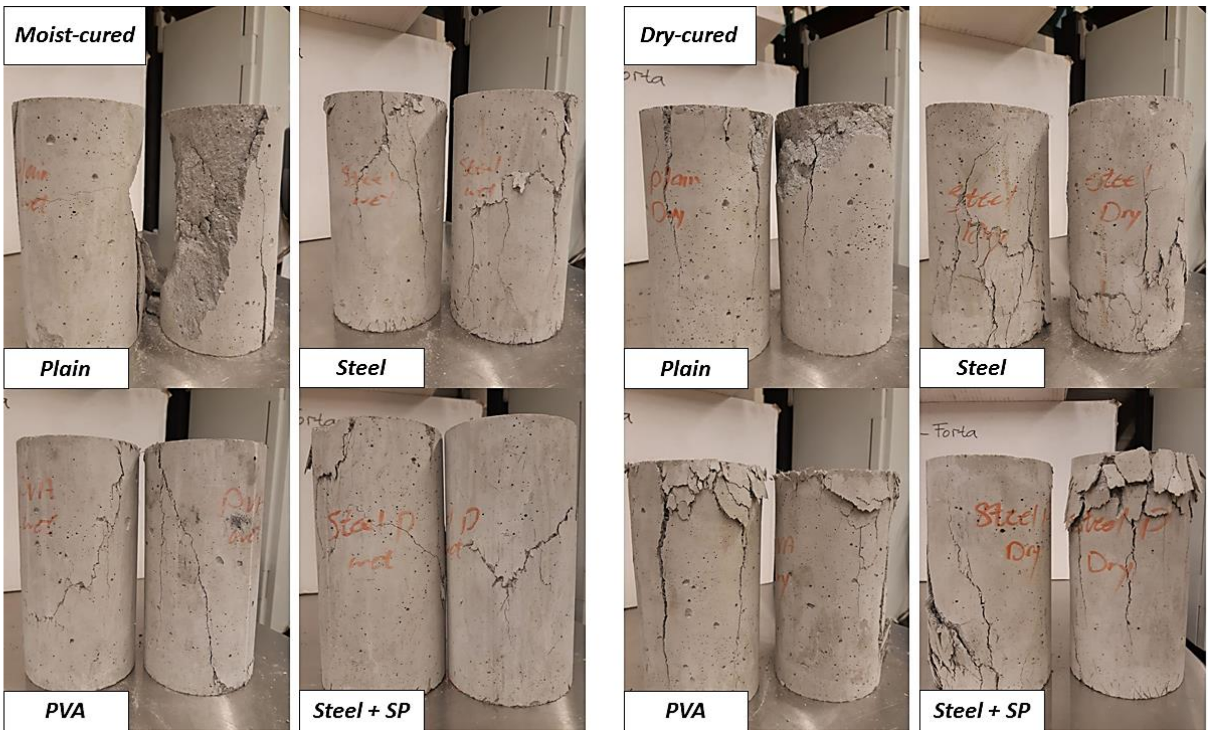

Figure 5.3: Failure mode of wet-cured vs. dry-cured specimens. Cracking patterns in wet-cured specimens are limited to diagonal cracks. In the case of dry-cured specimens, extra damage at their edges is present.

5.2.2 Capillary Absorption and Visual Inspection

Figure 5.4 shows the results of water absorption tests for the various composite systems. Almost all mix designs show higher water absorption when subjected to dry curing condition. Moreover, the trend of water mass – square root of time curve becomes more nonlinear where moving from moist cured to dry cured specimens. Higher water absorption and nonlinear trend indicate that higher temperature and lower relative humidity employed in dry curing regime has worked as anticipated and caused further shrinkage in the specimens.

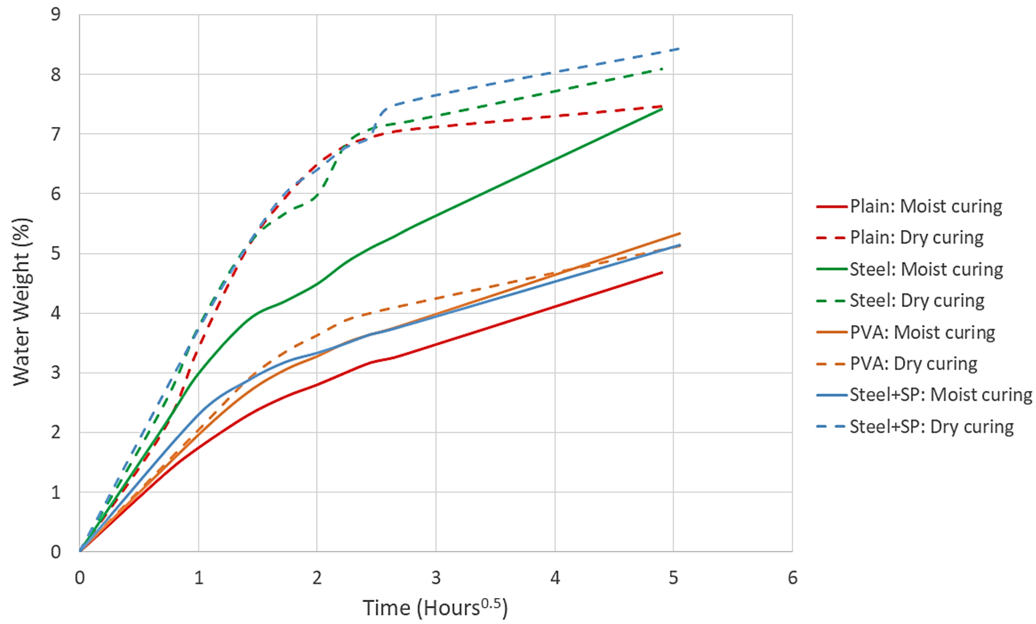

Figure 5.4: Results of capillary water absorption test

Among wet cured samples, steel FRC without superplasticizer tended to absorb more water. This can be attributed to higher permeability of steel FRC which has been investigated previously [Miloud, 2005], and confirmed by the results of this study. Three other mix designs exhibit quite similar water absorption when cured in the curing room. In the case of dry cured samples, however, specimens containing PVA fiber showed the lowest water absorption. This may be due to the ability of PVA fibers to mitigate deterioration by slowing down the evolution of local slippage, as a result of friction between the fiber and the matrix, and controlling crack widths [Al-Musawi et al., 2020, Branston et al., 2016; Magnat and Azari., 1990]. This suggests that PVA fibers have better performance in terms of mitigating shrinkage compared to plain material and steel FRC. Various factors may be responsible for better performance of PVA fibers including aspect ratio, modulus of elasticity, specific gravity etc. [Sun et al., 2001]. In the literature, it has been noted that fibers with a higher aspect ratio are better at mitigating shrinkage cracks and increasing tensile strength [Fang et al., 2020; Yoo et al., 2013]. This may explain the better performance of PVA fibers here which have much higher aspect ratio compared to steel fibers. These results are consistent with other research including the study performed by Qi et al. [2019] on effectiveness of steel versus synthetic fibers. Their results indicate that synthetic fibers reduce shrinkage to greater extent that steel fibers. The addition of synthetic fiber may have caused the cement particles to mix with coarse particles, leading to further friction and higher tensile strength. Synthetic fibers may have helped by reducing the movement of water and the rate of water evaporation [Van Breugel and Van Tuan, 2015] Moreover, PVA fibers have lower specific gravity than steel fibers which can help with smaller spacing between PVA fibers and their higher effectiveness [Sun and Mandel, 1989].

Plain and steel FRC with superplasticizer exhibited the biggest jump in absorption when moving from wet to dry curing conditions. This indicates that these two mix designs are vulnerable to harsh environmental conditions and are expected to have lower durability if not cured properly. In plain concrete, this is due to lack of sufficient resisting mechanisms against shrinkage and thermal cracks. Furthermore, adding superplasticizer to steel FRC shows a positive effect for wet cured specimens, however, both steel FRC systems exhibit same absorption capacity when subjected to dry curing regime. This suggests that adding superplasticizer to steel FRC is not a promising solution for repair works in harsh environments. This is in accord with previous research, which have demonstrated negative effects of superplasticizers on shrinkage. Such negative effects may be caused by improved cement dispersion and faster rate of hydration reactions in the matrix. In other terms, in absence of superplasticizer, heterogeneities within the matrix increase the internal restraining effect and reduce shrinkage damage [Beltzung and Wittmann, 2002].

Composite specimens prepared for microanalysis were examined using microscopy, and the effects of two different curing regimes were assessed visually. Figure 5.5 shows substrate-repair interface of various composite systems subjected to wet and dry curing regimes. It can be observed that in almost all cases samples have undergone extra damage due to high curing temperature under low relative humidity. This extra damage varies from presence of extra superficial and non-superficial shrinkage cracks to full debonding at the interface. Among four different repaired systems, the PVA fiber system exhibited the most promising results because full detachment was not observed in any specimen. This finding accords with the results obtained from capillary absorption test. Both techniques indicate that as far as shrinkage resistance of repaired systems is concerned, PVA FRC has a better performance compared to plain repair and steel FRC.

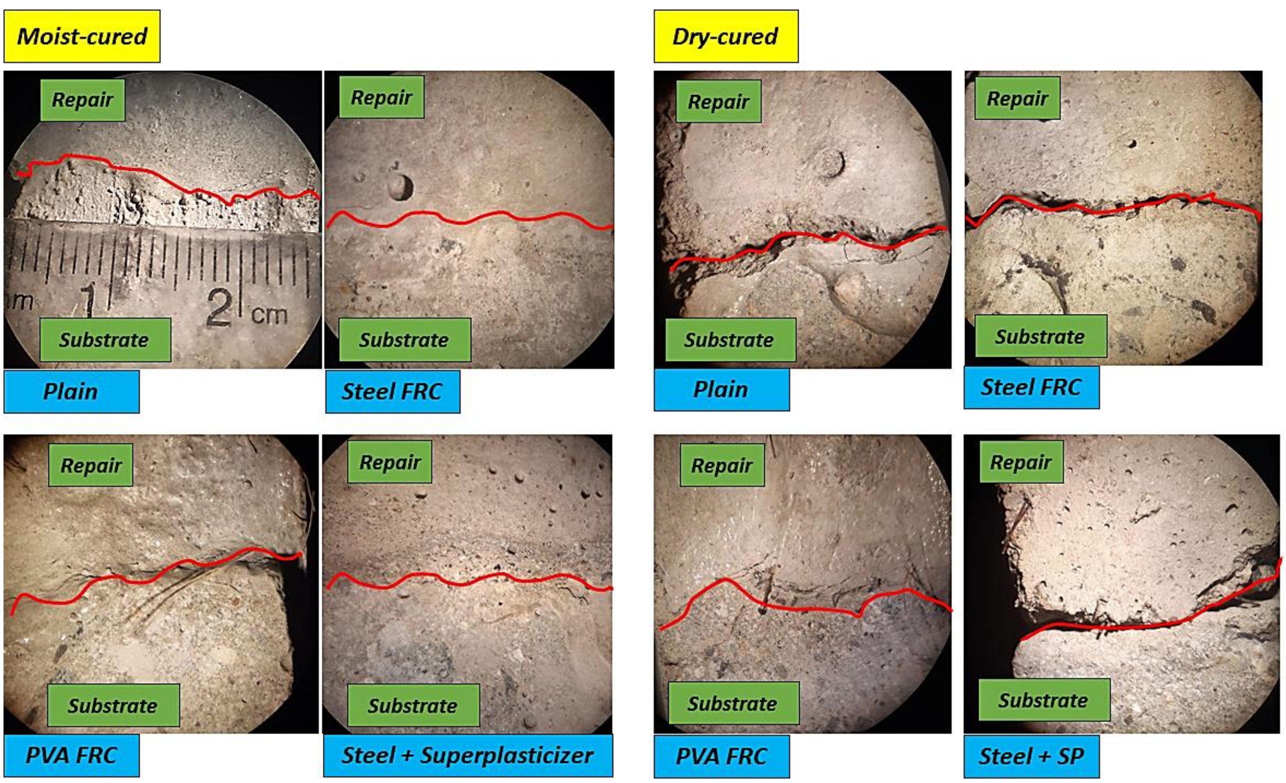

Figure 5.5: Substrate-repair interface of four different mix designs subjected to wet and dry curing regimes

5.2.3 Scanning Electron Microscopy and X-ray Micro-computed Tomography

Evaluating the microstructure of the interface between substrate and repair material helps to gain a better understanding of interface properties. In this study, SEM was used to investigate crack pattern and void distribution adjacent to the interface. After preparing specimens, multiple SEM images were taken from each sample with pixel size of 100 *nm*. These images were later put together to form a 4000 x 600 μm image (Figure 5.6). By thresholding dark pixels, which represent voids, a thresholded image containing only voids was obtained. Since concrete is a composite system, greyscale values of its components are different which complicates thresholding. Although SEM images have quite high resolution, they only provide information about outermost section of the specimen; that's why CT-scan images can be useful in evaluating other sections of the specimens.

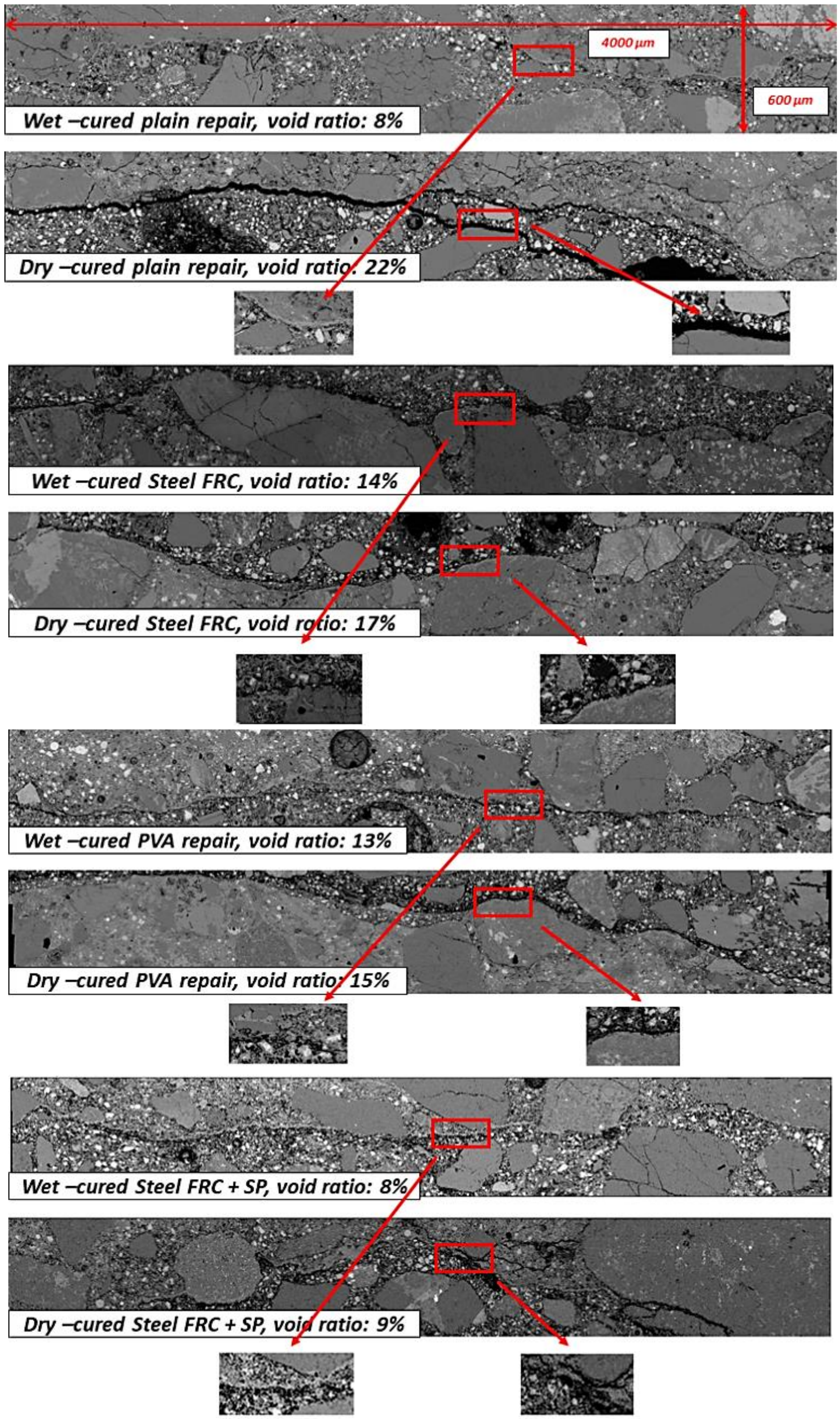

Figure 5.6: Microstructure of the substrate-repair interface at 500x and 1000x

As expected, dry-cured specimens exhibited greater damage at the interface. They contained higher numbers of larger cracks. Higher temperature may have caused more water evaporation in a shorter period of time period, which have led to shrinkage-induced cracking. Moreover, material mismatch at the interface might exacerbate crack formation. This was more evident in the composite systems containing plain repair material where no extra crack mitigating mechanisms were operated. Adding fiber to the repair layer had a positive impact in mitigating microcracks nucleation and propagation at the interface. This can be understood by comparing SEM images of Plain versus FRC repaired systems.

In order to quantify the porosity close to the interface, original images were thresholded using ImageJ based on their grayscale values. The void ratio is calculated as total void area divided by total area. All interfaces had higher porosity when subjected to the drying condition. Considering wet cured samples, adding fibers increased interfacial porosity. This was mitigated by adding superplasticizer to FRC repair layer. In the dry condition, steel FRC with added superplasticizer had the lowest porosity followed by PVA FRC. Plain repair material showed the highest increase in porosity when subjected to an unfavorable curing condition. As a result, adding fiber to repair material is expected to have a positive impact on durability of composite systems especially in dry and humid environments.

Some of the specimens were also scanned using CT to evaluate the effect of repair material and curing condition on microstructure of the composite systems (Figure 5.7). In comparison to SEM, CT obtains a larger region of interest around the interface. Moreover, microstructure was evaluated at various depths leading to a 3D perspective, whereas in SEM only external face of the interface was examined. To construct a 3D structure, all slices were aligned on top of each other covering 5 *mm* of the interface. The original images were thresholded and images of voids were obtained. To quantify void content, void area was divided by the area of region of interest in every image.

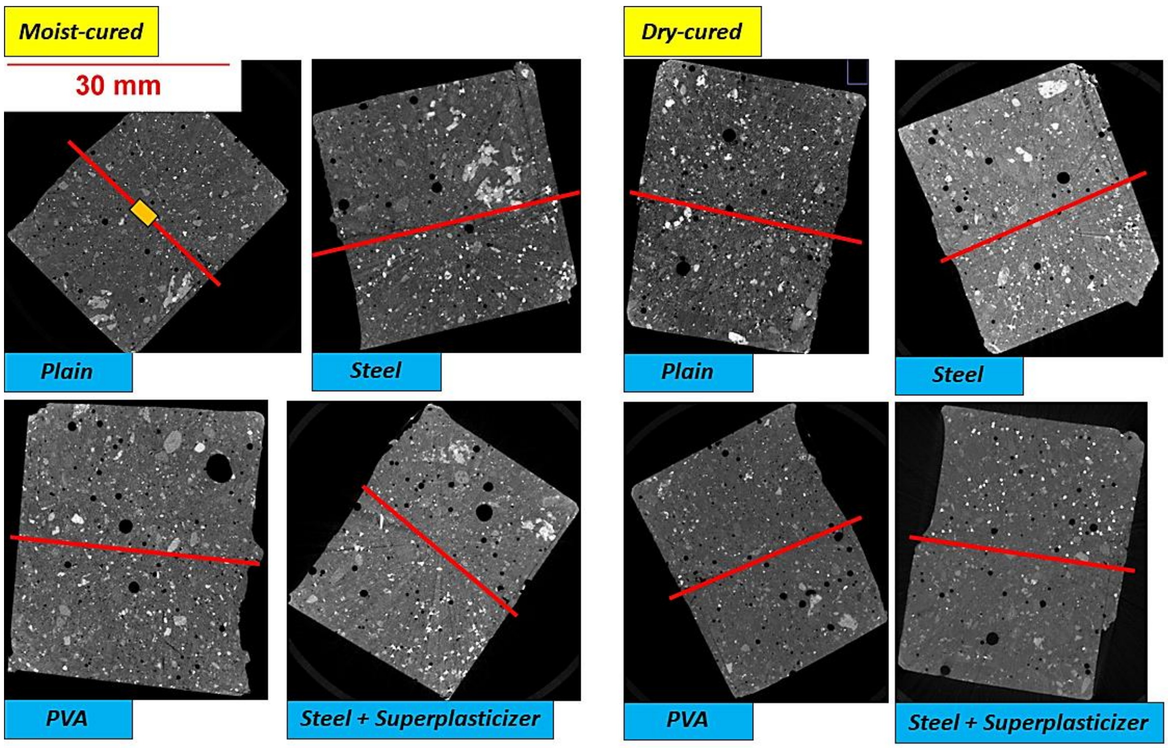

Figure 5.7: Structure of internal section of composite systems scanned by CT showing how porosity changes at the interface and within the bulk material for different composite systems subjected to wet and dry curing

Figure 5.8 shows how void ratio changes with depth in different composite systems subjected to wet and dry curing. The negative impact of dry curing can be observed in all cases. Moreover, better performance can be seen in PVA and Steel + SP mix designs which accords with SEM and capillary absorption results.

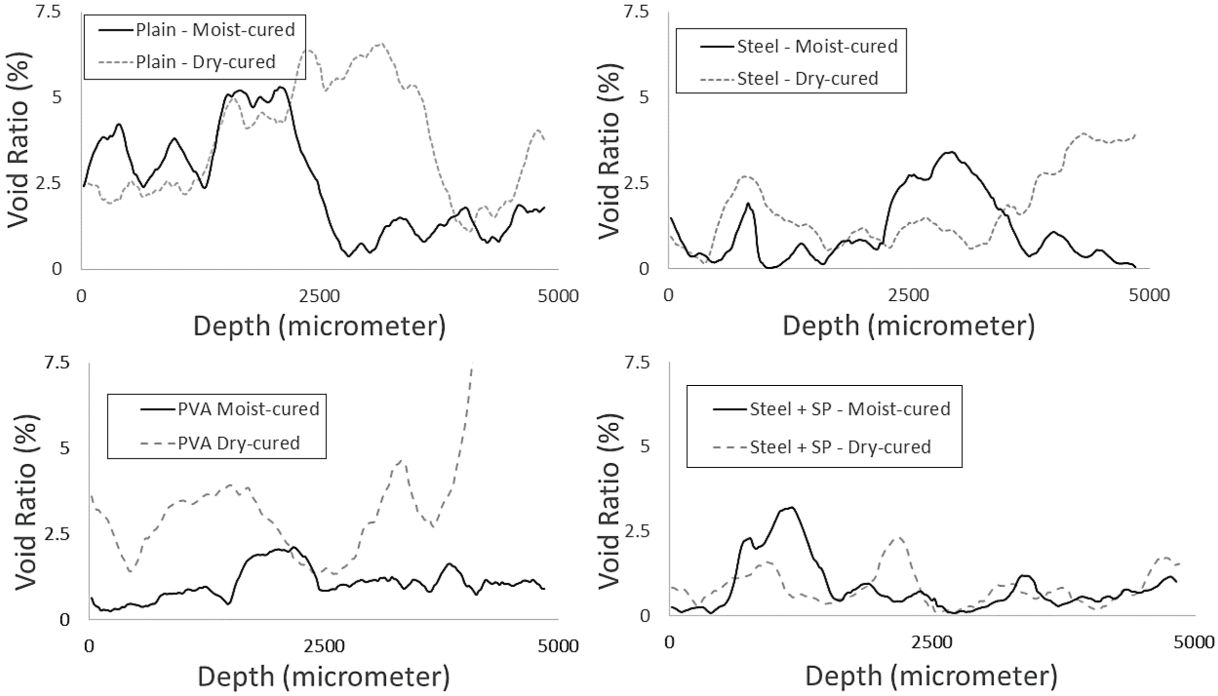

Figure 5.8: Void content in composite systems at different depths from the surface showing void ratio variations when going deeper in the specimens

5.2.4 Micro-indentation

Micro-indentation technique can be used for determining local mechanical properties as described above. A series of indents were applied to interfaces based on the grid shown in Figure 5.9. Samples were grinded and polished with sandpapers of increasing fineness (up to 1200 grit) to decrease surface roughness. After several trials on different combinations of indentation load and dwelling time, P_{max} = 50 gram-force (*gf*) and dwelling time of 15 *s* were chosen with loading rate of 50 *μm/sec*. Locations of indents were chosen in such a way to cover interface and its adjacent area for both repair and substrate layers. All specimens were studied under microscope prior to indentation to avoid having aggregate in the regions of interest near the interface.

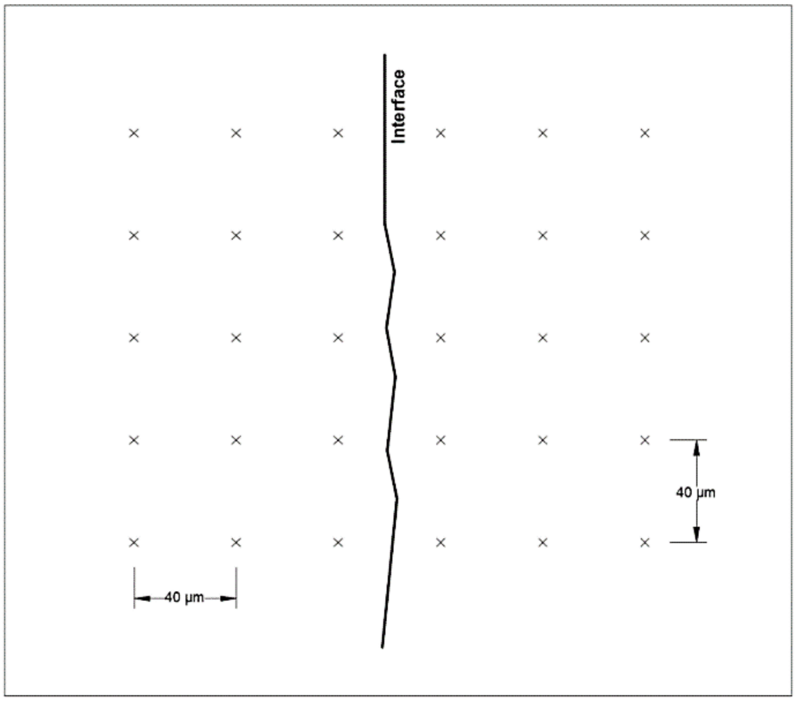

Figure 5.9: Pattern of locations for the micro-indentation test

Hardness data is presented in Figure 5.10. Hardness data range covers values up to 2.5 *GPa* in various color levels. Higher levels of hardness are shown using the same color as for 2.5 *GPa*. In this way, weak zones can be visualized more detail. Differences between hardness values are due to multiple phases within the indented grid. Indents with quantified hardness can be employed to evaluate porosity, microcracking, and general stability of the system [Lukovic, 2016]. The interface between old and new layers are shown by arrows.

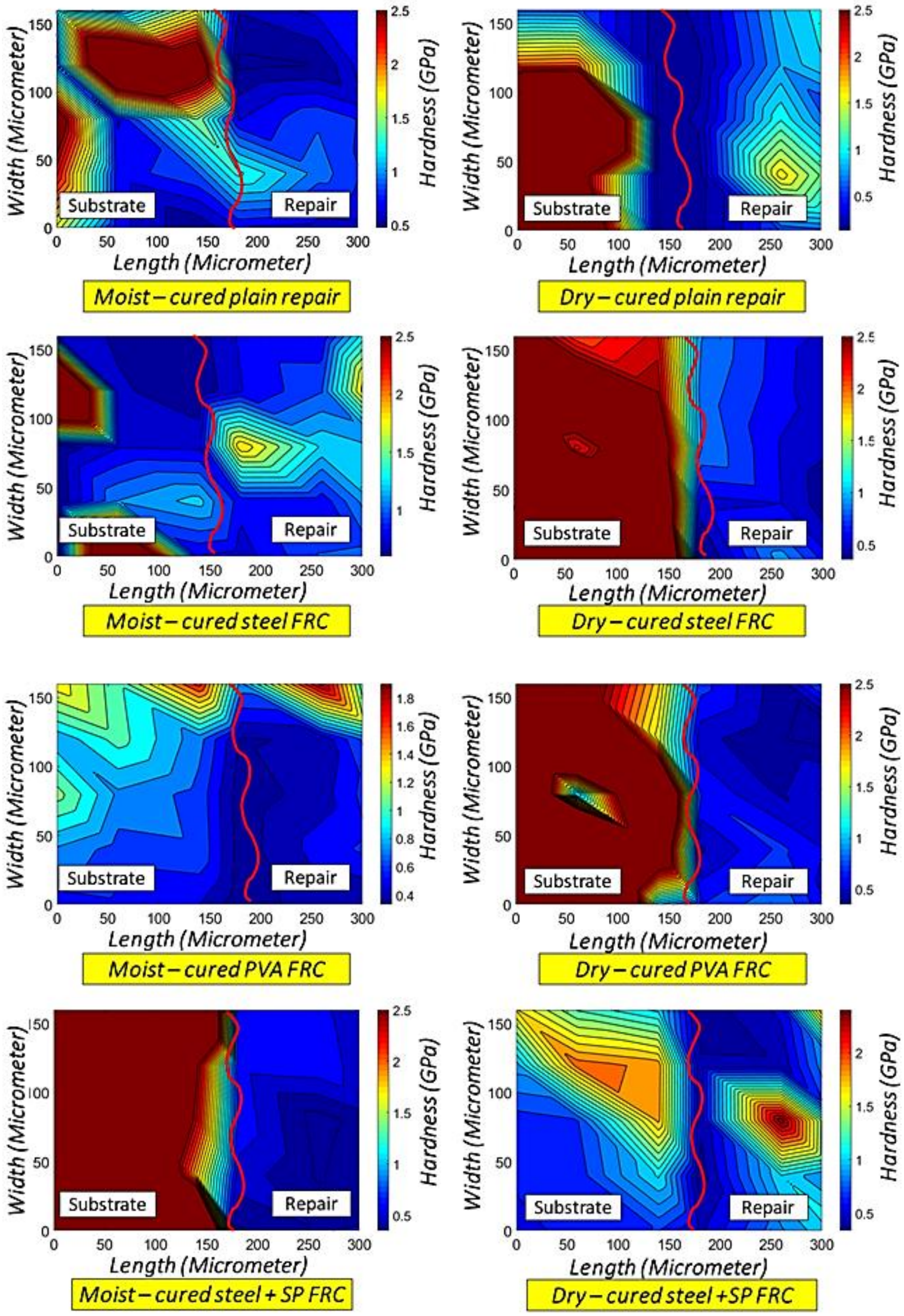

Figure 5.10: Pattern of micro-hardness alterations close to the interface for various composite systems subjected to dry and wet curing

In general, the concrete substrate had higher hardness values than the mortar repair layer. Non-uniform hardness values in concrete substrates are mainly due to the presence of various phases and constituent materials including aggregates [Lukovic et al., 2014]. While in the repair layer such non-uniformity is caused by the weakness of interfacial zone. Areas with lower hardness values can be linked to the interfacial zone and discrete locations within repair and substrate layers. It can be anticipated that these weak zones would be the place for initiation of microcracks. Lower hardness values at the interface are due to presence of weak media at the interface which is partially due to wall effects and fewer CSH particles. Also, discrete locations with lower hardness value are partially result of unhydrated cement particles within the system [Lukovic, 2016].

5.2.4.1 Ratio Between Interfacial Hardness of Dry and Wet-cured Specimens

Repair systems can be evaluated in terms of loss of hardness after being subjected to dry curing. The average hardness value of the interfacial region was calculated and the ratio between average hardness values compared for each repair mix (Figure 5.11). There is a large difference between plain repair versus FRC repair materials.

While composite specimens with plain repair material lost 75% of their interfacial hardness as a result of exposure to high temperature and low humidity, the values obtained for three other mix designs were much smaller. Among FRC repair materials, FRC containing steel and PVA fibers exhibited very small loss of microhardness values. However, this was not the case for FRC containing steel fiber and added superplasticizer. This finding accords with results of other studies, which have shown that addition of superplasticizer to concrete negatively affects the shrinkage and slows the development of early-age stiffness [Qian et al., 2020] [Brooks, 1989]. This finding is thought to be due to inhibiting the formation of hydration products at the early age of hydration and weakening of the CSH network, which leads to weaker micromechanical properties [Cheah et al., 2020]. Moreover, denser matrix, in presence of superplasticizer, increases volume of mesopores in smaller pore diameter inducing higher capillary stresses and higher drying shrinkage strains [Zhang et al., 2015]. In other words, there are more mesopores and fewer macropores in the mix design with superplasticizer which increases shrinkage [Qian et al., 2020]. This suggests that adding superplasticizer to steel FRC has some beneficial effects on long-term mechanical properties, but it is not the best option for improving early age interfacial response in concrete-FRC interfaces subjected to a shrinkage-inducing environment.

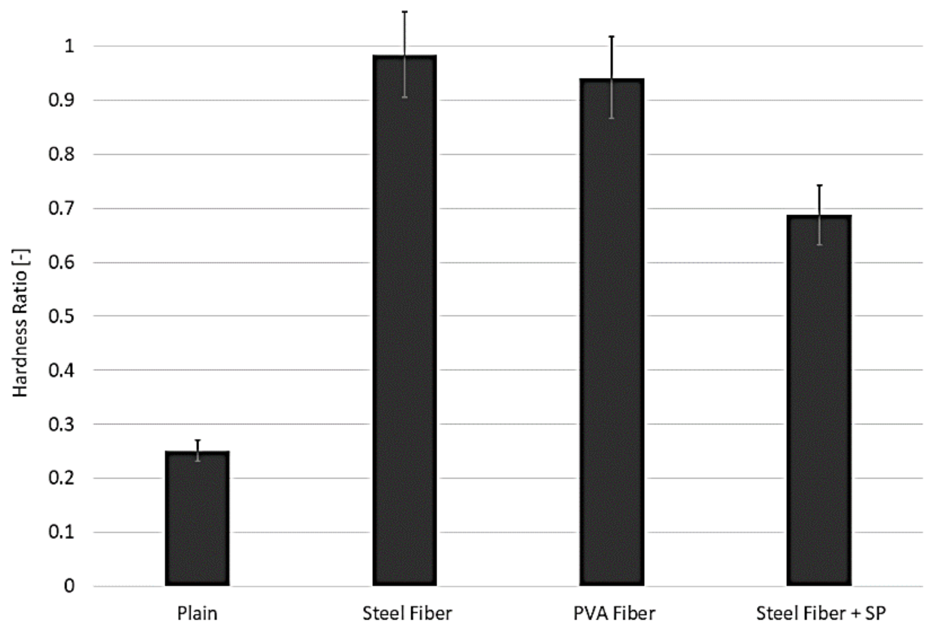

Figure 5.11: Ratio between the average hardness ratios (Hardness Ratio: dry-cured hardness / wet-cured)

5.3 Concluding Remarks

The focus of this chapter was on the microstructure and micromechanics of concrete-FRC interfaces. In order to study the response of concrete-concrete interfaces at the microlevel, various testing techniques were employed including capillary absorption test, visual inspection, X-ray micro-computed tomography, SEM, and microhardness. Based on the results, following conclusions can be drawn:

1. Curing can have a significant impact on absorption capacity, microstructure, and durability of repaired systems. In general, a dry curing regime causes more shrinkage-induced cracks

which in turn increases the vulnerability of repaired structures to penetration of harmful substances and decreases durability of composite systems. Among investigated repair materials, composite systems with FRC as repair material exhibited better mitigated the negative effect of dry curing.

2. Compressive strength of the repair material is highly dependent on the curing regime. Loss of compressive strength is observed among all dry-cured repair materials. The loss of strength in the repair material will in turn adversely affect the response of the composite system. In addition to having a lower strength, dry-cured specimens tend to exhibit further cracking and larger damaged zones around the edges which can be attributed to thermal and humidity effects.
3. Excessive shrinkage caused by high temperature and low humidity can cause extra damage at the concrete-FRC interfaces. This extra damage can be limited to only superficial cracks, major cracks, or even complete debonding. Visual inspection suggests that while all composite systems with plain, steel fiber, and steel fiber + superplasticizer exhibit some levels of damage, repaired systems containing PVA fibers did not undergo significant damage. This suggests efficiency of PVA fiber repaired systems in harsh environmental conditions.
4. Curing condition can remarkably affect micromechanical response of concrete-FRC interfaces. Composite systems with plain repair material are subjected to great loss of microhardness when subjected to adverse environmental condition. On the other hand, repaired systems with FRC material can effectively withstand high temperature, low humidity, and shrinkage cracking and hinder microhardness loss.

As anticipated, harsh dry curing can adversely affect the micromechanical properties of repaired systems and their microstructural stability, especially around the interface. In conclusion, adding PVA and steel fibers enhanced pre-loading stability minimizing changes in void structure and water absorption, and loss of hardness.

Chapter 6: Conclusions, Recommendations and Future Work

In this chapter, objectives of the research work are restated followed by associated results and contributions. Conclusions are drawn and recommendations for further research are suggested.

6.1 Significance of the Research Work

Employing FRC to retrofit old concrete elements is a common technique, however, there is a lot to do in order to fully understand composite behavior of FRC-concrete systems and develop better repair systems. Comprehensive experimental work was carried out on the mechanical response in Mode-I, long-term behavior, micro properties, and failure characteristics of various steel and PVA FRC-concrete interfaces. Macro and micro scale investigations were also carried out and a design expression was developed.

Chapter 3 was devoted to the evaluation of concrete-FRC interfaces under mode-I (tensile) stresses. Fracture parameters, as well as splitting load - CMOD behavior and maximum load bearing capacity of concrete-FRC systems containing 0*%*, 0.5*%*, and 1*%* of steel and PVA fibers were examined using contoured double cantilever beam tests, which is a closed-loop wedge-splitting test. 0*%*, 0.5*%*, and 1*%* volume fractions of 8 and 12 *mm* long PVA fibers and 13 *mm* long steel fibers were evaluated. The role of different fibers in improving interfacial bond and crack growth resistance was investigated. The role of crack deviation on tensile strength of monolithic specimens was investigated, and the impact of interfacial roughness on tensile bond strength of composite specimens was studied. Using 3D surface scans and optical microscope, the relationship between the number of fibers intersected at failure plane and tensile bond strength was investigated. Results of this chapter confirms positive effects of adding steel and PVA fibers, within the investigated range of fiber content, on crack growth resistance and maximum load bearing capacity of monolithic systems and concrete-FRC interfaces in Mode-I. Moreover, within the investigated range of data, beneficial impact of surface treatment and crack tortuosity on failure behavior of concrete-FRC interfaces under Mode-I was observed. Also, a correlation between fiber performance and surface preparation was detected. Based on the results, one can conclude that: (1) Steel and PVA FRCs are recommended for repair purposes in concrete structures as it can enhance mechanical performance of the repaired element; (2) Surface preparation is fundamental for having a strong and durable repair; (3) Impacts of fibers and surface roughness are correlated and they have to be considered simultaneously in designing a repair plan. The conclusions for this chapter are further explained in Section 3.3.

The focus of Chapter 4 was to obtain a design expression able to predict the interfacial bond strength and R-curve of concrete-concrete composite systems under tension. Various input parameters are addressed including surface texture, strength of the repair material, and level of ductility of the concrete-FRC system. Proposed models are based on more than 100 CDCB tests as well as multiple compressive and splitting tests. Results indicate that there is a strong correlation between interfacial bond and surface treatment. This correlation was further studied by introducing material properties as the second important variable. Moreover, the impact of ductility and elastic modulus mismatch was addressed for two different scenarios. Suggestive models are provided for crack growth resistance curves and maximum load bearing capacity of concrete-concrete interfaces under tensile stresses. Conclusions for this chapter can be found in Section 4.3.

Chapter 5 was focused on evaluation of properties of FRC-concrete systems at microscale. Porosity, crack patterns, micro-hardness, and water absorption of interfaces were investigated by means of SEM, CT-scanning, gravimetric tests, and microindentation techniques. In order to study the impact of environmental condition, two different curing regimes were employed. Effectiveness of steel and PVA fibers in mitigating pre-loading damages and shrinkage-induced cracks are demonstrated by the experimental results. Fiber addition has shown positive effects on capillary absorption, void content, and microstructure stability. Moreover, interfaces with FRC repair layers exhibit improved interfacial micromechanical properties compared to plain concrete. Detailed conclusions for this chapter can be found in Section 5.3.

With an increasing demand for repair and rehabilitation of deteriorating infrastructure, and the observed lack of durability and effectiveness of concrete repairs, the overarching goal of this research project was to provide engineered solutions and an enhanced understanding/predictability of complex interfacial behaviors in FRC concrete repairs, with special focus on factors' synergies and interactions at different scales. For this purpose, failure behavior of concrete-concrete interfaces under tensile stresses was researched with special focus on the response of FRC repairs, which represent a promising solution for achieving durable and reliable repaired systems, even though their interactions with the existing structure has lacked a systematic investigation. The research work was designed with a multi-faceted engineering approach to interface analysis so as to address the issue from different perspectives. The impact of steel and PVA fiber addition was evaluated not only under tensile loads but also in the pre-loading (i.e. curing) stage. Steel and PVA fibers, different fiber volume fractions, and curing conditions were considered. The behavior of concrete-FRC interfaces was studied at micro and macro levels; load bearing capacity and crack resistance of repaired systems in different environments were addressed. Based on the results, one can conclude that steel and PVA FRCs are promising options for repair and rehabilitation purposes in deteriorated concrete infrastructure, but their design requires proper consideration of several factors and their interrelations as discussed and quantified throughout the thesis (e.g. fiber stiffness, size, bonding, interface roughness, and elastic moduli of materials among other factors).

Fiber reinforcement positively affects micro and macro behavior of composite structures in terms of tensile strength and durability. Finally, a semi-empirical model is recommended for the prediction of the tensile load bearing capacity and crack growth resistance of various concrete-FRC interfaces, which can be employed for both practical design and more sophisticated numerical analysis.

The study presented here covers various knowledge gaps in the literature. It shows the synergistic effect of fibers and surface preparation and the importance of including both of these governing factors in designing concrete-FRC repairs. This is a continuation of what has already been demonstrated in previous research works on showing the effectiveness of fibers and surface preparation separately but not together. This thesis extends the previous knowledge on load-bearing efficacy of fibers into promising long-term performance of FRC as a repair material by investigating cracking behaviour and resistivity of concrete-FRC interfaces in harsh environmental conditions. This further strengthens the literature and helps with better understanding of concrete-FRC interfaces. The other important milestone of this thesis is providing a predictive model for failure of concrete-FRC interfaces in tension. This helps the previous efforts in the literature on modeling the behavior of concrete-FRC interfaces in shear. Moreover, proposed models for crack growth resistance of concrete-FRC interfaces are quite novel and are expected to inspire more studies on modelling fracture behavior of cementitious composite systems.

The proposed repair technique and recommendations of this study are expected to help with improving short-term and long-term effectiveness of concrete repairs. Moreover, showing positive impacts of FRC as a repair material and providing handy design equations are expected to promote employing FRC in more repair projects. This will lead into more durable repairs which helps with decreasing demand for demolishing and rebuilding deteriorated structures. It is expected that these changes positively affect carbon dioxide emissions of concrete industry which will improve sustainability of construction industry as well.

6.2 Limitations of the Current Study

- ✓ Although semi-empirical models were verified by comparing them to other studies in the literature, these models were built on limited types of fibers, fiber volume fractions, and surface roughness.
- ✓ The investigation presented in this thesis was limited to the response of concrete-FRC interfaces under tensile stresses. This study did not consider mixed-mode loading or concrete-FRC interfacial response under other modes of loading.
- ✓ Only monotonic loading regimes were studied; other loading conditions (e.g. fatigue or impact loading) were not included.
- ✓ Crack growth resistance curves and micro analysis provided an indication of the repairs' durability. However, other factors affecting long term behavior (such as corrosion, freeze-thaw) were not investigated.

6.3 Recommendations and Future Work

Based on the results of this study, the following future areas of investigation are recommended:

- ✓ In order to improve the semi-empirical model suggested in this study, further research is required to investigate the effects of other governing factors of FRC-concrete interfaces including more curing condition, or other types of fiber reinforcement.
- ✓ Mechanical response and fracture behavior of concrete-FRC interfaces should be extended to mixed-mode loading.
- ✓ Other loading regimes, such as impact loading, require analysis in the future.

- ✓ Additional microscale testing may be informative to gain a better understanding of chemical composition and mechanical behavior of FRC-concrete interfaces. It would be informative to have a test setup which provides information on micromechanical response of FRC-concrete interfaces under loading.
- ✓ Further durability tests, such as freeze-thaw and corrosion, may improve our understanding of long-term behavior of FRC-concrete interfaces.
- ✓ Performing full-scale field tests is highly suggested to capture size effect and include it in model expressions. A multiscale modelling approach should follow, including for instance correction factors corresponding to different scales should be obtained and incorporated into the proposed model expressions.

References

Abu-Tair A.L., Rigden S.R., Burley E., “Testing the Bond between repair Materials and Concrete Substrate”, ACI Materials Journal, Vol. 93, 1996, 553-558.

ACI 224R – 01, Control of Cracking in Concrete Structures, reported by ACI Committee 224, 2001.

ACI 308-01, Guide to Curing Concrete, reported by ACI Committee 308, 2001.

ACI 563-18, Specifications for repair of concrete in buildings, reported by ACI Committee 563, 2018.

Agliata R., Bogaard T. A., Greco R., Mollo L., Slob E. C., Steele-Dunne S. C., “Non-invasive estimation of moisture content in tuff bricks by GPR”, Construction and Building Materials, Vol. 160, 2018, 698-706.

Akazawa, T., “New test method for evaluating internal stress due to compression of concrete (the splitting tension test) (Part 1)”, Journal of Japanese Society of Civil Engineers, 1943.

Al-musawi Hajir, Huang Haidong, Guadagnini Maurizio, Pilakoutas Kypros, “A numerical study on the effect of restrained shrinkage on rapid hardening plain and recycled clean steel fiber concrete overlays”, Construction and Building Materials, Vol. 244, 2020.

Al-Osta M.A., Isa M.N., Baluch M.H., Rahman M.K., “Flexural behavior of reinforced concrete beams strengthened with ultra-high performance fiber reinforced concrete”, Construction and Building Materials, Vol. 134 2017, 279-296.

Anderson AR., “Composite designs in precast and cast-in-place concrete”. Prog. Archit. 1960; 41(9):172–9.

ASCE (American Society of Civil engineers), ASCE report cards for America’s infrastructure, 1998, 2001, 2003, 2005.

ASTM C39, Standard test method for compressive strength of cylindrical concrete specimens, 2020.

ASTM C150, Standard Specification for Portland Cement, 2016.

ASTM C469, Standard test method for Splitting Tensile Strength of Cylindrical Concrete Specimens, 2004.

ASTM C642 – 13, Standard Test Method for Density, Absorption, and Voids in hardened Concrete.

ASTM C882, Standard test method for bond strength of epoxy-resin systems used with concrete by slant shear, 2013.

ASTM D4541, Standard test method for pull-off strength of coatings using portable adhesion testers, 2017.

ASTM E92 - 17, Standard Test Method for Vickers Hardness and Knoop Hardness of Metallic Materials.

Austin S., Robins P., Pan Y., "Shear bond testing of concrete repairs", Cement and Concrete Research, Vol. 29, 1999, 1067-1076.

Austin S., Robins P., Pan Y., "Tensile bond testing of concrete repairs", Materials and Structures, Vol. 28, 1995, 249-259.

Balagaru P, Shah S., "Fiber reinforced cement composites", McGrow Hill, 1992.

Banthia N., Zanotti C., Sappakittipakorn M., "Sustainable fiber reinforced concrete for repair applications", Construction and Building Materials, Vol. 67, 2014, 405-412.

Banthia N., Gupta R., "Influence of Polypropylene Fiber Geometry on Plastic Shrinkage Cracking in Concrete", Cement and Concrete Research, Vol. 36(7), 2006, 1263-1267.

Banthia N., Nandakumar N., "Crack growth resistance of hybrid fiber reinforced cement composites", Cement and Concrete Composites, Vol. 25, 2003, 3-9.

Banthia N., Nandakumar N., "Crack growth resistance of concrete reinforced with a low volume fraction of polymeric fiber", Journal of Materials Science Letters, Vol. 20, 2001, 1651-1653.

Banthia N., Moncef A., Chokri K, Sheng J., “Micro-fiber reinforced cement composites. Uniaxial tensile response”, Canadian Journal of Civil Engineering, Vol. 21, No. 6, 1994, 999-1011.

Banthia N., Debeau S., “Carbon and steel microfiber-reinforced cement based composites for thin repairs”, Journal of Materials in Civil Engineering, 1994.

Barenblatt GI., “The mathematical theory of equilibrium cracks in brittle fracture”, Advanced Applied Mechanics, Vol. 7 (1), 1962, 55–129.

Barkhordari Bafghi M.A., Amini F., Safaye Nikoo H., Sarkardeh H., “Effect of Steel Fiber and Different Environments on Flexural Behavior of Reinforced Concrete Beams”, Applied Sciences, Vol. 7(10), 2017, 1011.

Bazant Z.P., “Fracture mechanics of concrete structures”, Proceedings of the first international conference (FraMCoS-1), Breckenridge, Colorado, 1992, Elsevier, London, 1040p.

Bažant ZP, Kim J-K, Pfeiffer PA, Determination of fracture properties from size effect tests”, J. Struct. Eng., ASCE 112 (2): 289–307, 1986.

Bažant ZP, “Size effect in blunt fracture: Concrete, rock, metal.”, J. Eng. Mech., ASCE 110 (4): 518–535, 1984.

Bažant ZP, Oh BH, “Crack band theory for fracture of concrete”, Mater. Struct., Vol. 16 (93): 155 177, 1983.

Bazant N., Cedolin L., “Blunt crack bond propagation in finite element analysis”, Journal of Engineering Mechanics Division, March/April 1979, Vol. 105, No. 2, 297-315.

Beaupre D., “Bond strength of shotcrete repair”, Shotcrete magazine, 1999.

Beltzung F., Wittmann F., “Influence of Cement Composition on Endogenous Shrinkage, Self-desiccation and its importance in Concrete Technology, Report TVBM3104, ISBN 573185343, 2002.

Bentur A., Mindess S., "Fiber Reinforced Cementitious Composites", Taylor and Francis, New York, 2007.

Bentur, A., Gray, R.J. and Mindess, S., “Cracking and pull-out processes in fiber reinforced cementitious materials”, Developments in Fiber Reinforced Cement and Concrete, (eds R.N.Swamy, R L.Wagstaffe and D.R.Oakley), Proceedings RILEM Conference, Sheffield, paper 6.2, 1986.

Birkeland HW., “Precast and prestressed concrete”, Class notes for course, University of British Columbia, Spring; 1968.

Birkeland PW, Birkeland HW., “Connections in precast concrete construction”, Journal of American Concrete Institute, Vol. 63, 1966, 345–68.

Bogas J. A., Gomes M. G., Real S., “Capillary absorption of structural lightweight aggregate concrete”, Materials and Structures, 2015, 2869-2883.

Bonaldo Everaldo, Barros Joaquim, Lourenco Paulo, “Bond characterization between concrete substrate and repairing SFRC using pull-off testing”, International Journal of Adhesion and Adhesives, 2005, 463-474.

Bonen D. and Diamond S., ‘Occurrence of large silica fume-derived particles in hydrated cement paste’, Cement and Concrete Research, Vol. 22 (6) pp.1059-1066, 1992.

Branston J., Das S., Kenno Y., Taylor C., “Influence of basalt fibers on free and restrained plastic shrinkage”, Cement and Concrete Structures, 2016, 182-190.

Brocken H., Spiekman M., Pel L., Kopinga K., and Larbi J., “Water extraction out of mortar during brick laying: a nmr study”, Materials and Structures, Vol. 31, 1998, 49-57.

Brooks J.J., “Influence of Mix Proportions, Plasticizers and Superplasticizers on Creep and Drying Shrinkage of Concrete”, Magazine of Concrete Research, 1989, 145-153

Carol I., Prat P.C., Lopez C.M., “Normal/shear cracking model: Application to discrete crack analysis”, Journal of Engineering Mechanics, 1997, 765-773.

CAN/CSA A23.3. “Design of concrete structures - Structures design”, Canadian Standards Association, 178 Rexdale Boulevard, Rexdale, Ontario, M9W 1R3, Canada, 2004, 258 p.

Carneiro F.L., Barcellos A., “Tensile strength of concrete (in French)”, RILEM Bulletin, Vol.13, 98-125, 1949.

Chalioris C.E., Thermou G.E., Pnatazopoulou S.J., “Behavior of rehabilitated RC beams with self-compacting concrete jacketing – Analytical model and test results”, Construction and Building Materials, 2014, 257-273.

Cheah C.B., Chow W.K., Oo C.W., Leown K.H., “The influence of type and combination of polycarboxylate ether superplasticizer on the mechanical properties and microstructure of slag-silica fume ternary blended self-consolidation concrete’, Journal of Building Engineering, 2020.

Chen Pu-Woei, Fu Xuli, Chung D.D.L., “Improving the bonding between old and new concrete by adding caron fibers to the new concrete”, Cement and Concrete Research, 1995, 491-496.

Chestney M.A., “Concrete Patch Repair Bond Strength, Department of Civil and Building Engineering”, Loughborough University, 1996.

Chmielewska B, “Czarnecki L, Krupa P. Influence of selected factors on the results of pull-off tests for industrial floors”. Proceedings of the fifth international colloquium−Industrial Floors ‘ 03. Technische Akademie Esslingen, January 21‑23, 2003.

CSCE (Canadian Society for Civil Engineering), The technology road map, 2003.

Collin R.G., “Cement and concrete as an engineering material: an history appraisal and case study analysis”, Engineering Failure Analysis, 2014, 114-140.

Courard L., Piotrowski T., Garbacz A., “Near-to-surface properties affecting bond strength in concrete repair”, Cement and Concrete Composites, 2014, 46:73-80.

Crow J.M., “The concrete conundrum”, Chemical World, Vol. 5, 2008, 62-66.

Cui, D., Sun, W., Wan, K., and Banthia, N., “Porosity Characterization in Interfacial Transition Zone Using Dual CT Scans”, Journal of Testing and Evaluation, Vol. 45, No. 2, 2017, 408-418.

Dai S., Liu X., Nawnit K., "Experimental Study on the Fracture Process Zone Characteristics in Concrete Utilizing DIC and AE Methods", Applied Sciences, 2019, 9(7):1346.

Dai J., Ueda T., Sato Y., "Unified analytical approaches for determining shear bond characteristics of FRP-Concrete interfaces through pullout tests", Journal of Advanced Concrete Technology, 2006, 133-145.

D'Ambrisi A., Feo L., Focacci F., "Bond-slip relations for PBO-FRCM materials externally bonded to concrete", Composites: Part B, 2012, 2938-2949.

D'Antino T., Carloni C., Sneed L.H., Pellgrino C., "Matrix-fiber bond behavior in PBO FRCM composites: A fracture mechanics approach", Engineering Fracture Mechanics, 2014, 94-111.

De Borst R., "Application of advanced solution techniques to concrete cracking and non-associated plasticity", in Taylor, C. et al: Numerical method for non-linear problems, 1984, Vol. 2, 314-325, Pineridge press, Swansea, UK.

Delatte N.J., Williamson M.S., Fowler D.W., "Bond strength development with maturity of high-early strength bonded concrete overlays", ACI Materials Journal, 2000, 201-207.

Diamond Sidney, "The microstructure of cement paste and concrete – a visual primer", Cement and Concrete Composite, 2004, 919-933.

Diamond S., Huang J., "The ITZ in concrete – a different view based on image analysis and SEM observations", Cement and Concrete Composites, 23, 2001, 179-188.

Dias-da-Costa D., Alfaiaye J., Julio E.N.B.S., "FE modelling of the interfacial behavior of composite concrete members", Construction and Building Materials, 2012, 233-243.

Dugdale, D.S. (1960) "Yielding of steel sheets containing slits," Journal of the Mechanics and Physics of Solids, 8(2), 100–104.

Elser M, Tschegg E.K., Stanzl-Tschegg S.E, "Fracture behavior of polypropylene-fiber-reinforced concrete under biaxial loading: An experimental investigation", Composite Science and Technology, 1996, 933-945.

EN B. 1-1:2004. “Eurocode 2: design of concrete structures”, General rules and rules for buildings, European Committee for Standardization, Avenue Marnix 17, B-1000 Brussels, Belgium, 2004, 225 pp.

EN 1504: Products and systems for the protection and repair of concrete structures; definitions, requirements, quality control and evaluation of conformity, 2004.

Emmons P.H., “Concrete Repair and Maintenance Illustrated”, R.S. Means company, INC., Construction Publishers and Consultants, 1994.

Emmons P.H., Vaysburd A.M., McDonald E.J., “A Rational Approach to Durable Concrete Repairs”, Concrete International, September 1993, 40-45.

Espeche A.D., Leon J., “Estimation of bond strength envelopes for old-to-new concrete interfaces based on a cylindrical splitting test”, Construction and Building Materials, 2011, 1222-1235.

Fang Chengfeng, Ali Mohamed, Xie Tianyu, Visintin Philip, Sheikh Abdul, “The influence of steel fiber properties on the shrinkage of ultra-high performance fiber reinforce concrete”, Construction and Building Materials, 2020.

Faure P., Care S., Po C., and Rodts S., “An mri-spi and nmr relaxation study of drying-hydration coupling effect on microstructure of cement-based materials at early age”, Magnetic resonance imaging 23, 2005, 311-314.

Ferreira Tiago, Wayne Rasband, “ImageJ User Guide”, 2012.

Genois “Fracture resistance of micro-fiber reinforced cement composites, 155p, Masc. Thesis, University of British Columbia, Department of Civil Engineering, Vancouver, 1995.

Gettu R., Mobasher B., Carmona S., Jancen D., “Testing of Concrete Under Closed-Loop Control”, Advanced Cement-based Materials, 1996, 54-71.

Gohnert M., “Horizontal shear transfer across a roughened surface”. Cement and Concrete Composites, 2003;25(3):379–85.

Griffith A.A., "The phenomena of rupture and flow in solids", Philosophical transactions of the royal society of London, 1920, Series A, Vol. 221, 163-198.

Guide to concrete repair, U.S. department of internal bureau of reclamation, 2015.

Guruprasad Y. K., Ramaswamy A., "Micromechanical analysis of concrete and reinforcing steel exposed to high temperature", Construction and Building Materials, Vol. 158, 2018, 761-773.

Hall C., "Water Sportively of Mortars and Concretes: A Review", Magazine of Concrete Research 41, 1989, 105-109.

Hansen T.S., Frederiksen J.M., "Micro structural analysis – An essential tool for diagnosis of concrete deterioration and choice of repair strategy", Materials and Corrosion, 2012, 1165-1172.

He Ming-Yuan, Bartlett Andrew, Evan Anthony G., "Kinking of a crack out of an interface: role of in-plane stress", Journal of the American Ceramic Society, 1991, 767-771.

Hemalatha T., "Studies on characterization of self-compacting concrete: microstructure, fracture and fatigue", PhD thesis, Indian Institute of Science, 2013.

Hillerborg A, Results of three comparative test series for determining the fracture energy GF of concrete. Mater Struct 18 (5): 407–413, 1985.

Hillerborg A., "Analysis of fracture by means of the fictitious crack model. Particularly for fiber reinforced concrete", The International Journal of Cementitious Composites, Vol. 2, 1980, 177-184.

Hillerborg, A., Modeer, M., and Petersson, P.E., "Analysis of crack formation and crack growth in concrete by means of fracture mechanics and finite elements," Cement and Concrete Research, 6(6), 773–782, 1976.

Hofbeck JA, Ibrahim IO, Mattock AH., "Shear transfer in reinforced concrete". Journal of American Concrete Institute, 1969; 66(2):119–28.

Hrberk V., Koudelkova V., Prosek Z., Tesarek P., "Micro-mechanical performance of concrete used as recycled raw material in cementitious composite", Acta Polytechnica CTU Proceedings, 2017.

Inglis, C. E., “Stresses in a plate due to the presence of cracks and sharp corners”, Transactions of the Institution of Naval Architects, 55, 219–241, 1931.

Irwin, G.R., Fracture, Handbook der Physik, VI. Flugge, ed., Berlin Springer, pp. 551–590, 1958.

Irwin G.R., Plastic zone near a crack and fracture toughness. Proceedings of the 7th Sagamore Conference, p. IV–63, 1960.

ISO 4287-1997 “Geometrical Product Specification - Surface Texture: Profile method – Terms definitions and surface texture parameters”, 1997.

Jenq YS, Shah SP, “Two parameter fracture model for concrete”, J. Eng. Mech., ASCE 111 (10): 1227–1241, 1985.

Jenq YS, Shah SP, “Crack-propagation in fiber reinforced concrete, Journal of structural engineering”, ASCE, 1986, 19-34.

Jenq, Y. S. and Shah, S. P., ‘On the concrete fracture testing methods’, in Fracture Toughness and Fracture Energy—Test Methods for Concrete and Rock (edited by H. Mihashi, H. Takahashi and F. H. Wittmann) (A. A. Balkema Publishers, Rotterdam, Netherland, 1989, pp. 443–463).

Kabiri far B., Zanotti C., “Concrete-concrete bond in Mode-I: a study on the synergistic effect of surface roughness and fiber reinforcement”, Applied Sciences, Special Issue “Fiber-Reinforced Concrete, 2019, 2556.

Kamada Toshiro, Li V. C., “The effects of surface preparation on the fracture behavior of ECC/Concrete repair system”, Cement and Concrete Composites, 2000, 423-431.

Kaplan, M. E., “Crack propagation and fracture of concrete”, Journal of ACI , 58(5), 591–610, 1961.

Kaufmann R., Flisch A., Griffa M., Hartmann S., Hofmann J., Jerjen I., Liu Y. Luthi T., Neeld A., Plamondon M., Reifler E., Schuetz P., Stritt C., Yang E., and Dommann A., “New directions in x-ray tomography, in 11th European Conference on Non-Destructive Testing (ECNDT 2014), , Prague, Czech Republic, October 6- 10, 2014.

Kazemi Kamyab M., Denarie E., Bruhwiler E., Wang B., Thiery M., Faure P. F., and Broghel-Bouny V., "Characterization of moisture transfer in uhpfrc-concrete composite systems at early age, in Proceedings of the 2nd International Conference on Microstructural-related Durability of Cementitious Composites, EPFL-CONF-177049, 2012.

Krafft JM, Sullivan AM, Boyle RW, Effect of dimensions on fast fracture instability of notched sheets. Proceedings of the Crack Propagation Symposium, College of Aeronautics, Cranfield, England, Vol. 1, 1961, 8-26.

Krenchel H., "Fiber reinforcement", Akademisk Forlag, Copenhagen, 1964.

Kriegh, J.D., "Arizona Slant Shear Test: A Method to Determine Epoxy Bond Strength", American Concrete Institute, Journal of the American Concrete Institute, Vol. 73, No. 3 pp. 372-373, 1976.

Kumar S., Barai S.V., "Concrete fracture models and applications", Springer-Verlag Berlin Heidelberg, 2011.

Lampropoulos A.P., Paschalis S.A., Tsioulou O.T., Dritsos S.E., "Strengthening of reinforced concrete beams using ultra high performance fiber reinforced concrete (UHPFRC)", Engineering Structures, 2016, 370-384.

Landis E. N., Bolander J. E., "Explicit representation of physical process in concrete fracture", Journal of Physics D: Applied Physics, 42, 2009.

Lea, F.M., "The Chemistry of Cement and Concrete", Third Edition, Chemical Publishing Co., Inc., New York, 1970.

Leung C.K.Y., Chi J., "Derivation of crack bridging force in random ductile fiber reinforced brittle matrix composites", ASCE J. Eng. Mech., 1995.

Li Zongjin, "Advanced Concrete Technology", John Wiley & sons, Inc., 2011.

Li V.C., "Engineered Cementitious Composites (ECC) – Material, Structural, and Durability Performance", In E. Nawy, Concrete Construction Engineering Handbook, CRC Press, 2007.

Li V.C., “On engineered cementitious composites: a review of the material and its applications”, Journal of Advanced Concrete Technology, 2003, Vol 1, No. 3, 215-230.

Li V.C., Leung C.K.Y., “Steady state and multiple cracking of short random fiber composites”, ASCE Journal of Engineering Mechanics, 2246-2264, 1992.

Lieboldt M., Mechtcheine V., “Capillary transport of water through textile-reinforced concrete applied in repairing and/or strengthening cracked RC structures”, Cement and Concrete Research, 52, 2013, 53-62.

Lim Y. M., Li V.C., “Durable repair of aged infrastructure using trapping mechanism of engineered cementitious composites”, Cement and Concrete Composites, 1997, 19:373-385.

Lin, C.K., Chen, J.N. & Lin, C.C., ‘An NMR, XRD and EDS study of solidification/stabilization of chromium with Portland cement and C3S’, Journal of Hazardous Materials, vol. 56 (1-2), 1997, 21-34.

Lin IJ, Chen YL., “Shear transfer across a crack in reinforced high strength concrete”, In: Proceedings 2nd east Asia–Pacific conference on structural engineering & construction, Chiang Mai, Thailand, January 1989. p. 505–10.

Liu Y., Wang F., Hu S., Liu M., “Compatibility of repair materials with substrate low-modulus cement and asphalt mortar (CA mortar)”, Construction and Building Materials, 2016, 304-312.

Locher F.W., Richartz W., Sprung S., ‘Erstarren von Zement’ (in German), Zement Kalk Gips vol. 29 (10) pp. 435-442, 1976.

Loov RE., “Design of precast connections”, Paper presented at a seminar organized by Compa International Pt., Ltd. Singapore, 1978, 8 p.

Lukovic M., “Influence of Interface and Strain Hardening Cementitious Composite (SHCC) Properties on the Performance of Concrete Repairs”, PhD Thesis, Delft University of Technology, 2016.

Lukovic M., Dong H., Savija B., Schlangen E, Ye G, Van Bruegel K., “Tailoring strain-hardening cementitious composite repair systems through numerical experimentation”, Cement and Concrete Composites, 2014, 53: 200-213.

Lukovic M., Schlangen E., Ye G., Savija B., “Impact of surface roughness on the debonding mechanics in concrete repairs”, J.G.M van Mier, G. Ruiz, C. Andrabe, R.C. Yu, X. Zhang (eds), Fracture Mechanics of Concrete and Concrete Structures, Proceedings of the 8th International Conference of Fracture Mechanics of Concrete and Concrete Structures (FraMCoS-8), 11-14 March 2013, Toledo, Spain, 611-621.

Lukovic M., Ye G., Van Breugel K., “Reliable concrete repair: A critical review”, Conference: Structural faults and repair, 2012.

Magnet P., and Azari M., “Plastic shrinkage of steel fiber reinforced concrete”, Materiaux et Constructions, 1990.

Maiti Surjya Kumar, “Fracture mechanics, fundamentals and applications”, Cambridge University Press, 2015.

Mansur MA, Vinayagam T, Tan KH. Shear transfer across a crack in reinforced high-strength concrete. ASCE J Mater Civil Eng 2008; 20 (4):294–302.

Mattock AH. Shear friction and high-strength concrete. ACI Struct J 2001; 98(1):50–9.

Mattock AH. Reader comments of paper ‘‘Influence of concrete strength and load history on the shear friction capacity of concrete members’’ published in PCI Journal, January–February 1987, 66-84.

Mattock AH. Shear transfer in concrete having reinforcement at an angle to the shear plane. American Concrete Institute. Special Publication 42-2, January 1974, 17–42.

Mattock AH, Hawkins NM. Shear transfer in reinforced concrete – recent research. PCI J 1972; 17(2):55–75.

McDonald J., Campbell R., U. A. E. W. E. Station, M., “Repair, Evaluation, and R. R. Program, The Condition of Corps of Engineers Civil Works Concrete Structures”, Technical report (Repair, Evaluation, Maintenance and REHABILITATION Research Program (U.S.): REMR-CS), U.S. Army Engineer Waterways Experiment Station, 1985.

McGill-FCM (McGill University and Federation of Canadian Municipalities), Canadian municipal infrastructure: the present state, 1996.

Miloud B., "Permeability and porosity characteristics of steel reinforced concrete", Asian Journal of Civil Engineering, 2005, 317-330.

Mindess S., Young J., Darwin D., "Concrete", Pearson Education Inc., 2003.

Mindess S., "The fracture process zone in concrete", in Shah S.P.: Toughening mechanisms in quasi brittle materials, Kluwer academic publishers, The Netherlands, 1991, 271-286.

Mindess S., Banthia N., Yan C., "The fracture toughness of concrete under impact loading", Cement and Concrete Research, 17, 1987, 231-241.

Mindess, S. and Young, J.F., Concrete, Prentice-Hall, Englewood Cliffs, 1981.

Mirza Saeed, "Durability and sustainability of infrastructure – a state-of-the-art report", Can. J. Civ. Eng. 33, 2006, 639 – 649.

Mirza M.S., "Urgency of addressing Canada's infrastructure needs", In Canadian p3: Under the Microscope, 12th Annual Conference on Public-Private Partnership, Toronto, 22-23 November 2004.

Mohamad ME, Ibrahim IS., "Interface shear strength of concrete-to-concrete bond with and without projecting steel reinforcement", Journal Teknologi, 2015, 75(1):169-172.

Momayez A., Ehsani M.R., A.A. Ramezanianpour, Rajaie H., "Comparison of methods for evaluating bond strength between concrete substrate and repair materials", Cement and Concrete Research, 2005, 35:748 – 757.

Moser R. D., Allison P. G., Chandler M. Q., "Characterization of Impact Damage in Ultra-High Performance Concrete Using spatially Correlated Nanoindentation/SEM/EDX", Journal of Materials Engineering and Performance, 22, 2013, 3902-3908.

Mostovy S., Crosley P.B., Ripling E.J., “Use of crack-line-loaded specimens for measuring plane strain fracture toughness”, Journal of Materials, Vol. 2, No. 3, 1967, 661-681.

Nallathambi P, Karihaloo BL, “Determination of specimen-size independent fracture toughness of plain concrete”, Magn. Concr. Res., 38 (135), 1986, 67–76.

NEN-EN 480-5 Admixtures for concrete, mortar and grout – Test methods – Part 5: Determination of capillary absorption, 2005.

Neshvadian Keivan, “Evaluation of bond strength between overlay and substrate in concrete repairs”, KTH University, 2010.

Neto P., Alfaiate J. Almeida J.R., Pires E.B., “The influence of mode II fracture on concrete strengthened with CFRP”, Computers and Structures, 2004, 1495-1502.

Oliver W. C., and Pharr G. M., “Measurement of hardness and elastic modulus by instrumented indentation: Advances in understanding and refinements of methodology”, Journal of Materials Research, 19, 2004, 3-20.

Papanicolaou CG, Triantafillou TC., “Shear transfer capacity along pumice aggregate concrete and high-performance concrete interfaces”, Mater. Struct., 2002, 35(4):237–45.

Pattnaik R.R., Rangaraju P.R., “Analysis of compatibility between repair material and substrate concrete using simple beam with third point loading”, Journal of Materials in Civil Engineering, 2007, 1060-1069.

Qi C., Wiess J., Olek J., “Characterization of plastic shrinkage cracking in fiber reinforced concrete using image analysis and a modified Weibull function”, Mater. Struct., 2003, 36:386-395.

Qi Cao, Quanqing Gao, Ruibin Wang, Zhibin Lin, “Effect of fibers and expansive agent on shrinkage of self-consolidating concrete under two curing schemes”, Journal of Materials in Civil Engineering, 2019.

Qiao P., Chen Y., “Cohesive fracture simulation and failure modes of FRP-concrete bonded interfaces”, Theoretical and Applied Fracture Mechanics 49, 2008, 213-225.

Qian X., Yu C., Zhang L., Qian K., Fang M., Lai J., “Influence of superplasticizer type and dosage on early-age drying shrinkage of cement paste with consideration of pore size distribution and water loss”, Journal of Wuhan University of Technology, 2020, 758-767.

Ramey G.E., Strickland A.M., “An experimental evaluation of rapid-setting patching materials used in repair of concrete bridges and pavements”, HPR Report, 1984, 149 p.

Randl N. Investigations on transfer of forces between old and new concrete at different joint roughness. PhD thesis, University of Innsbruck, 1997, 379 p. [in German].

Raths CH. Reader comments of paper ‘‘Design proposals for reinforced concrete corbels’’, published in PCI Journal, May–June 1976;21(3):18–42, by Mattock A. PCI J 1977, 22(2):93–8.

Reinhardt H., Cornelissen H.A.W., “Post-peak cyclic behavior of concrete in uniaxial tensile and alternating tensile and compressive loading”, Cement and Concrete Research, Vol. 14, No. 2, 1994, 263-270.

Richardson I.G., “The nature of C-S-H in hardened cements”, Cement and Concrete Research, 1999, 1131-1147.

Rice, J.R., “A path independent integral and the approximate analysis of strain concentration by notches and cracks,” Journal of Applied Mechanics, ASME, 35(6), 1968, 379–386.

RILEM Report 11, “Interfacial Transition Zone in Concrete”, Chapman and Hall, 1996.

Roels S. and Carmeliet J., “Analysis of moisture flow in porous materials using microfocus x-ray radiography”, International Journal of Heat and Mass Transfer, 49, 2006, 4762-4772.

Rokugo, K., Iwasa, M., Suzuki, T. and Koyanagi, W., “Testing method to determine tensile strain softening curve and fracture energy of concrete”, in Fracture Toughness and Fracture Energy, Balkema, 1989, 153-163.

Rots J.C., Blaauwendrad J., “Crack models for concrete: discrete or smeared? Fixed, multi-directional or rotating”, HERON, Vol. 34, No. 1, 1989, 1-59.

Rots J.G., “Computational modelling of concrete fracture”, PhD Thesis, Civil Engineering and Geosciences, Delft University of Technology, Delft, The Netherlands, 1988.

Sadowski L., Stefaniuk D., “Microstructural Evolution within the Interphase between Hardening Overlay and Existing Concrete Substrates”, Applied Sciences, 2017, 7(2):123.

Sadowski L., “Adhesion in Layered Cement Composites”, Springer Nature Switzerland AG, 2019.

Sadowski L., Stefaniuk D., Hola J., “The effect of the porosity within the interfacial zone between layers on pull-off adhesion”, Construction and Building Materials, 2017, 152: 887-897.

Sadowski L., “Multi-Scale Evaluation on the interphase Zone between the Overlay and Concrete Substrate: Methods and Descriptions”, Applied Sciences, 2017, 7(9):893.

Sadouki H., Denarie E., Bruhwiler E., “Validation of a FEA model of structural response of RC-cantilever beams strenghned with a R-UHPFRC layer”, Construction and Building Materials, 2017, 100-108.

Safdar M., Matsumoto T., Kakuma K., “Flexural behavior of reinforced concrete beams repair with ultra-high performance fiber reinforce concrete (UHPFRC)”, Composite Structures, 2016, 279-296.

Sahoo, P.K., Soltani, S. and Wong, A.K.C., ‘A survey of thresholding techniques,’ Computer Vision, Graphics, and Image Processing, vol. 41, 1998, 233-260.

Sakulich A. R. and Li V. C., “Nanoscale characterization of engineered cementitious composites (ecc)”, Cement and Concrete Research, 41, 2011, 169-175.

Santos P.M.D., Jùlio E., “Interface shear transfer on composite concrete members”, ACI Structural Journal, Vol. 111(1), 2014, 113-122.

Santos P.M.D., Jùlio E., “A state-of-art review on roughness quantification methods for concrete surfaces”, Construction and Building Materials, Vol. 38, 2013, 912-923.

Santos P.M.D., Julio E.N.B.S., “Factors Affecting Bond between New and Old Concrete”, ACI Materials Journal, Vol 108, No. 4, 2011, 449-456.

Santos P.M.D., Júlio ENBS, “Recommend improvements to current shear-friction provisions of model code”, In: 3rd fib international congress, Washington, DC, May 29–June 02, 2010.

Schaefer C., Kupwade-Patil K., Ortega M., Soriano C., Buyuzkozturk O., White A., Short M., “Irradiated recyclyed plastic as a concrete additive for improved chemo-mechanica properties and lower carbon footprint”, Waste Management, Vol. 71, 2018, 426 – 439.

Scrivener K.L., ‘The use of backscattered electron microscopy and image analysis to study the porosity of cement paste’, Proc. Material Research Society Symposium, vol. 137, Pore structure and permeability of cementitious materials, 1988, 129-140.

Shah S. G., Kishen J. M. C., “Nonlinear fracture properties of concrete-concrete interfaces”, Mechanics of Materials, 42, 2010, 916-931.

Shrestha J., Zhang D., Ueda T., “Bond-slip models for FRP-concrete interfaces subjected to moisture conditions”, International Journal of Polymer Science, 2017.

Silfwerbrand J., Beuhausen H., Courard L., Bond. In: Bissonnette B., Courard L., Fowler D.W., Granju J. L., “Bonded Cement-Based Material Overlays for the Repair, the Lining on the Strengthening of Slabs or Pavements”, State-of-the-Art Report of the RILEM Technical Committee 193-RLS, 51-79, 2011.

Silfwerbrand J., “Shear bond strength in repaired concrete structure”, Materials and Structures, Vol. 36, July 2003, 419-424.

Slowik V., Lukovic M., Wagner C., Van Zijl G., “Behavior of bonded SHCC overlay systems”, Chapter 8 in A Framework for Durability Design with Strain-Hardening Cement-Based Composites (SHCC), Van Zijl GPAG and Slowik V (eds.), RILEM, ISBN 978-94-024-1012-9, 2017, 125-146.

Sorelli L., Banthia N., Plizzari G.A., “Crack growth resistance of thin mortar layers with hybrid fiber reinforcement”, Special Publication 224, Paper N. 12, American Concrete Institute, Farmington Hills, MI, USA: 161-178, 2014.

Soleimani-Dashtaki Salman, "Seismic Strengthening of Unreinforced Masonry Walls Using Sprayable Ecofriendly Ductile Cementitious Composite (EDCC), PhD Thesis, University of British Columbia, 2018.

Struble, L.J., 'Quantitative phase analysis of clinker using X- diffraction', Cement and Concrete Aggregates, Vol. 13 (2), 1991, 97-102.

Stutzman P.E., 'Scanning Electron Microscopy in Concrete Petrography', Proc. Materials Science of Concrete Special Volume: Calcium Hydroxide in Concrete, J. Skalny, J. Gebauer and I. Odler, eds ., The American Ceramic Society. November 1-3, 2000, Anna Maria Island, Florida, 59-72.

Sun W., Mandel J.A., "The effect of fiber spacing on interfacial layers, J. Chin. Ceram. Soc., 1989.

Sun Wei, Chen Huisu, Luo Xin, Qian Hongpin, "The effect of hybrid fibers and expansive agent on the shrinkage and permeability of high-performance concrete", Cement and Concrete Research, Vol.31, 2001, 595-601.

Suzuki T., Shiotani T., Ohtsu M., "Evaluation of cracking damage in freeze-thawed concrete using acoustic emission and E-ray CT image", Construction and Building Materials, 136, 2017, 619-626.

Tabor, L.J., "Evaluation of Resin Systems for Concrete Repair", Magazine of Concrete Research, Vol. 30, No. 105, December 1978, 117-125.

Tamulenas V., Ramanauskas R., Kaklauskas G., "Experimental and numerical investigation on tensile concrete elements bonded with external CFRP sheets", Procedia Engineering, 2017, 1146-1153.

Taylor, H.W.F., "The Chemistry of cement", Vol. 1, Academic Press, London, 1964.

Tekieli M., De Santis S., De Felice G., Kwiecien A., Roscini F., "Application of Digital Image Correlation of Composite Reinforcement Testing", Composite Structures, 2017, 160:670 – 688.

Tilly G. and Jacobs J., "Concrete repairs: performance in service and current practice", ConRepNet Project Report, HIS BRE Press, Watford, UK, Tech. Rep., 2007.

Trainor K. J., Foust B.W. Landis E.N., “Measurement of Emery Dissipation Mechanisms in Fracture of Fiber-Reinforced Ultrahigh-Strength Cement-Based Composites”, Journal of Engineering Mechanics, 2013, 771-779.

Trtik P., Munch B. and Lura P., “A critical examination of statistical nanoindentation on model materials and hardened cement pastes based on virtual experiments”, Cement and Concrete Composites, Vol. 31, 2009, 705-714.

Trtik P., Bartos P.J.M., “Micromechanical properties of cementitious composites”, Materials and Structures, Vol. 32, 1999, 388–393.

Tschegg E.K., Ingruber M., Suberg C.H., Monger F., “Factors influencing fracture behavior of old-new concrete bonds”, ACI Structural Journal, 2000, 447-453.

Tschegg E.K., “New equipments for fracture tests on concrete”, Karl Hanser Verlag, 1991.

Tsoukantas SG, Tassios TP., “Shear resistance of connections between reinforced concrete linear precast elements”, ACI Structural Journal, 1989, 86 (3):242–249.

Tudjono S., Lie H.A., Hidayat A., Purwanto, “Experimental study on the concrete surface preparation influence to the tensile and shear bond strength of synthetic wraps”, Procedia engineering, Vol. 171, 2016, 1116-1122.

Van Belleghem B., Montoya R., Dewanckele J., Van den Steen N., De Graeve I., Deconinck J., Cnudde V., Van Tittelboom K., De Belie N., “Capillary water absorption in cracked and uncracked mortar: A comparison between experimental study and finite element analysis”, Construction and Building Materials, Vol. 110, 2016, 154-162.

Van Bruegel K., Van Tuan N., “Autogenous Shrinkage of HPC and Ways to Mitigate it”, Key Engineering Materials, 2014, 3-20.

Van Mier J.G.M., “Mode I fracture of concrete: discontinuous crack growth and crack interface grain bridging”, Cement and Concrete Research, , Vol. 21, No. 1, 1991, 1-15.

Visalvanich K., Naaman A. E., “Fracture methods in cement composites”, Journal of the Engineering Mechanics Division, Vol. 107, No. 6, 1981, 1155 – 1171.

Vision 2020: A vision for the concrete repair protection and strengthening industry, the Strategic Development Council (SCD), Technical Report, 2016.

Wagner C., Bretschneider N., Slowik V., “Characterization of the interface between strain hardening cementitious repair layers and concrete subgrade”, FraMCoS-8, 2013, Toledo, Spain.

Wagner C., Bretschneider N., Villman B., Slowik V., “Modelling of the bond between strain hardening cementitious repair layers and concrete substrate”, 3rd international RILEM conference on strain hardening cementitious composites, November 2014, The Netherlands.

Walraven J, Frénay J, Pruijssers A., “Influence of concrete strength and load history on the shear friction capacity of concrete members”, PCI Journal 1987; 32(1):66–84.

Wang X., Petru M., “Mode I fracture evaluation of CFRP-to-concrete interfaces subject to aggressive environments agents: Freeze-thaw cycles, acid and alkaline solutions”, Composites Part B, Vol. 168, 2019, 581-588.

Wang L., Ueda T., “Mesoscale modelling of water penetration into concrete by capillary absorption”, Ocean Engineering, Vol. 38, 2011, 519-528.

Wang X.H., Jacobsen S., He J.H., Zhang Z.L., Lee S.F., and Lein H.L., “Application of nanoindentation testing to study of the interfacial transition zone in steel fiber reinforced mortar”, Cement and Concrete Research, Vol. 39, 2009, 701-715.

Wang X., Wu B., Wang Q., “Online SEM investigation of microcrack characteristics of concretes at various temperatures”, Cement and Concrete Research, Vol. 35, 2005, 1385-1390.

Worrell E., Price L., Martin N., Hendriks C., Media L.O., “Carbon dioxide emissions from global cement industry”, Annual Review of Energy and Environment, Vol. 206, 2001, 303-329.

Wu Z.S., Yoshizawa H., “Analytical/Experimental Study on Composite Behavior in Strengthening Structures with Bonded Carbon Fiber Sheets”, Journal of Reinforced Plastics and Composites, 1999.

Xiao J., Li W., Sun Z., Lange D.A., and Shah S.P., “Properties of interfacial transition zones in recycled aggregate concrete tested by nanoindentation”, Cement and Concrete Composites, Vol. 37, 2013, 276-292.

Xiong G., Liu J., Li G., Xie H., “A way for improving interfacial transition zone between concrete substrate and repair materials”, Cement and Concrete Research, Vol. 32, 2002, 1877 – 1881.

Xu S, Zhang X, “Determination of fracture parameters for crack propagation in concrete using an energy approach”, Engineering Fracture Mechanics, Vol. 75, 2008, 4292–4308.

Xu S, Reinhardt HW, “Determination of double-K criterion for crack propagation in quasi-brittle materials, part I: Experimental investigation of crack propagation”, International Journal of Fracture, Vol. 98, 1999, 111–149.

Xu S, Reinhardt HW, “Crack extension resistance and fracture properties of quasi-brittle materials like concrete based on the complete process of fracture”, International Journal of Fracture, Vol. 92, 1998, 71–99.

Ye G., “Experimental study and numerical simulation of the development of the microstructure and permeability of cementitious materials”, PhD thesis, Delft University Press, 2003.

Yin H., Shirai K., Teo W., “Numerical model for predicting the structural response of composite UHPC-concrete members considering the bond strength at the interface”, Composite Structures, 2019.

Yin H., Teo W., Shirai K., “Experimental investigation on the behavior of reinforced concrete slabs strengthened with ultra-high performance concrete”, Construction and building materials, , Vol. 215, 2017, 185-197.

Yoo DY, Lee JH, Yoon YS, “Effect of fiber content on mechanical and fracture properties of ultra-high performance fiber reinforced cementitious composites”, Composite Structures, Vol. 106, 2013, 742-753.

Zanotti C., Randl N., “Are concrete-concrete bond tests comparable?”, Cement and Concrete Composites, Vol. 99, 2019, 80-88.

Zanotti C., Rostagno G., Tingley B. “Further evidence of interfacial adhesive bond strength enhancement through fiber reinforcement in repairs”, Construction and Building Materials, Vol. 160, 2018, 775 – 785.

Zanotti C., Banthia N., Plizzari G., "Towards sustainable repairs: Substrate-repair interface Mode-I fracture analysis", International Journal of Sustainable Materials Structural Systems, Vol. 1(3), 2014a, 265-281.

Zanotti C., Banthia N., Plizzari G., "A study of some factors affecting bond in cementitious fiber reinforced repairs”, Cement and Concrete Research, Vol. 63, 2014b, 117-126.

Zhang Y.R., Kong X.M., Lu Z.B., Lu S.S., Hou S.S., “Effects of the charge characteristics of polycarboxylate superplasticizers on the adsorption and the retardation in cement pastes, Cement and Concrete Research, Vol. 67, 2015, 184-196.

Zhou J., “Performance of Engineered Cementitious Composites for Concrete Repairs, PhD Thesis, Delft University of Technology, 2011.

Zhou Y., Wu Y., Yun Y., “Analytical modelling of the bond-slip relationship at FRP-concrete interfaces for adhesively-bonded joints”, Composites: Part B, Vol. 41, 2010, 423-433.

Zhu W., Bartos P., “Assessment of interfacial microstructure and bond properties in aged GRC using novel microindentation method”, Cement and Concrete Research, Vol. 27, 1997, 1701-1711.

Zou X., Sneed L.H., D’Antino Tommaso, Carloni C., “Analytical Bond-Slip Model for Fiber-Reinforce Cementitious Matrix-Concrete Joints Based on Strain Measurements”, Journal of Materials in Civil Engineering, Vol. 31, 2019.

Appendix

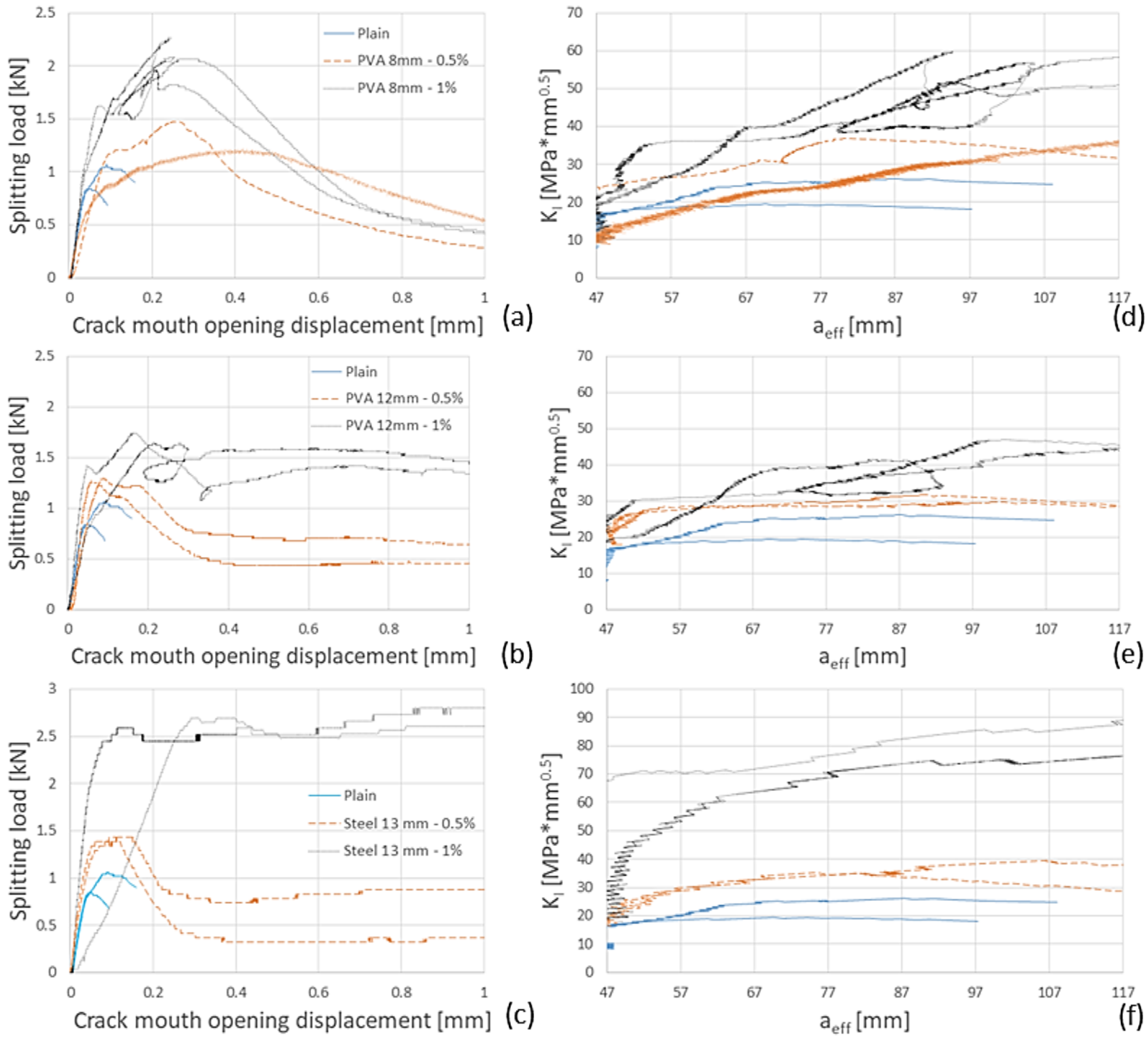

Figure A1. Splitting load (SL) vs. crack mouth opening displacement (CMOD) curves of (a) 8 mm PVA FRC (b) 12 mm PVA FRC (c) 13 mm Steel FRC, Crack growth resistance curves (in terms of SIFs, KI, vs. effective crack length, aeff) of (d) 8 mm PVA FRC, (e) 12 mm PVA FRC (f) 13 mm steel FRC

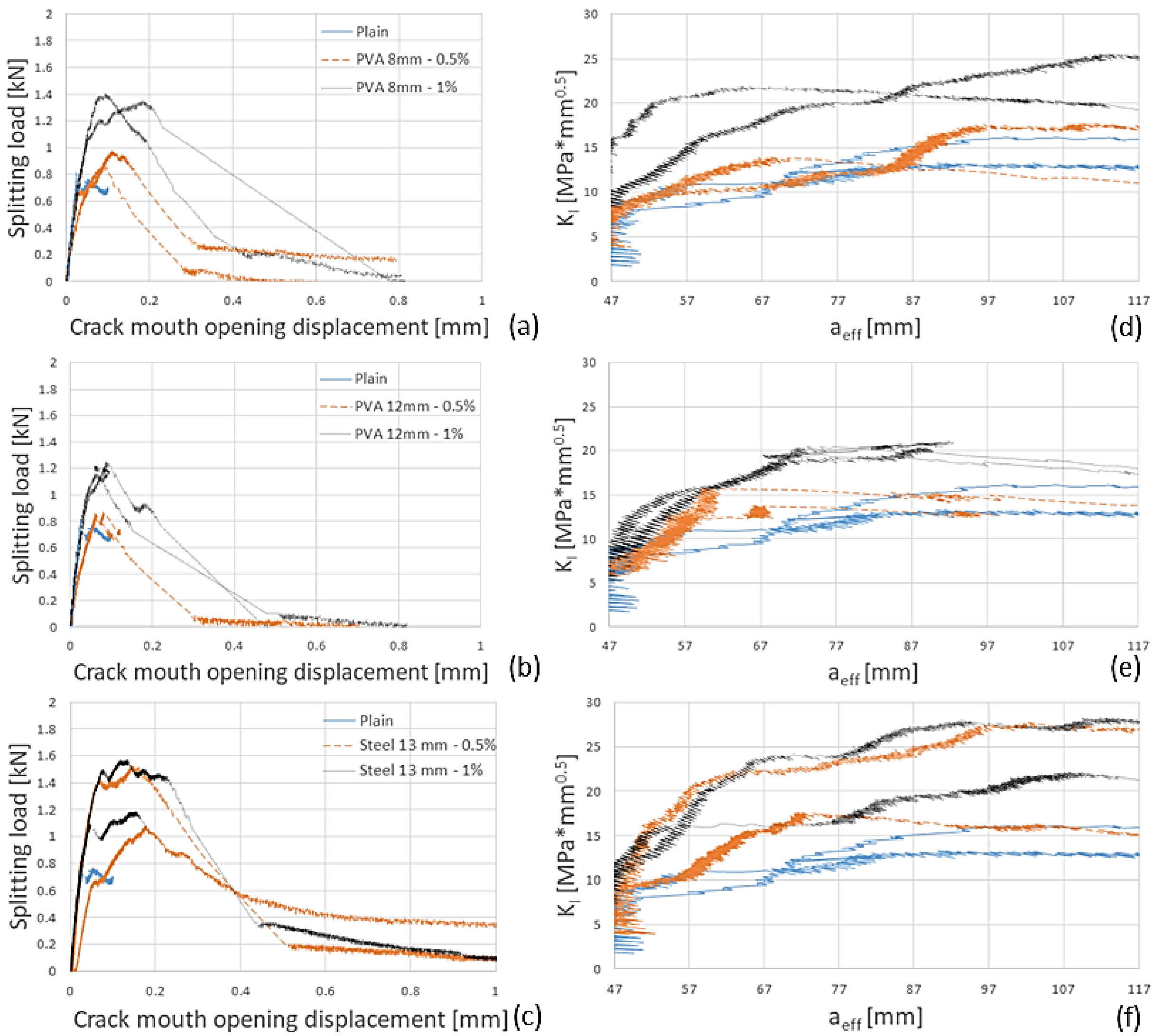

Figure A2. Splitting load (SL) vs. crack mouth opening displacement (CMOD) curves of (a) 8 mm PVA interface (b) 12 mm PVA interface (c) 13 mm Steel interface, Crack growth resistance curves (in terms of SIFs, KI, vs. effective crack length, aeff) of (d) 8 mm PVA interface, (e) 12 mm PVA interface (f) 13 mm steel interface